EXPERIMENTAL INVESTIGATION OF ENERGY-BASED SEISMIC RESPONSE ANALYSIS FOR SDOF STEEL COLUMNS

by

Babak Ebadi Tabrizi

B.S., Civil Engineering, Islamic Azad University South Tehran Branch, 2007

Submitted to the Institute for Graduate Studies in
Science and Engineering in partial fulfillment of
the requirements for the degree of
Master of Science

Graduate Program in Civil Engineering
Boğaziçi University
2016

ACKNOWLEDGEMENTS

Firstly, I would like to express my sincere gratitude to my advisor Assoc. Prof. Cem Yalçin for the continuous support of my Master's study and research, for his patience and immense knowledge. His guidance helped me throughout of research and writing of this thesis.

Next, I wish to extend my appreciation to Assist. Prof. Ahmet Anil Dindar for his guidance and sharing his own experience in the development of the study. Without his assistance, this research would not have been possible.

Additionally, I would like to thank Assoc. Prof. Ercan Yüksel due to his guidance and effort especially during experimental part of this study.

Moreover, I would like to thank Istanbul Technical University Structural and Earthquake Engineering laboratory staff for their fruitful cooperation. I also would like to thank PhD students Ahmet Güllü and Burak Horoz for their invaluable support.

Finally, I must express my very profound gratitude to my parents for providing me with unfailing support and continuous encouragement throughout my years of education from the very first day and through the process of researching and writing this thesis. This accomplishment would not have been possible without them.

ABSTRACT

EXPERIMENTAL INVESTIGATION OF ENERGY-BASED SEISMIC RESPONSE ANALYSIS FOR SDOF STEEL COLUMNS

Earthquake Engineering is a field of engineering which deals with seismic forces and their effects on structures. Earthquake engineers are responsible for estimating the earthquake risk surrounding structure's region and their appropriate design to make sure that the structure can resist severe consequences of probable future earthquakes. The main purpose of the current study, aims to verify formulation of Energy-Based seismic analysis of the structures by conducting experimental tests and includes four main steps. Firstly, an algorithm which performs Energy-Based seismic analytical analysis for any Single Degree of Freedom (SDOF) affected by a given earthquake. The algorithm also has the capability of generating input and plastic energy response spectra. Secondly, seismic experimental tests on shake table were performed using SDOF steel box-sectioned columns under dynamic loadings with two earthquake records which have similar Acceleration Response Spectrum (ARS) while their input energy spectra have obvious differences. The third step includes different energy components that were calculated using the data obtained from sensors during tests, including acceleration and displacement responses along with strain data. Finally, the obtained experimental energy components values have been compared with those calculated by the analytic analyses algorithm mainly considering the input energy response spectra. Additionally, to verify the results, modal analyses have been conducted in SAP2000 for all test specimens. Totally twelve tests with elastic behavior were conducted. Six specimens were subjected to the two earthquake records with two different scale factors. Analytical and experimental results were compared and found out that they were very close. Thus, experimental verified analytical derivations of Energy-Based methodology.

ÖZET

TEK SERBESTLİK DERECELİ ÇELİK KOLONLAR İÇİN ENERJİ BAZLI SİSMİK DAVRANIŞ ANALİZİNİN DENEYSEL İNCELEMESİ

Deprem mühendisliği yer hareketleri ve onların yapılar üzerindeki etkilerini inceleyen bir mühendislik dalıdır. Deprem mühendisleri ise yapı bölgesindeki deprem riskini tahmin etmekle, ve bu yapıların gelecekte meydana gelebilecek şiddetli bir olası deprem halinde dayanıklılık gösterebileceğini ispat eden tasarımlarını yapmakla yükümlüdürler. Deneysel çalışma ile yapıların enerji bazlı deprem analizlerini formüle etmeyi amaçlayan bu çalışma, dört adımdan oluşmaktadır. Ilk adımda, verilmiş bir deprem etkisi altında herhangi bir tek serbestlik dereceli (TSD) sistemin enerji-bazlı deprem analizlerini gerçekleştiren bir algoritma ele alınmıştır. Bu algoritma aynı zamanda veri girişi sağlama ve plastik enerji tepki spektrumu oluşturma yeteneğine de sahiptir. Ikinci olarak,TSD çelik kutu-kesitli kolonlar, birbirine benzer ivme tepkisi spektrumuna sahip (ASR) ancak belirgin farklılıkları olan girdi enerji spektrumlu iki adet depremin dinamik yüklemesi altında sarsma masası testlerine tabi tutulmuştur. Üçüncü adımda, testler süresince sensörlerden elde edilen birim şekil değiştirme verilerine ek olarak ivme ve deplasman tepkilerini de içeren veriler aracılığıyla farklı enerji bileşenleri hesaplanmıştır. Son olarak, deneysel olarak elde edilen enerji bileşen değerleri, analitik analiz algoritması ile elde edilen bileşenler ile temelde girdi enerji tepki spektrumunu dikkate alarak birbiriyle kıyaslanmıştır. Buna ek olarak, güvenli tarafta bulunmak maksadıyla, tüm analizler için SAP2000 aracılığıyla modal analizler gerçekleştirilmiştir. Toplamda, iki adet farklı katsayı ile tanımlanan bahsedilmiş deprem yükleri altında altı adet numune için on iki adet elastik test gerçekleştirilmiştir. Deneysel sonuçlar ile analitik sonuçlar arasında önemli bir tutarlık gözlemlenmiştir.

TABLE OF CONTENTS

LIST OF FIGURES

LIST OF TABLES

LIST OF SYMBOLS

c	Damping coefficient
E_a	Absorbed energy
E_d	Damping energy
E_I	Input energy
E_k	Kinetic energy
E_p	Plastic energy
E_s	Strain energy
F	Force
f_s	Restoring force
J	Joule
k	Stiffness
m	Mass
M	Moment
R	Force Reduction Factor
T_D	Natural Period of Damped Vibration
T_n	Natural period
σ_y	Yielding stress
ξ	Damping ratio

LIST OF ABBREVIATIONS

2D	Two Dimensional
ADS	Acceleration Design Spectrum
ARS	Acceleration Response Spectrum
ASCE	American Society of Civil Engineering
ASD	Allowable Stress Design
EBD	Energy-Based Design
EOM	Equation of Motion
EPP	Elastic Perfectly Plastic
FAS	Fourier Amplitude Spectrum
ITU	Istanbul Technical University
LVDT	Linear Variable Differential Transducer
MDOF	Multi Degrees of Freedom
PGA	Peak Ground Acceleration
RC	Reinforced Concrete
SDOF	Single Degree of Freedom

1. INTRODUCTION

1.1. General

Earthquake is a natural phenomenon which cannot be predicted with current human knowledge. Therefore, development of some rational procedures to evaluate the existing buildings and design of new structures is absolutely necessary.

Current commonly used design methods in seismic design codes, such as Allowable Stress Design method (ASD) and Performance-Based Design methods (PBD) neglect the actual behavior of the structure. Earthquake loads are reversible rather than being monotonic and structural elements are exposed to the hysteretic ground acceleration-induced loading during strong earthquake event. Thus, the amount of energy, especially which the elements are supposed to dissipate, has to be included in the analysis process.

This study aims to utilize energy concepts in the seismic analysis of structures in terms of calculating energy components and carry out experiments on Single Degree of Freedom systems (SDOF) with steel columns having hollow cross section in order to verify the theoretical derivations. In the experimental study, shake table was used with two seismic records which have similar Acceleration Response Spectra (ARS) yielding different Energy Spectra. In order to prove that the ARS analysis methodology including performance criteria could underestimate the level of damage on the structure.

1.2. Current Design Methods

In order to have proper understanding of how the Energy-Based design approach is advantageous compared to current methods, which are mostly used in order to design structures under seismic loadings, it is helpful to consider a review of their main concepts and procedures.

1.2.1. Force-Based Method

Despite those facts that the Force-Based method is utilized in numerous design codes and it has been amended during decades to include dynamic terms such as soil-structure interaction, however, it does not include the performance of building structures. In addition, the absolute maximum response values of the structures are considered to determine the extreme action of forces. Although this method is very straight forward and easy to apply in earthquake-resistant analysis and design, it does not truly represent the dynamic problems. This method is primarily based on elastic Acceleration Design Spectrum (ADS) which depends on constant critical damping ratio of the structure, the seismicity of the area in which the structure will be constructed and the type of soil the structure will be built on. The ADS charts are drawn for a range of natural period (T_n) for SDOF systems. Calculating reasonably the period of a structure, it is feasible to find out the elastic seismic demand force based on acceleration (Rahman *et al.* 2011).

The general process of designing a structure using Forced-Based design method could be stated as follows (Farahmand, 2006):

(i) Estimation of the dimension of the structural members and subsequently the elastic rigidity of the system.

(ii) Estimation of natural period of the system using empirical or analytic formulations.

(iii) Determination of maximum elastic acceleration response of the structure utilizing Acceleration Design Spectrum which is mostly a function of soil classification and seismicity of the area.

(iv) Applying the acceleration obtained from third step to the system and calculation of elastic forces.

(v) Reduction of the obtained elastic forces using Force Reduction Factor.

(vi) Controlling the absolute and relative displacements with allowed values.

This method has some disadvantages which lead to introduction of more modern procedures such as Displacement-Based design method. Since the period of the structure is unknown, the designer needs to estimate the period using the empirical formulations from seismic codes. In this way, estimated periods are generally less than the real values (Farhamand, 2006). Also, applying Force Reduction Factor causes the design results not to be properly reliable. Additionally, displacements have few importance and their values are only controlled at the end of the design process. However, in some other methods displacements play significant role in instability of the structures and determination of failure of structural members is more practical and easier by taking displacements into account. Moreover, this approach neglects the cumulative damage effect of seismic loading as the method considers only the maximum response which is a significant deficiency of the method (Chopra, 1995).

The most unreasonable feature of using the elastic design spectrum while analyzing those structures which displace beyond their elastic ranges is the estimation of Force Reduction Factor which is related to ductility and period of the structures (Dindar, 2009). There have been many researches aimed to find a relationship between Force Reduction Factor (R), ductility factor and its natural Period of a system (Newmark and Hall, 1982; Vidic *et al.* 1994; Dimova *et al.* 2004). It is generally proposed that (R) is a function of the other two characteristics of the system.

1.2.2. Displacement-Based Method

The performance of a structure is defined in accordance with capability of its members to deform while effected by earthquake loads. Thus, the member deformation and consequently the displacement of the structural system needs to be considered in the design method. The idea of Displacement-Based Design was introduced almost 40 years ago. Gülkan and Sözen (1974) conducted a set of experimental research on the behavior of one-story, one-bay reinforced concrete frames by subjecting them to dynamic base motion, simulated earthquake motion and lateral static loadings in order to investigate the effect of displacement on stiffness reduction and incremental energy dissipation. They proposed an equivalent elastic model assuming a linear behavior and a viscous damping equivalent to the nonlinear response. The method was developed by Kowalsky *et al.* (1994) for SDOF Reinforced Concrete (RC) systems and Calvi and Priestly (1997) for both Single Degree of Freedom and Multi Degrees of Freedom system (MDOF) buildings starting from a target maximum displacement. They offered such an approach beginning with a preliminary design and continues with push-over analysis which results the yield and ultimate displacement of a system and an elastic acceleration spectrum is formed along with the capacity curve derivation. In almost all design procedures which are proposed based upon displacement - based design approach seismic demand is specified as either a displacement spectrum or an acceleration displacement response spectrum (Xue and Moehle, 2001).

Displacement-Based approach is more suitable for seismic design in comparison with Forced-Based approach since it included the nonlinear behavior of the systems while Force-Based design method considers only elastic forces as the main factor of design process. Moreover, designer of the structure has the option of selecting the performance level of the system which is more rational than using a tabulated force reduction factor obtained from the design codes.

Although PBD method considers hysteretic behavior of structural elements for the last ten years this method has the shortcoming of ignoring the actual behavior of the system under reversible cycling seismic loads. Because the major reason of the accumulated damage occurred in the structural members are the duration and the frequency content of the earthquake and the same damage occurrence is not obtained from capacity curve that is plotted for the top displacement versus base shear which is in fact nonlinearly increase of lateral force in one direction.

1.3. Introduction to Energy-Based Method

Energy-Based Design could be assumed as a seismic design methodology which does not include the shortcomings of the currently used design approaches. The design of earthquake-resistant structures is not only a function of the peak response demand but also a function of the time history response demand. The cumulative inelastic response such as plastic energy is a significant parameter to reflect time history response. It is a good indicator of how hysteresis nonlinear behavior of a structure is during ground motions. Energy-Based Design method proves to be appropriate under this circumstance.

Moreover, as it is widely known, the structures should endure the seismic forces by their strength capacity and also should remain under a certain deformation (or displacement) limit that classified as the performance level (Krawinkler and Nassar, 1992; Priestly *et al.* 1996). However, having enough energy dissipation capacity in terms of plastic deformation and viscous damping for the structures is necessary. The approaches discussed in the previous section, either completely neglect or do not appropriately take the energy dissipation capacity into account.

It is possible that two similar structures which holds the same yield and displacement capacities may not have equal energy dissipation capacity due to constitutive behavior. Despite having identical yield and ultimate deformation, the surrounded area of hysteresis (loading and unloading force-displacement) curves, which are known as plastic energy dissipation value of a member (Chopra, 1995) could be clearly different. That is to say, both structures absorb the same amount of energy, while Structure 1 dissipates more energy than Structure 2. The explained concept is shown in Figure 1.1.

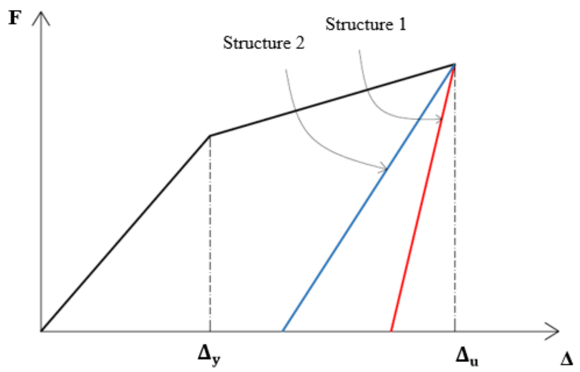

Figure 1.1. Two Identical Structures with Different Energy Dissipation Capacity.

An adequate earthquake-resistant design of the system is performing such a design which properly represents the destructive potential expected in a given site. Methods based upon determination of input energy and other energy parameters has been considered being effective to determination of earthquake-resistant design owing to the fact that they provide an approach to appropriately characterize different kinds of time histories which correspond to earthquake (Deanini and Mollaioli, 2001).

It is widely known that the damage occurred in a member is directly related to the plastic energy dissipated in the member (Park and Ang, 1985). Thus, a method which considers force, deformation capacity along with energy dissipation capacity of structural members in its formulations covers all the required aspects of the seismic analysis and consequently the earthquake resistant design of new buildings.

Since it is difficult to visualize the physical concept of the energy, it could be inconceivable to use it as a structural design parameter. In addition, it could not be easy to estimate either deformation or resisting rate of the structural members. As a solution to the problem in the members needs to be thoroughly investigated (Dindar, 2009).

1.4. Literature Review

Energy-Based approach considers the cumulative damage occurrence due to hysteresis behavior of components of a structure. This advantage has attracted researchers' attention to conduct various investigations in this area for the last three decades.

The earliest researchers mainly discussed the fundamental concept of Energy-Based seismic analysis and paved the way for further investigators to propose a variety of analysis and design procedures based on energy principles. Zaharah *et al.* (1984) made an investigation on the amount of energy imparted into the structure, the amount of energy dissipated by inelastic deformation and damping as well as defining a possible effective motion criterion based on the amount of energy imparted into a structure. Akiyama (1985) publish a book in which he derived and utilized energy formulation in order to analyze and design of MDOF structures. Uang and Bertero (1988) conducted an extended research to implicate the earthquake records on seismic design of buildings and focused on the significance of input energy, hysteresis energy and number of yielding reversals in the formulation of design criteria as a part of their study. They drew the conclusion that using relative energy formulation is more effective than absolute energy formulation for Energy-Based seismic analysis. Kuwamura *et al.* (1989) discussed that when the structural collapse energy absorption capacity is greater than the input earthquake energy, the structure can survive.

Numerous researches performed analytical investigations in Energy-Based earthquake analysis and proposed different numeric procedure of analysis and design considering energy principles. Fajfar and Vidic (1994) developed a procedure for the determination of inelastic design spectra (for strength, displacement, hysteresis and input energy) for systems with a prescribed ductility factor. Akbas. (1997) conducted an analytical study regarding energy demand prediction on steel moment resisting frames. He discussed the distribution of absorbed energy through the height of the building in beam and column connections at the same floor level beginning from the top floor and in accordance with strong-column weak-beam principle. He finally proposed energy dissipation capacity tables for steel members in his procedure. Decanini *et al.* (1998) introduced a procedure for the determination of elastic design earthquake input energy spectra considering the effect of earthquake magnitude, soil type and the distance between surface projection and the fault. Same researchers proposed a method for assessment of seismic energy demands starting with developing inelastic design input energy spectra for systems with a prescribed displacement ductility ratio. Because earthquake records are random in nature, the proposed indices needed to be based on simplifying assumption. Manfredi (2001) proposed such a method to obtain a simplified representation of the equivalent number of loops correlated to the earthquake properties by the proposed seismic index. However, given the fact that seismic demand is strongly influenced by structural response and seismic record, an energy demand spectrum has to be derived by taking into account the diverse characteristics of a structure and seismic records (Chai, 2004). Wong and Yang (2002) proposed a computational based on force analogy method in order to characterize the energy in nonlinear structures and the transfer among different energy forms during an earthquake for a SDOF system and extended it to investigate the transfer of energy among various forms in a MDOF system. However, since this approach appeared not to be appropriate for the analysis of real structures, Wong and Wang (2003) modified derivation of the previous force analogy formulation using static condensation. Akbas (2006) proposed a neural network to model the nonlinear relationship between the structural and earthquake parameters and the hysteresis energy demand in steel moment resisting frames. Leelataviwat *et al.* (2009) investigated on seismic demand and the structural response utilizing energy vs displacement (capacity) curve derived from displacement response spectra. In his procedure, energy demand is estimated, whereas the energy components has to be analyzed. In spite of simplicity, their formulation properly meets the shortcomings of elastic spectra calculation. On the contrary, the proposed energy-displacement curve is based upon push-over analysis and does not consider cumulative damage in the structural components during cycling loads. Dindar (2009) carried out a study into both Energy-Based seismic analysis of structures and determination of the energy dissipation capacity of reinforced concrete columns. Haddad Shargh and Hosseini (2010) undertook an analytical research into the existence of an optimal distribution of stiffness over the height of mid-to-high rise buildings in order to minimize the seismic input energy. Jiao *et al.* (2011) investigated the effect of earthquake characteristics like intensity, frequency content, duration and the structural properties such as ductility, damping and cyclic behavior on the distribution of input energy for a five story building using both short and long duration seismic records. Erbrik *et al.* (2015) conducted a research into inelastic displacements of reinforced concrete systems using an Energy-Based approach. They introduced such a hysteresis model which includes stiffness, strength degradation and pinching. Özakgül (2015) developed a numerical approach based upon inelastic dynamic analysis taking into account material, geometric and connection nonlinearity in order to investigate the seismic response of inelastic steel structures under earthquake-type loadings.

Experimental investigations have been performed in the area of seismic Energy-Based analysis for different purposes. By showing correlation between results from analytic prediction of absolute input energy of a SDOF model with those obtained from experimental measurement of input energy for a six-story steel building with geometric scaling of 0.3. Uang and Bertero (1986) concluded that pseudo velocity, defined in their study, is an appropriate factor to estimate input energy. Kunnath *et al.* (1997) conducted an empirical fatigue research in order to investigate the relation between the load path and the plastic damage occurred in reinforced concrete (RC) structural members. They concluded that energy dissipation is absolutely dependent on loading history and the confinement is highly influenced by the energy dissipation of the member. Erbik and Sütçüoglu (2004) experimentally tested RC beam members in terms of fatigue and their findings were very close to those of .Kunnath *et al.* (1997). Poljansek *et al.* (2009) tested RC columns in order to conduct a research on the relation between hysteretic energy dissipation and drift ratio of the specimens. The outcomes of their study showed that the simplest damage index of drift should be assumed a reliable performance limit for RC structural members. Due to wide application of strong-column weak-beam design tendency among structural engineers, Jiao *et al.* (2011) performed an experimental investigation into the effects of various loading histories on the deformation capacity and energy dissipation capacity of the steel beams. Acun and Sütçüoglu (2012a) performed a research on energy dissipating capacity of reinforced concrete columns under inelastic displacements using experimental test. They introduced an analytic approach to evaluate the energy dissipation under variable-amplitude displacement cycles using the energy dissipation capacity under constant-amplitude displacements. They (2012b) also developed an Energy-Based hysteresis model for the moment-rotation response of RC columns in flexure using experimental specimens.

Various procedures have been developed in order to estimate the performance of structures under seismic loadings considering both Energy-Based concept and pushover analysis during recent years. Chou *et al.* (2003) proposed a procedure to determine absorbed energy in a multistory frame from energy spectra with help of pushover analysis. Montes *et al.* (2004) studied on an Energy-Based formulation for first and multiple mode pushover analysis. Prasanth *et al.* (2008) conducted a research into a method in which an equivalent SDOF system is used instead of a MDOF in order both to estimate hysteretic energy demand through a pushover analysis and to introduce a suitable procedure for design guidelines. Hesegawa *et al.* (2008) proposed a seismic response estimation method in order to predict maximum inter-story drift and damage in each member for steel moment resisting frames using inelastic strain energy achieved from pushover analysis. Climent and Zahran. (2010) proposed a methodology considering estimation of the total input energy amount and hysteresis energy which a structure can dissipate until collapse under seismic loads using static pushover analyses in order to assess the seismic capacity of existing buildings. Manoukas *et al.* (2011) proposed an Energy-Based pushover method to estimate structural performance under heavy earthquakes. The main idea of their method was the determination of equivalent SDOF system by calculating the external work done by lateral force acting on the MDOF system under consideration to the strain energy of the equivalent SDOF system. Lin *et al.* (2014) used a method named modified modal cyclic pushover which reflects the dual criterion of deformation and energy to provide an assessment on seismic performance of the steel reinforced concrete piers and concrete bridge piers. They concluded that seismic capacity of steel reinforced concrete bridge piers is better than reinforced concrete bridge piers. Uçar *et al.* (2015) investigated on calculation of energy dissipation of reinforced concrete frames, which are designed according to Turkish Earthquake Code (2007), based on inelastic behavior using pushover analysis.

Some investigators conducted various studies into the efficiency and design of dampers taking the advantage of Energy-Based principles. Shen *et al.* (1996) addressed the importance of energy concept in the design of energy dissipating devices for structural applications, and proposed a design procedure in accordance with damage control concept. Sütçü (2006) investigated on an Energy-Based damper design method assuming a uniform displacement distribution in order to determine the necessary viscous damping coefficient. He made the conclusion that by using the obtained viscous damping coefficient from the proposed method, seismic displacement response of the multi-story structure is effectively reduced under the target inter-story value. Takewaki (2007) developed a method to estimate the earthquake input energy to two building structures connected by viscous dampers. He discussed that the input energy imparted into structures and added viscous connecting dampers could be defined as works done by the boundary forces between the subsystems on their corresponding displacements. Climent (2011) introduced a method for seismic retrofitting of existing buildings by adding hysteresis energy dissipating devices. The methodology was based upon energy balance equation of the structure and it is applied to determine the lateral strength, energy dissipating devices required in each story to reach prescribed target performance levels for a given earthquake hazard.

Recently, different researchers tried to develop a variety of seismic design procedures considering Energy-Based approach Climent *et al.* (2002, 2010) proposed input energy spectra to seismic design of structures located in both low-to-moderate and moderate-to-high seismic region. They also suggested an equation to estimate the energy contributable to damage from the total input energy for both regions. Leelataviwat *et al.* (2002) investigated the use of energy in order to derive seismic design forces for multi-story moment frames. They extended and modified the general energy balance concept, which is used to derive design response spectra, to include the plastic yield mechanism and the distribution of seismic forces along the height of investigated frames. Since seismic response spectra neglect the reduction in stiffness and energy dissipating capacity, Malhotra (2002) carried out an investigation to propose a cyclic demand spectrum based on energy principles. Ghosh *et al.* (2006) investigated the potential in the development of a probabilistic design methodology considering hysteresis energy demand within the framework of Performance-Based design seismic design of buildings. Gilmore and Jirsa. (2005) proposed a formulation to estimate cumulative plastic deformation demands for using in seismic design. Kalkan and Kunnath (2007) investigated the effective cyclic energy (sum of damping and hysteretic energies) for proposing a spectrum in order to estimate target energy demands. Hosseini *et al.* (2008) performed a research on variation of input energy with the variation of dynamical characteristics of building considering both linear and nonlinear behavior, and how this variation could be utilized in reliable seismic design of structures. Bojorquez *et al.* (2008) proposed a procedure for the preliminary design of structures. They explicitly considered the maximum and cumulative plastic deformation demands in the earthquake-resisting structures. Dindar (2009) proposed a design methodology to determine amount of the longitudinal reinforcement of reinforced concrete members considering energy balance equation. He also proposed an algorithm in order to derive input and dissipated (plastic) energy spectra based on earthquake intensity, ductility requirement and soil types. Ye *et al.* (2009) conducted a valuable study in order to propose a seismic design framework considering the Energy-Based approach and performance-based methods. They draw the conclusions that peak ground responses are not suitable to be considered as earthquake intensity index to represent the structural seismic capacity. Terapathana (2012) investigated into plastic design of reinforced concrete moment resisting frames based on inelastic energy demand. Almansa *et al.* (2013) explained a methodology in order to generate design energy spectra based on equivalent velocity using numerous strong ground motions obtained from various sites in Turkey. Khampanit *et al.* (2014) proposed an Energy-Based seismic design procedure in order to strengthen non-ductile reinforced concrete frames utilizing buckling-restrained braces. Keke and Chen. (2014) undertook a study to develop a practical design and assessment approach of steel frames considering damage control behavior in order to increase the structural resilience. They proposed a procedure for designing and assessing the structural system based upon energy demand and energy capacity. D'ambrisi and Mezzi. (2015) proposed an Energy-Based methodology for inelastic static analysis of structures in which both the demand and capacity is defined based upon energy parameters. They calculated demand in from maximum displacement response and the maximum force. The capacity in their method, is computed from an energy capacity curve that at each step the work of lateral forces is equal to the structure internal work.

Despite all the valuable conducted researches regarding development of the Energy-Based approach in seismic analysis and design, it is still opened for investigation from its various aspects. Also, the approach has not become suitable in order to be included in design codes. However, the time this method is sufficiently extended, it will most probably be a part of seismic design codes.

1.5. Objective and Scope of the Study

Having considered the above the literature review, it could be stated that various studies regarding diverse aspects of Energy-Based seismic analysis and design have been performed. Most investigated aspects could be generally categorized as fundamental concept of Energy-Based approach, introducing analytical analyses procedures, proposal for design methodologies and experimental research on RC members. However, experimental work on SDOF steel members using a shaking table experimental setup emphasizing on finding the energy components, spectra, and comparison of energy and damage levels for a number of input earthquake records that have similar acceleration response spectra. Along with a verification of analytical work on energy components, especially relative energy values is missing in the literature.

Thus, the objective of this study is shake table experimental evaluation of energy formulations on SDOF steel column members with scaled input earthquake acceleration records.

The scope of the research is limited to two dimensional (2D) hollow cross section SDOF steel cantilever columns. Various amounts of mass were installed on top of the columns in order to perform the tests for different period ranges. The earthquake loadings were applied in only one direction.

This study could be helpful for different related researches in future. First, as a continuation of this research, a set of nonlinear tests could be performed and the results could be compared with the proposed algorithm in this study. Second, it could be helpful to follow the same objective for MDOF systems. Third, the developed algorithm could be used in order to perform analytical dimensional analyses and the experimental results can be considered as a reference for future dimensional analysis. Last but not least, the study could be an opening to further more experimental investigations on Energy-Based seismic analysis and design.

1.6. Organization of the Thesis

This thesis consists of five chapters. The first Chapter provides an introduction and literature review, as well as objective and scope of the study.

Chapter 2 discusses the analytic part of the study including an introduction to Equation of Energy (Energy Balance Equation) and the components of the equation, development of the algorithm to calculate energy components and to generate the input and plastic response energy spectra.

Chapter 3 discusses the experimental part of the study including test setup, properties of SDOF systems along with experimental results.

Chapter 4 provides analyses of the results and comparison between the experimental and analytical results.

Chapter 5 presents conclusions and recommendations for relevant investigations in future.

2. ENERGY-BASED APPROACH AND ANALYTIC ANALYSIS OF THE RESEARCH

This Chapter discusses the energy responses of SDOF systems subjected to seismic ground motions loads. The Chapter also describes the derivation and definition of energy terms based upon SDOF systems. Also, an algorithm to compute the values of time-history energy components as well as generating input and plastic energy response spectra is presented within the Chapter.

2.1. Energy Balance Equation

The major concern for the structural engineers is formulating the influence of the earthquake on a structure, Figure 2.1.

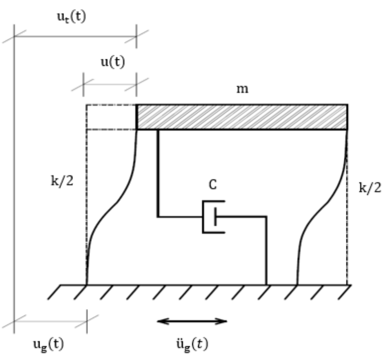

Figure 2.1. SDOF under Effect of Earthquake with Absolute Displacement.

The time-based force effects on a SDOF system could be stated in two ways; first, displacement of system from the resting point of the ground (absolute motion terms) and second, from the resting point of the system (relative motion terms). The difference of these two ways is observed only in the terms in which mass of the structure is included. The general Equation of the Motion (EOM) of the system is as follows (Chopra, 1995):

$$m\ddot{u}_t(t) + c\dot{u}(t) + f_s(u(t), \dot{u}(t)) = 0 \tag{2.1}$$

where m, c and fs are the mass, damping coefficient and restoring force of the system respectively. The terms $\ddot{u}_t(t), \dot{u}(t)$ and $u(t)$ are the dynamic time history responses of total acceleration, relative velocity and relative displacement of the system, respectively. Since the term $\ddot{u}_t(t)$ includes both the acceleration of the system $\ddot{u}(t)$ and that of the ground $(\ddot{u}_g(t))$, the Equation 2.1 could be written in a different way:

$$\ddot{u}_t\left(t\right) = \ddot{\mathrm{u}}\left(t\right) + \ddot{u}_g\left(t\right) \tag{2.2}$$

Therefore, the EOM becomes

$$m\ddot{u}\left(t\right) + c\dot{u}\left(t\right) + f_s\left(u\left(t\right), \dot{u}\left(t\right)\right) = -m\ddot{u}_g\left(t\right) \tag{2.3}$$

Studying EOM considering relative values may yield a better Studying EOM considering relative values may yield a better understanding to the physical concept of the components. The first term represents inertia force of the mass, the second term is the damping force due to inherent damping of structural members and the third term is the restoring spring force which tries to keep the system in its initial position. The component on the right side of the EOM is the excitation external force introduced to the system due to strong ground motion (Dindar, 2009).

If the structural system remains in the elastic region due to responses produced by given strong ground motion, the third part of the Equation 2.3 could be simplified as ku(t), where k is the stiffness (rigidity) of the SDOF system (Chopra, 1995). Therefore, EOM, in this case only, could further be simplified as then following:

$$m\ddot{u}\left(t\right) + c\dot{u}\left(t\right) + ku\left(t\right) = -m\ddot{u}_g\left(t\right) \tag{2.4}$$

The EOM is actually a mathematical formula which describes displacement, velocity and acceleration of a system due to dynamic force or a representative acceleration records of an actual or artificial earthquake, and it is driven by earthquake motion's properties (Clough and Penzien, 1995).

2.1.1. Derivation of Absolute and Relative Equations of Energy

Uang and Bertero (1988) derived two definitions of energy method; absolute energy and relative energy. The formulations of the two approaches results in similar formulations for all the energy parameters except form the input and kinetic energies.

Taking integration of Equation 2.1 while multiplying each term by displacement and referring to Figure 2.1, based on relative displacement $u(t)$, shown in Figure 2.1) the following energy equation could be obtained:

$$\int m\ddot{u}\,(t)\,du + \int c\dot{u}\,(t)\,du + \int f_s du = 0 \tag{2.5}$$

Since $u_t\,(t) = u_g\,(t) + \mathrm{u}\,(t)$, Equation 2.5 could be rewritten as below:

$$\int m\ddot{u}_t\,(t)\,du_t + \int c\dot{u}\,(t)\,du + \int f_s du = \int m\ddot{u}_t du_g \tag{2.6}$$

The Equation 2.16 is known as Absolute Energy Equation and its terms are known as, from left to right, Absolute Kinetic Energy, Damping Energy, Absorbed Energy and Absolut Input Energy, respectively. Thus, in terms of energy components Equation 2.16 could be represented as shown below:

$$E_K + E_d + E_a = E_I \tag{2.7}$$

The third component, E_a, of the above equation includes both the Elastic Strain Energy and Plastic (Inelastic Strain) Energy, which is the energy which is dissipated due to plastic deformation of the structural member.

$$E_a = E_s + E_p \tag{2.8}$$

However, integrating Equation 2.3, which is mathematical statement of Figure 2.2, with respect to relative displacement ($u(t)$, shown in Figure 2.2) the derived energy formulation would be as Equation 2.9 that is known as Relative Energy Equation

(Terapathana, 2012).

$$\int mu\left(t\right)du + \int c\dot{u}\left(t\right)du + \int f_s du = -\int m\ddot{u}_g\left(t\right)du \tag{2.9}$$

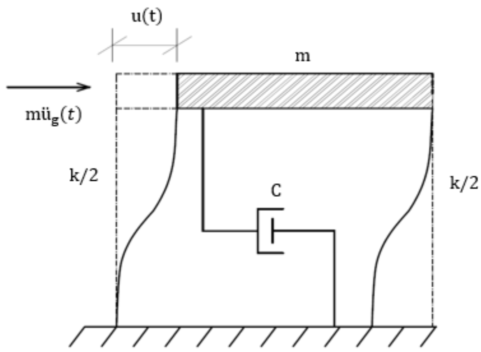

Figure 2.2. Fixed-Based SDOF System with Relative Displacement.

In a similar way to absolute energy terms, the terms in Equation 2.9 are known as Relative Kinetic, Damping Energy, Absorbed Energy and Relative Input Energy, respectively. Therefore, Relative Energy Equation can be restated as below;

$$E'_k + E_d + (E_s + E_p) = E'_I \tag{2.10}$$

The relative energy equation is the physical work done by equivalent lateral force, $\int m\ddot{u}_g\left(t\right)du$, on a system as shown in Figure 2.2, whereas the same physical concept in the absolute energy equation depends on the work done by total base shear,$\int m\ddot{u}_t\left(t\right)du_g$, (Bertero and Uang, 1992; Terapathana, 2012).

Once again, the third term of left hand side of the Equation 2.9 is the summation of elastic strain and plastic energies.

Since the concentration of this thesis is on experimental investigation on relative energy computation, the related kinetic and relative input energies will be shown as E_k and E_I rather than E'_k and E'_I. The appearance of E'_k and E'_I was only to distinguish the difference between Equation 2.7 and Equation 2.9.

2.2. Concept and Formulation of Energy Components

Each term in equation of energy represents a specific physical characteristics of the structure. If the relations between the derivatives of relative displacement in equation 2.9 are used in order to redefine of integration terms each energy form becomes more intelligible during ground motions.

A brief explanation of physical concept along with redefinition of the formulation of each energy component is stated separately as follow;

2.2.1. Input Energy

As it is mentioned earlier, the physical concept of relative input energy is the work done by equivalent lateral force, $\int m\ddot{u}_g\,(t)\,du$,, on a system. The related formulation could be derived from the right hand side in Equation 2.9.

As it is mentioned earlier, the physical concept of relative energy equation is the work done by equivalent lateral force, $\int m\ddot{u}_g\,(t)\,du$, on a system. The related formulation could be derived from the right hand side in Equation 2.9.

$$E_I = -\int m\ddot{u}_g\,(t)\,du = -\int m\ddot{u}_g\,(t)\,du \times \frac{dt}{dt} = -m\int \ddot{u}_g\,(t)\,\dot{u}dt \tag{2.11}$$

2.2.2. Kinetic Energy

Kinetic energy is in fact the energy of motion. In other words, it is the energy that an object possesses due to its motion. This kind of energy is physically defined as the work required in order to accelerate an object from its resting position to its velocity. The formulation of kinetic energy could be derived from the first term of left hand side in Equation 2.9.

$$E_K = \int m\ddot{u}du = \int m\ddot{u}\frac{dt}{dt}du = \int m\ddot{u}\dot{u}dt = \int m\dot{u}\frac{d\dot{u}}{dt}dt = m\int \dot{u}d\dot{u} = \frac{m\dot{u}^2}{2} \tag{2.12}$$

2.2.3. Damping Energy

Damping could be generally defined as restriction or prevention against velocity. In other words, damping is the energy dissipating property of a system against its oscillations. Damping energy has the characteristic of being cumulative. Its formulation could be resulted from the second term of Equation 2.9.

$$E_d = \int c\dot{u}du\frac{dt}{dt} = c\int \dot{u}^2dt \tag{2.13}$$

2.2.4. Absorbed Energy

As it is noticed from Equation 2.8, absorbed energy in the equation of energy includes elastic strain energy (called as strain energy in this study) and inelastic strain energy (called as plastic energy in this study). The formulation is derived from the third term of Equation 2.9.

$$E_a = \int f_s(t)\,du = \int f_s(t)\,du \times \frac{dt}{dt} = \int f_s(t)\,\dot{u}dt \tag{2.14}$$

Strain energy (also known as potential energy) is the energy stored in a system upon elastic deformation. The physical concept of strain energy could be stated as the total work done on the system in linear deformations. Uang and Bertero (1990) stated the formulation of strain energy due to the elastic stiffness (k) of the system as Equation 2.15.

$$E_s = \frac{(f_s(t))^2}{2k} \tag{2.15}$$

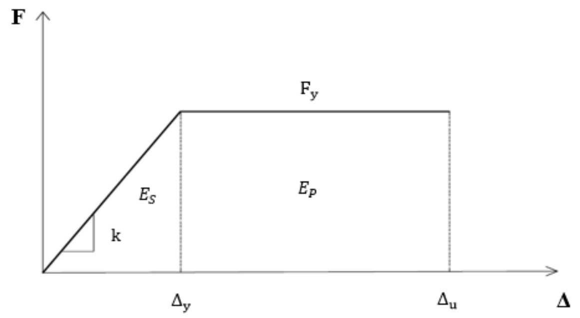

Figure 2.3. Elastic and Plastic Strain Energies.

If the system remains in the elastic region, while subjected to earthquake-type or any other kinds of loading, amount of strain energy will be equal to the area of linear part of force - displacement relationship as shown in Figure 2.3.

$$E_s = \frac{1}{2}F\Delta = \frac{1}{2}k\Delta^2 \tag{2.16}$$

Plastic energy is actually the amount of dissipated energy upon inelastic deformations of the system. Therefore, while the structural system stays in elastic region while subjected to seismic loadings, the amount of plastic energy is considered as zero. Formulation of plastic energy is not as straightforward as the other energy components since it is needed to be calculated in nonlinear range of the system (shown in Figure 2.3 as the area under the inelastic section of the graph). The common method to compute the value of plastic energy is subtracting the summation of kinetic, damping and strain energy from the amount of input energy (Equation 2.16). Similar to damping energy, plastic energy is also considered as being cumulative. Thus, plastic energy term becomes as the following:

$$E_p = E_I - (E_k + E_d + E_s) \tag{2.17}$$

The traditional method to compute the plastic energy is to calculate the area enveloped by hysteresis graph (Mahin and Bertero 1981). The advantage of this method has been taken in this study as well.

The derived energy formulations in Equation 2.11-Equation 2.13 and Equation 2.15 are used in the proposed algorithm to compute the energy components. The algorithm will be discussed in the next section in detail.

It is supposed that the input energy which is the system received due to the earthquake is divided by two main groups as recoverable and irrecoverable energy (Figure 2.4). The basic difference between two categories is the way they behave in terms of value. The kinetic and elastic strain energies obtain some numeric values throughout the strong motion duration and vanish gradually at the end of the duration. On the contrary, damping and plastic energy increase instantly during the earthquake and they do not diminish at the end of the seismic motion. This explanation will be observed in the graphs of the next section.

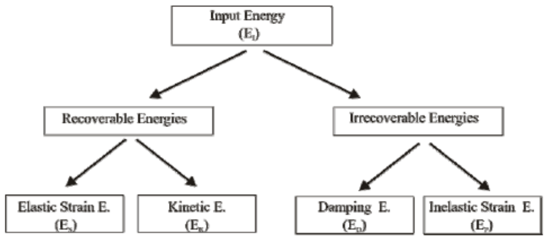

Figure 2.4. Energy Components (Dindar, 2009).

2.3. Energy Response Time-Histories and the Proposed Algorithm

As the derivation of energy formulations in the previous section implies, in order to obtain the responses from time histories for each energy component, the displacement (u) and velocity ($\dot{u}$) of the SDOF system need to be calculated throughout the duration of the strong ground motions in each time increment. Since it is impossible to analytically solve the EOM (Equation 2.3) due to arbitrary nature of the ground accelerations, which means it does not follow any specific function or series, it is necessary to utilize some numeric time-stepping methods. There are numerous numeric time-stepping methods to solve the differential equation of motion such as Taylor's Series, Finite Difference, Runga-Kutta, Central Difference and Newmark methods (Chopra, 1995). In all the methods the loading and the system response histories are divided into a sequence of time intervals named "steps" and the responses are computed for each step based on the initial conditions (displacement, velocity and acceleration) existing at the beginning of the step (Clough and Penzien, 1995). The method used in this study is Newmark which would be discussed in the following section.

2.3.1. Newmark Time Integration Methods

Newmark procedure is decided to be utilized in order to accomplish the linear and nonlinear dynamic time history analysis due to its versatility and wide usage in many researches. Newmark integration can be used in two different ways named as Constant Acceleration and Linear Acceleration methods. The derivation of both the methods would be discussed in this part of the study.

Figure 2.5 depicts the basic logic of Newmark constant acceleration procedure. This method assumes the variation of acceleration is constant and equal to average accelerations of two continuous steps. The parameter, $\ddot{u}(\tau)$ is indicateor of the variation of acceleration between two time steps

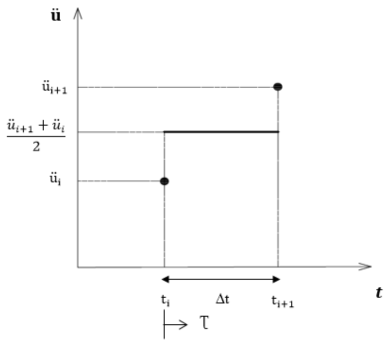

Figure 2.5. Constant Acceleration.

The equations derivation of the method is as follows;

$$\ddot{u}(\tau) = \frac{1}{2}(\ddot{u}(i) + \ddot{u}(i+1)) \tag{2.18}$$

Integrate Equation 2.18

$$\int_{t(i)}^{\tau} \ddot{u}(\tau)\,dt = \int_{t(i)}^{\tau} \left(\frac{1}{2}\left(\ddot{u}(i) + \ddot{u}(i+1)\right)\right) dt \tag{2.19}$$

Velocity Response

$$\dot{u}(\tau) = \dot{u}(i) + \frac{\tau}{2}\left(\ddot{u}(i) + \ddot{u}(i+1)\right) \tag{2.20}$$

Integrate Equation 2.20

$$\int_{t(i)}^{\tau} \dot{u}(\tau) = \int_{t(i)}^{\tau} \left(\dot{u}(i) + \frac{\tau}{2}\left(\ddot{u}(i) + \ddot{u}(i+1)\right)\right) dt \tag{2.21}$$

Displacement Response

$$u(\tau) = u(i) + \dot{u}(i)\,\tau + \frac{\tau^2}{4}\left(\ddot{u}(i) + \ddot{u}(i+1)\right) \tag{2.22}$$

If $\tau = \Delta t$ then from Equation 2.20:

$$\dot{u}(i+1) = \dot{u}(i) + \frac{\Delta t}{2}\left(\ddot{u}(i) + \ddot{u}(i+1)\right) \tag{2.23}$$

From Equation 2.21:

$$u(i+1) = u(i) + \dot{u}(i)\,\Delta t + \frac{\Delta t^2}{4}\left(\ddot{u}(i) + \ddot{u}(i+1)\right) \tag{2.24}$$

By definition we know

$$\Delta u(i) = u(i+1) - u(i) \tag{2.25}$$

$$\Delta \dot{u}(i) = \dot{u}(i+1) - \dot{u}(i) \tag{2.26}$$

$$\Delta\ddot{u}\left(i\right)=\ddot{u}\left(i+1\right)-\ddot{u}\left(i\right) \tag{2.27}$$

Now from (2.20)

$$\Delta\dot{u}\left(i\right)=\frac{\Delta t}{2}\left(\ddot{u}\left(i\right)+\ddot{u}\left(i+1\right)\right) \tag{2.28}$$

and from Equation 2.23:

$$\Delta u\left(i\right)=\dot{u}\Delta t+\frac{\Delta t^{2}}{4}\left(\ddot{u}\left(i\right)+\ddot{u}\left(i+1\right)\right) \tag{2.29}$$

Find $\Delta\ddot{u}(i)$ from Equation 2.29

$$\Delta u\left(i\right)-\dot{u}\left(i\right)\Delta t=\frac{\Delta t^{2}}{4}\left(\ddot{u}\left(i\right)+\ddot{u}\left(i+1\right)\right) \tag{2.30}$$

$$\ddot{u}\left(i\right)+\ddot{u}\left(i+1\right)=\frac{4}{\Delta t^{2}}\left(\Delta\dot{u}\left(i\right)-\dot{u}\left(i\right)\Delta t\right) \tag{2.31}$$

$$\Delta\ddot{u}\left(i\right)=\frac{4}{\Delta t^{2}}\left(\Delta\dot{u}\left(i\right)-\dot{u}\left(i\right)\Delta t\right)-2\ddot{u}\left(i\right) \tag{2.32}$$

Subscribe (2.31) into (2.28):

$$\Delta\dot{u}\left(i\right)=\frac{\Delta t}{2}\left(\frac{4}{\Delta t^{2}}\left(\Delta\dot{u}\left(i\right)-\dot{u}\left(i\right)\Delta t\right)\right)=\frac{2}{\Delta t}\left(\Delta\dot{u}\left(i\right)-\dot{u}\left(i\right)\Delta t\right) \tag{2.33}$$

from EOM (Equation 2.4):

$$\Delta m\Delta\ddot{u}\left(i\right)+c\Delta\dot{u}\left(i\right)+K\left(i\right)\Delta u\left(i\right)=\Delta F\left(i\right) \tag{2.34}$$

$$\begin{aligned}&m\left(\tfrac{4}{\Delta t^{2}}\left(\Delta\dot{u}\left(i\right)-\dot{u}\left(i\right)\Delta t\right)-2\ddot{u}\left(i\right)\right)\\&\qquad+c\left(\tfrac{2}{\Delta t}\left(\Delta\dot{u}\left(i\right)-\dot{u}\left(i\right)\Delta t\right)\right)+k\left(i\right)\Delta u\left(i\right)=\Delta F\left(i\right)\end{aligned} \tag{2.35}$$

$$\begin{aligned}&\left(\tfrac{4m}{\Delta t^2}+\tfrac{2}{\Delta t}c+k\left(i\right)\right)\Delta u\left(i\right)\\&\qquad=\Delta F\left(i\right)+\left(\tfrac{4}{\Delta t}m+2c\right)\dot{u}\left(i\right)+2m\ddot{u}\left(i\right)\end{aligned} \tag{2.36}$$

$$\hat{k}\left(i\right)=k\left(i\right)+\frac{4m}{\Delta t^2}+\frac{2}{\Delta t}c \tag{2.37}$$

$$\Delta\hat{F}\left(i\right)=\Delta F\left(i\right)+\left(\frac{4m}{\Delta t}+2c\right)\dot{u}\left(i\right)+2m\ddot{u}\left(i\right) \tag{2.38}$$

$$\hat{K}\left(i\right)\Delta u\left(i\right)=\Delta\hat{F}\left(i\right) \tag{2.39}$$

$$\Delta u\left(i\right)=\frac{\Delta\hat{F}\left(i\right)}{\hat{K}\left(i\right)} \tag{2.40}$$

$$u\left(i+1\right)=u\left(i\right)+\Delta u\left(i\right) \tag{2.41}$$

$$\dot{u}\left(i+1\right)=\dot{u}\left(i\right)+\Delta\dot{u}\left(i\right) \tag{2.42}$$

$$\ddot{u}\left(i+1\right)=\frac{-m\Delta F\left(i+1\right)-c\dot{u}\left(i+1\right)-\left(f_k\left(i+1\right)\right)}{m} \tag{2.43}$$

It is important to note that for inelastic cases $f_k(i)$ needs to be defined by a Hysteresis Model. Elastic Perfectly Elastic (EPP) model, shown in Figure 2.6, is utilized in this investigation since it is appropriate for nonlinear steel behavior.

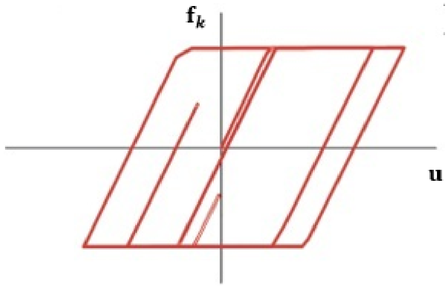

Figure 2.6. Elastic Perfectly Elastic (EPP) Model.

Figure 2.7 depicts the basic concept of linear acceleration method. This method assumes that the acceleration variation is in a linear way. So, the parameter $\ddot{u}(\tau)$, which is again indicates the variation of acceleration between two time steps, is defined the Equation 2.44:

$$\ddot{u}\left(\tau\right)=\ddot{u}\left(i\right)+\frac{\tau}{\Delta t}\Delta\ddot{u}\left(i\right) \tag{2.44}$$

The equations derivation of the method is as follows;

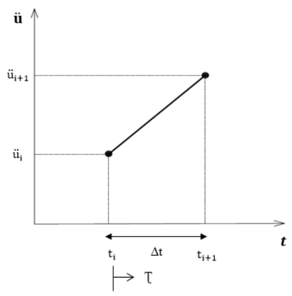

Figure 2.7. Linear Acceleration.

Integrate Equation 2.44

$$\int\limits_{t(i)}^{\tau}\ddot{u}\left(\tau\right)dt=\int\limits_{t(i)}^{\tau}\left(\ddot{u}\left(i\right)+\frac{\tau}{\Delta t}\Delta\ddot{u}\left(i\right)\right)dt \tag{2.45}$$

Velocity Response

$$\dot{u}\left(\tau\right)=\dot{u}\left(i\right)+\ddot{u}\left(i\right)\tau+\frac{\tau^{2}}{2\Delta t}\Delta\ddot{u}\left(i\right) \tag{2.46}$$

Integrate Equation 2.46

$$\int_{t(i)}^{\tau} \dot{u}(\tau)\,dt = \int_{t(i)}^{\tau} \left(\dot{u}(i) + \ddot{u}(i)\,\tau + \frac{\tau^2}{2\Delta t}\Delta\ddot{u}(i) \right) dt \tag{2.47}$$

Displacement Response

$$u(\tau) = u(i) + \frac{\ddot{u}(i)\,\tau^2}{2} + \frac{\tau^3}{6\Delta t}\Delta\ddot{u}(i) + \dot{u}(\tau) \tag{2.48}$$

If $\tau 0 \Delta t$ then from Equation 2.46:

$$\begin{aligned} \dot{u}(i+1) &= \dot{u}(i) + \ddot{u}(i)\,\Delta t + \tfrac{\Delta t^2}{2\Delta t} \rightarrow \dot{u}(i+1) \\ &= \dot{u}(i) + \ddot{u}(i)\,\Delta t + \tfrac{\Delta t}{2}\Delta\ddot{u}(i) \end{aligned} \tag{2.49}$$

$$\begin{aligned} u(i+1) &= u(i) + \dot{u}(i)\,\Delta t \\ &\quad + \tfrac{\Delta t^3}{6\Delta t}\Delta\ddot{u}(i) + \tfrac{\ddot{u}(i)(\Delta t)^2}{2} \end{aligned} \tag{2.50}$$

$$u(i+1) = u(i) + \dot{u}(i)\,\Delta t + (\Delta t)^2 \left(\frac{1}{6}\ddot{u}(i+1) + \frac{1}{3}\ddot{u}(i) \right) \tag{2.51}$$

By definition we know

$$\Delta u(i) = u(i+1) - u(i) \tag{2.52}$$

$$\Delta\dot{u}(i) = \dot{u}(i+1) - \dot{u}(i) \tag{2.53}$$

$$\Delta\ddot{u}(i) = \ddot{u}(i+1) - \ddot{u}(i) \tag{2.54}$$

Now from Equation 2.49

$$\Delta\dot{u}\left(i\right) = \ddot{u}\left(i\right)\Delta t + \frac{\Delta t}{2}\Delta\ddot{u}\left(i\right) \tag{2.55}$$

and from Equation 2.51

$$\Delta u\left(i\right) = \dot{u}\Delta t + \frac{\Delta t^2}{6}\Delta\ddot{u}\left(i\right) + \frac{\ddot{u}\left(i\right)\Delta t^2}{3} \tag{2.56}$$

Find $\Delta\ddot{u}(i)$ from Equation 2.56

$$\frac{\Delta t^2}{6}\Delta\ddot{u}\left(i\right) = \Delta u - \dot{u}\left(i\right)\Delta t - \frac{\ddot{u}\left(i\right)\Delta t^2}{2} \tag{2.57}$$

$$\Delta\ddot{u}\left(i\right) = \frac{6\Delta u\left(i\right)}{\Delta t^2} - \frac{6\dot{u}\left(i\right)}{\Delta t} - 3\ddot{u}\left(i\right) \tag{2.58}$$

Subscribe Equation 2.58 into Equation 2.55:

$$\Delta\dot{u}\left(i\right) = \ddot{u}\left(i\right)\Delta t + \frac{3\Delta u\left(i\right)}{\Delta t} - 3\dot{u}\left(i\right) - \frac{3}{2}\ddot{u}\left(i\right)\Delta t \tag{2.59}$$

$$\Delta\dot{u}\left(i\right) = \frac{3\Delta u\left(i\right)}{\Delta t} - 3\dot{u}\left(i\right) - \frac{1}{2}\ddot{u}\left(i\right)\Delta t \tag{2.60}$$

From EOM (Equation 2.4):

$$m\Delta\ddot{u}\left(i\right) + c\Delta\dot{u}\left(i\right) + k\left(i\right)\Delta u\left(i\right) = \Delta F\left(i\right) \tag{2.61}$$

$$\begin{split} m\left(\tfrac{6\Delta u(i)}{\Delta t^2} - \tfrac{6\dot{u}(i)}{\Delta t} - 3\ddot{u}\left(i\right)\right) \\ + c\left(\tfrac{3\Delta u(i)}{\Delta t} - 3\dot{u}\left(i\right) - \tfrac{1}{2}\ddot{u}\left(i\right)\Delta t\right) + k\left(i\right)\Delta u\left(i\right) = \Delta F\left(i\right) \end{split} \tag{2.62}$$

$$\begin{aligned}&\tfrac{6m}{\Delta t^2}\Delta u\left(i\right)-\tfrac{6\dot{u}(i)}{\Delta t}m-3\ddot{u}\left(i\right)m\\&\quad+\tfrac{3\Delta u(i)}{\Delta t}c-3\dot{u}\left(i\right)c-\tfrac{1}{2}\ddot{u}\left(i\right)\Delta tc+k\left(i\right)\Delta u\left(i\right)=\Delta F\left(i\right)\end{aligned} \tag{2.63}$$

$$\hat{K}\left(i\right)=k\left(i\right)+\frac{3}{\Delta t}c+\frac{6m}{\Delta t^2} \tag{2.64}$$

$$\Delta\hat{F}\left(i\right)=\Delta F\left(i\right)+\left(\frac{6\dot{u}\left(i\right)}{\Delta t}+3\ddot{u}\left(i\right)\right)m+\left(3\dot{u}\left(i\right)+\frac{1}{2}\ddot{u}\left(i\right)\Delta t\right)c \tag{2.65}$$

$$\hat{K}\left(i\right)\Delta u\left(i\right)=\Delta\hat{F}\left(i\right) \tag{2.66}$$

$$\Delta u\left(i\right)=\frac{\Delta\hat{F}\left(i\right)}{\hat{k}\left(i\right)} \tag{2.67}$$

$$u\left(i+1\right)=u\left(i\right)+\Delta u\left(i\right) \tag{2.68}$$

$$\dot{u}\left(i+1\right)=\dot{u}\left(i\right)+\Delta\dot{u}\left(i\right) \tag{2.69}$$

$$\ddot{u}\left(i+1\right)=\frac{-m\Delta F\left(i+1\right)-c\dot{u}\left(i+1\right)-\left(f_k\left(i+1\right)\right)}{m} \tag{2.70}$$

The derived formulations for both constant acceleration and linear acceleration Newmarks methods were utilized to develop an algorithm that determines the time history dynamic responses. The detailed description of the algorithm is provided in the next section.

2.3.2. The Development of an Algorithm for Time-History Energy Response Analysis

A computer algorithm using MATLAB (Release 2012a) was developed in order to determine the energy time histories of the relative energy components discussed in Section 2.2 for a lumped-mass cantilever steel column. However, the dynamic time history responses (relative displacement and velocity) are required to be accomplished before energy computations. Since the behavior of the structural system may fall beyond the elastic range while subjecting to earthquake loads, the moment-curvature analysis should be performed in order to find out the yielding moment of the cross Section. Thus, the methodology (Figure 2.8) developed in this study has three main steps (three MATLAB sub programs).

Moment-Curvature sub program: Moment-Curvature (Sectional analysis) is performed in order to determine the yielding moment and consequently the yielding force values of the SDOF system, which will be used in step-by-step time history analysis procedure. The algorithm has the capability of conducting the analysis for any steel Sections regardless of the geometric property (general Section is considered). That is to say, the Section is divided to different finite strips and the area of each strip are calculated. Then, by gradually increasing the strain value of the outermost bar from 0.0001 to 0.1, the amount of curvature corresponding to each strain value is calculated. Afterwards, the values of stress, internal force and moment due to neutral axis of the Section are calculated for each bar respectively. Ultimately, the summation of the moment values of the bars is the moment amount of the Section corresponding to the calculated curvature. This sub program results in the value of yielding moment and the moment-curvature graph.

Step-by-step time history analysis sub program: Linear or nonlinear dynamic time history analysis is performed in this step. As it is mentioned in Section 2.3.1, EPP model is selected as the hysteresis behavior of the material for this study (Figure 2.6). The main inputs of the computer code are the properties of the SDOF system such as mass, initial stiffness and the yielding moment value, accomplished from the previous step, as well as the earthquake acceleration records. This analysis gives the outputs of relative displacement, velocity and acceleration responses and hysteresis graph.

Computation of energy components sub program: Time-history energy terms are determined from the results of the dynamic time history analysis in previous sub program using the formulation derived in Sections 2.2.1 up to 2.2.4. This sub program results in time history values of graphs for relative input energy, damping, strain and plastic energies along with relative input energy.

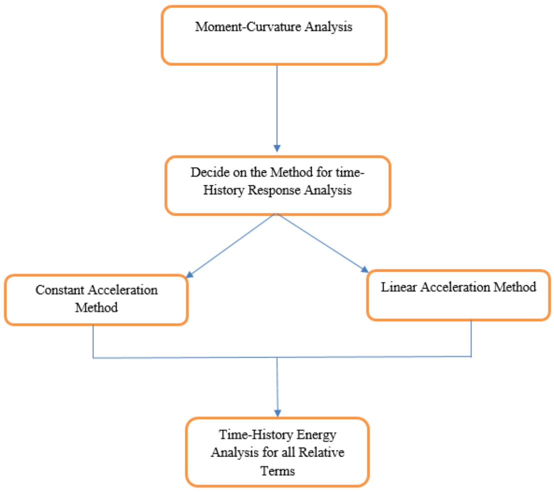

Figure 2.8. Flowchart for Time-History Energy Responses.

2.3.3. Verification of the Algorithm for Energy Time-History Analysis

The developed algorithm was verified with a published literature (Wong and Yang, 2002) in terms of dynamic response results and energy components for the both elastic and inelastic cases. Figure 2.8 depicts the SDOF model in the mentioned literature and states its properties which was assumed to be subjected to Northridge earthquake occurred at Sylmar in 1994, Peak Ground Acceleration (PGA) is 0.84g and Figure 2.9 shows the time history of the ground motion.

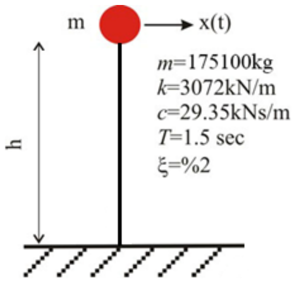

Figure 2.9. The used SDOF System for Verification.

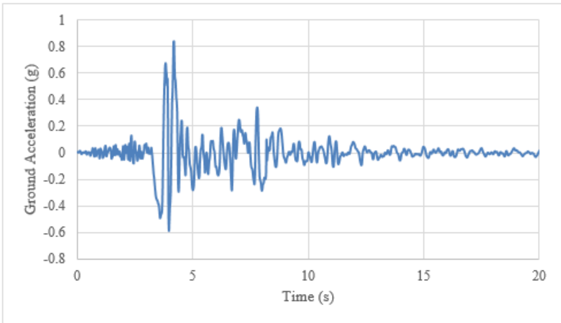

Figure 2.10. Northridge-Sylmar 1994 Ground Acceleration.

Figure 2.11 up to Figure 2.13 depict the relative elastic dynamic responses resulted from both linear and constant acceleration formulations derived in Section 2.3.1. The responses have perfect agreement with those mentioned in the literature.

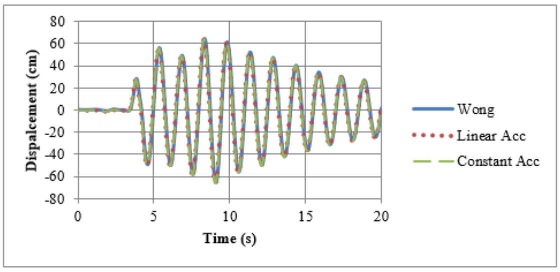

Figure 2.11. Displacement Response in Linear Model.

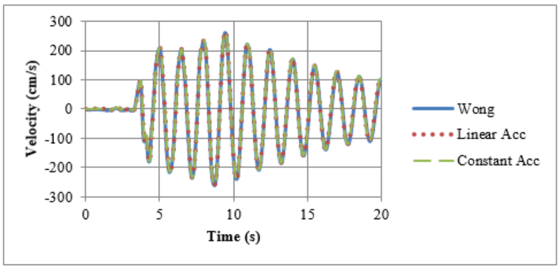

Figure 2.12. Velocity Response in Linear Model.

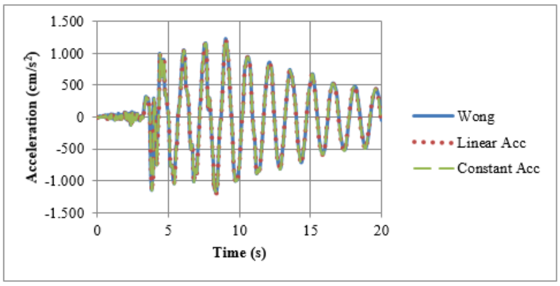

Figure 2.13. Acceleration Response in Linear Model.

Figure 2.14 up to Figure 2.17 show the verification of energy terms time histories for elastic case. They are in excellent agreement.

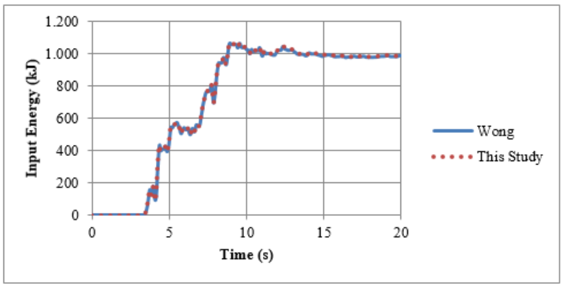

Figure 2.14. Input Energy in Linear Model.

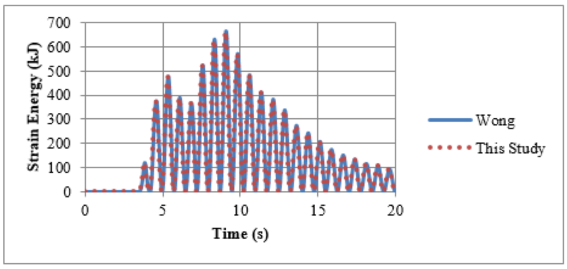

Figure 2.15. Strain Energy in Linear Model.

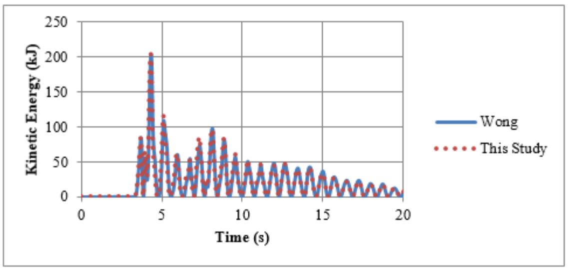

Figure 2.16. Kinetic Energy in Linear Model.

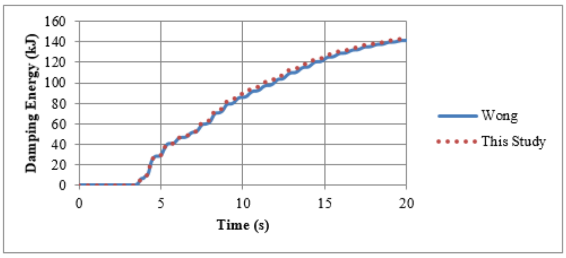

Figure 2.17. Damping Energy in Linear Model.

Nonlinear response verification could be observed in Figure 2.18 to Figure 2.20. The used hysteresis model is elastic perfectly plastic as already mentioned (Figure 2.6).

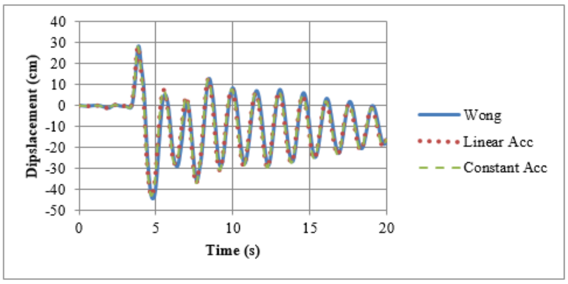

Figure 2.18. Displacement Response in Nonlinear Model.

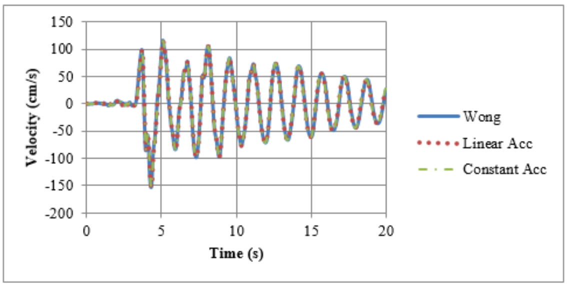

Figure 2.19. Velocity Response in Nonlinear Model.

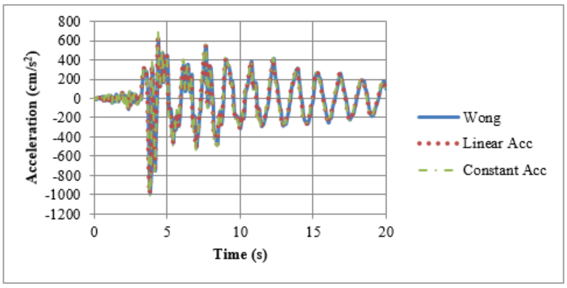

Figure 2.20. Acceleration Response in Nonlinear Model.

Energy Components Verifications for inelastic case are shown in Figure 2.21 to Figure 2.25.

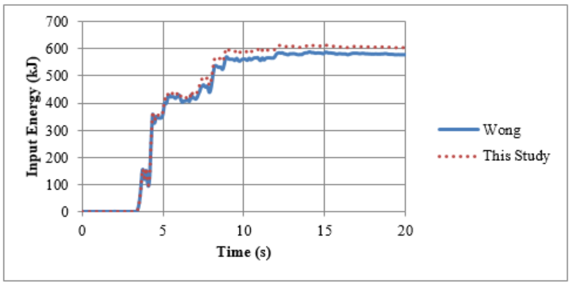

Figure 2.21. Input Energy in Nonlinear Model.

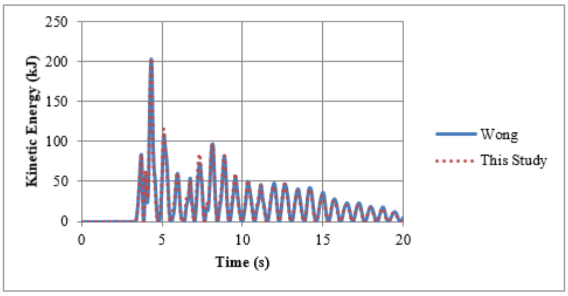

Figure 2.22. Kinetic Energy in Nonlinear Model.

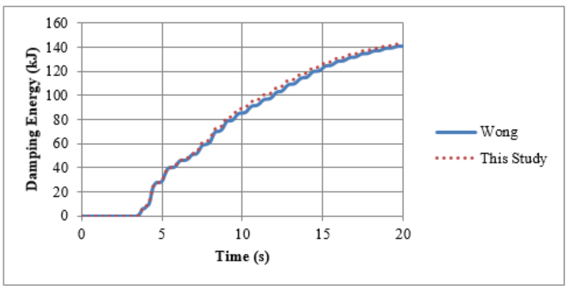

Figure 2.23. Damping Energy in Nonlinear Model.

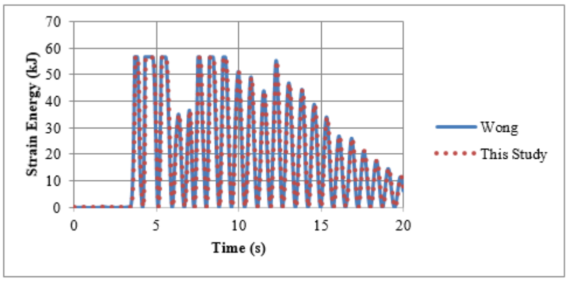

Figure 2.24. Strain Energy in Nonlinear Model.

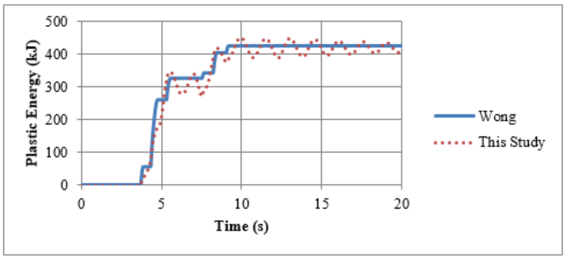

Figure 2.25. Plastic Energy in Nonlinear Model.

All the Figure 2.11 to Figure 2.25 imply that the results of analytical analyses (MATLAB Code) are very close to Wong and Yang (2002) analyses. Moreover, the data obtained from Newmark Constant and Linear Acceleration methods are compatible to each other in terms of dynamic time history response analyses. Thus, it could be concluded that the proposed algorithm works properly for conducting time history dynamic and energy responses in both elastic and inelastic states.

However, since the moment-curvature analysis is a part of the developed algorithm, it needs to be verified to make sure that all the algorithm is reliable to perform a pure analytical energy time history analysis for a given SDOF system.

Because the only important result from the part of the developed algorithm is calculating the yielding moment of a given Section, it is sufficient to verify that the calculated yielding moment from the algorithm is the same as that of classic formulations. For this purpose, a box steel Section (40x40x2 mm) is taken as an example as shown in Figure 2.26.

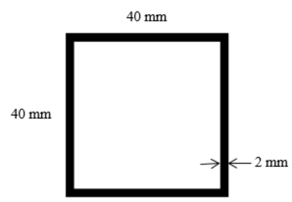

Figure 2.26. Steel Box Section of 40x40x2 mm.

The assumed stress-strain behavior of the material is given as EPP shown in Figure 2.27.

Using the algorithm developed for moment-curvature relationship depicted in Figure 2.28, the value of yielding moment (M_y) was calculated as 1540586.88 Nmm.

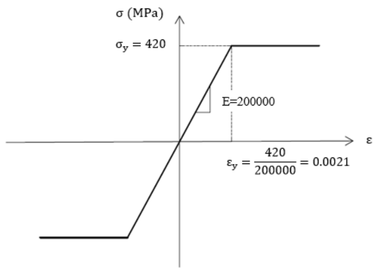

Figure 2.27. Stress Strain Model.

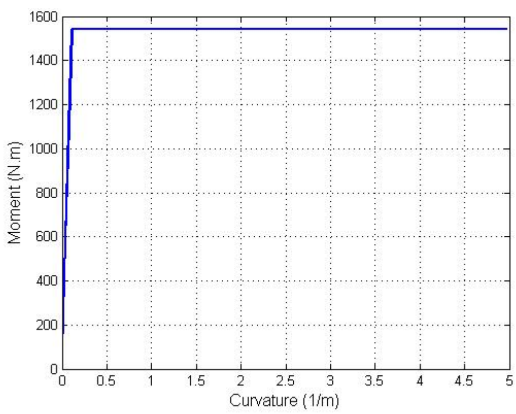

Figure 2.28. Moment Curvature Graph for Box 40x40x2 mm.

The yielding moment of a Section is calculated from Equation 2.71 (Wong, 2009).

$$M_y = \frac{\sigma_y \times I}{y_{max}} \tag{2.71}$$

where σ_y is the yielding stress as shown in Figure 2.27, I is moment of inertia of the Section and y_{max} is the distance of the furthest fiber in the Section to the Neutral Axis. Therefore,

$$M_y = \frac{\sigma_y \times I}{y_{max}} = \frac{420 \times 73361.28}{20} = 1540586.88 N.mm \tag{2.72}$$

As it could be observed the computed value for yielding moment of the analyzed Section from the computer algorithm is exactly the same as that of calculated by classic formulation.

By taking into the account the results of the verification process for all the three main steps of the algorithm (Sectional, dynamic time history and energy analyses), it could be concluded that the developed algorithm is reliable for conducting an energy time history analysis for a given SDOF system.

2.4. Energy Response Spectra and the Developed Algorithm

Spectra concept in structural analysis is widely preferred compared to seismic forces as it is more advantageous and practical. Due to the fact that a spectrum includes diverse structural parameters such as natural frequency (or period) and damping ratio of the system, it is capable to cover and explain many cases and conditions of structures. The kind of spectra which has the most application in seismic analysis are the response spectra, which depend only on natural period, damping ratio and soil condition of the structures, resulted from time history response (displacement, velocity and acceleration) analysis of a SDOF while affected by earthquake accelerations. That is to say, response spectrum is one of the useful tools of earthquake engineering for analyzing the performance of structures especially while subjected to earthquakes, since many systems behave as single degree of freedom systems. Thus, if the natural frequency (or natural period) of the structure is known, then the peak response of the building could be estimated by reading the acceleration value from the response spectrum for the appropriate frequency. In most seismic design building codes, this value, especially value of acceleration response spectrum, forms the basis for calculating the forces that a structure must be designed to resist.

Although the extreme structural response is reflected in the response spectra, it is widely known that seismic design using these methods neglect important information found within the whole duration of earthquake (Gupta 1990; Ye, 2009). This is utilized as the spectral values of energy components are taken at the end of the motion, whereas the values in response spectra are actually the absolute greatest numbers in response time-histories (Dindar, 2009). Taking the extreme values in a response time-history may lead to wrong conclusions Such a case occur when two ground motion records hold close acceleration spectra but different input energy response spectra. Figure 2.29 and Figure 2.30 show Chile 1985 and San Salvador 1986 earthquake records and their duration, respectively.

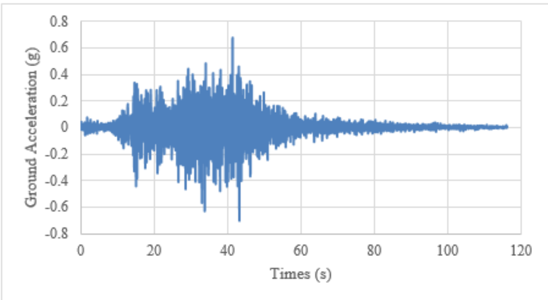

Figure 2.29. Chile 1985 Earthquake Records.

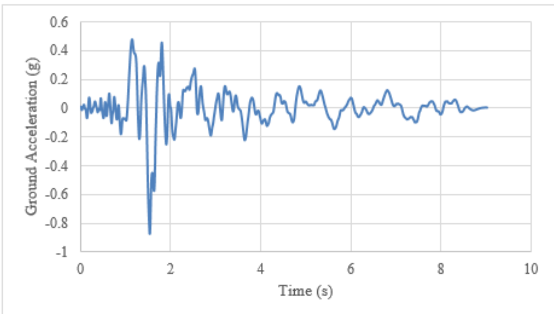

Figure 2.30. San Salvador 1986 Earthquake Records.

As it can be inferred from Figure 2.31 (acceleration response spectra of San Salvador and Chile earthquake records) and Figure 2.32 (input energy response spectra of San Salvador and Chile earthquake records), the two seismic records have clearly different input energy response spectra despite holding the similar acceleration response spectra.

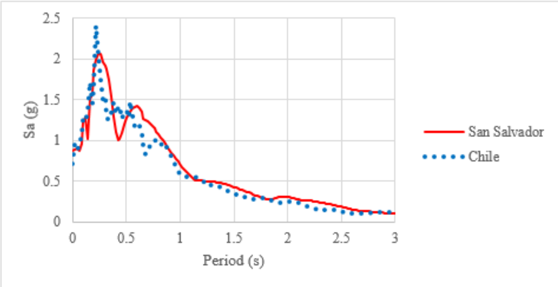

Figure 2.31. ARS of San Salvador and Chile Earthquakes (Uang and Bertero, 1988).

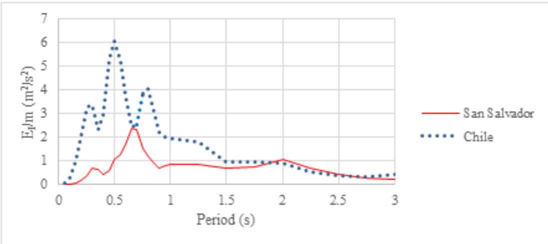

Figure 2.32. Input Energy Response Spectra of San Salvador and Chile Earthquakes (Uang and Bertero, 1988).

In fact, Figure 2.31 and Figure 2.32 represents the advantage of utilizing Energy-Based approach in seismic analysis to other common design methods. That is, using ADS leads the designer to similar designs while designing a structure subjected to the San Salvador and Chile earthquakes. However, by considering the input energy response spectra of the mentioned earthquakes, the design results would be considerably different. For example, if a building has natural period of T=0.50s, it would be designed using the same lateral earthquake force while considering the Chile and San Salvador earthquakes. On the contrary, the input energy response spectra, which include the whole duration of the earthquakes (duration of Chile is longer than that of San Salvador as shown in Figures 2.29 and Figure 2.30) imply an obvious damage potential difference in the assumed period. Furthermore, the difference in frequency content of the discussed to earthquakes is another reason for the two input energy response spectra. Figures 2.33 and Figure 2.34 depicts the Fourier Amplitude Spectra (FAS) of the earthquakes which clearly describe the different frequency content of the mentioned ground motions. These significant information is not included in those seismic design approaches which only take the dynamic response spectra into account (Dindar, 2009).

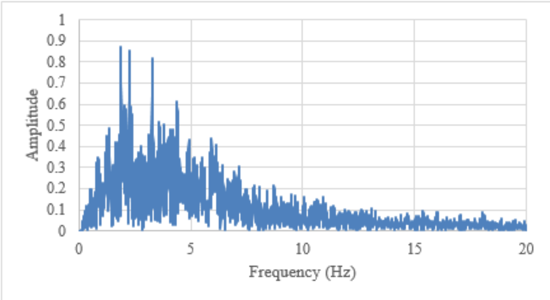

Figure 2.33. Fourier Amplitude Spectrum of Chile Earthquake.

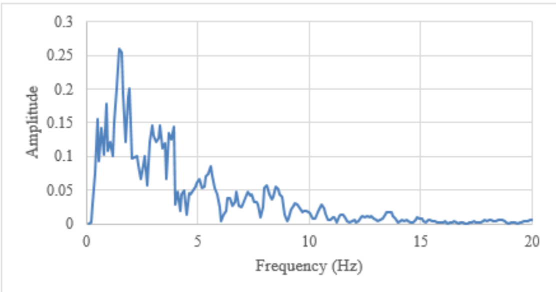

Figure 2.34. Fourier Amplitude Spectrum of San Salvador Earthquake.

2.4.1. The Development of an Algorithm for Energy Response Spectrum

In Energy-Based seismic analysis, the whole duration of ground motion and the frequency content is considered for the energy terms discussed before (E_I, E_K, E_D, E_S, E_P) at the very end of the earthquake, which is totally diverse from common dynamic response spectra that takes into account the maximum absolute value of dynamic responses. In order to generate energy spectra of an earthquake, time history response analysis of SDOF system needs to be performed (using the derived formulation in

Section 2.3.1) and the resulted responses are required to be inserted in the energy components (Equation 2.11-Equation 2.13 and Equation 2.15 for input, kinetic, damping and strain energies, respectively as well as the area of enclosed in force-displacement graph for plastic energy). Needless to say that the structural properties (natural period and damping ratio) and the model of seismic behavior (elastic or inelastic) play major roles in the dynamic responses and consequently the energy components values. Some supplements to the developed computer algorithm, discussed in Section 2.3.2, are used in order to develop a new algorithm for deriving the input and plastic energy response spectrum for a given SDOF subjected to earthquake-type loading in a range of period. This algorithm includes two steps (two MATLAB sub programs) stated below.

Step (Sub program) 1: Moment-Curvature (Section) analysis is needed to be performed in order to determine the yielding moment and consequently the yielding force values of the SDOF system, which will be used in dynamic time history response analyses in the next step. The process of the analysis is exactly the same as discussed in Section 2.3.2.

Step (Sub programs) 2: Linear or nonlinear dynamic along with input and plastic energy time history analyses for a range period (from 0.05s to 3s) are performed in this step. The Algorithm is capable of computing all the spectral values using any desirable period time increments determined by the user. However, in order to generate a comprehensive input energy response graph, period time increments higher than 0.02s is not recommended (as the results for some periods would be missed in the generated spectrum). In tis sub program, it is possible to use Newmark's linear or constant acceleration method in order to calculate the dynamic responses (displacement, velocity and acceleration) using the formulation derived in Section 2.3.1. Moreover, values of mass corresponding to each period is calculated by the algorithm itself. It is highly important to mention that spectral values are calculated by dividing the last value of time history input (or plastic) energy response by the related mass (mass normalized) in each period as it is represented in Figure 2.35. The main inputs of the sub program are the properties of the SDOF system, initial stiffness, the yielding moment value, the earthquake acceleration records and period time increment. These analyses result in the outputs of input and plastic energy response spectra.

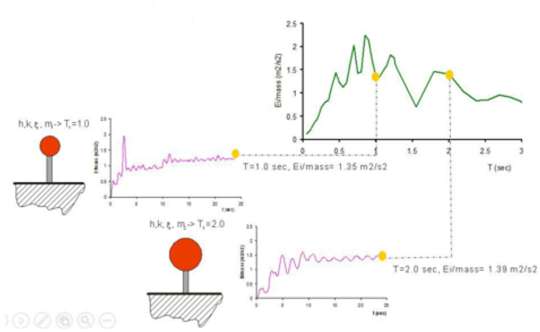

Figure 2.35. Energy Response Spectral Values (Dindar *et al.*2012).

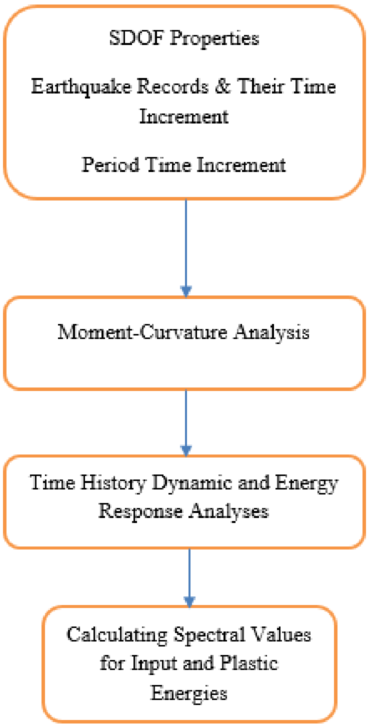

Figure 2.36. Flowchart for Energy Response Spectra.

2.4.2. Verification of the Algorithm for Energy Response Spectra

Chile and San Salvador earthquakes, which used in the previous parts of the study are considered to verify the Energy Response Spectra algorithm. Uang and Bertero (1988) derived the elastic input response spectra of the ground motions. Figure 2.37 and Figure 2.38 show the comparison between the elastic input energy response spectra represented in Uang and Bertero's (1988) research and the spectra derived from the algorithm developed in this study considering Chile and San Salvador earthquakes.

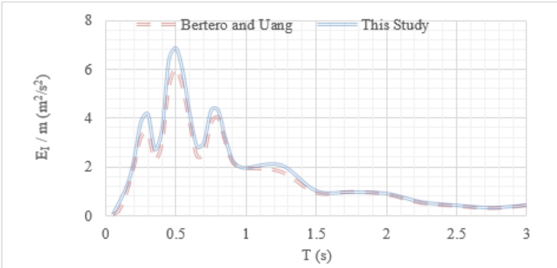

Figure 2.37. Elastic Input Energy Spectrum of Chile Earthquake.

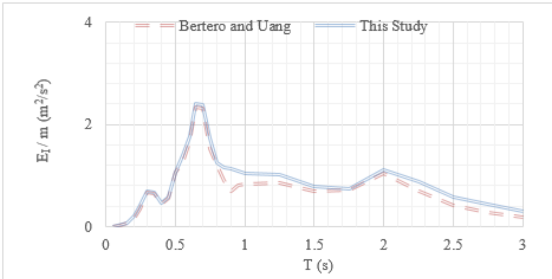

Figure 2.38. Elastic Input Energy Spectrum of San Salvador Earthquake.

Observing Figure 2.37 and Figure 2.38, it is possible to conclude that results of the two studies are in perfect agreement.

Figure 2.39 and Figure 2.40 depicts the inelastic input spectra of Chile and San Salvador earthquakes and their plastic energy response spectra respectively.

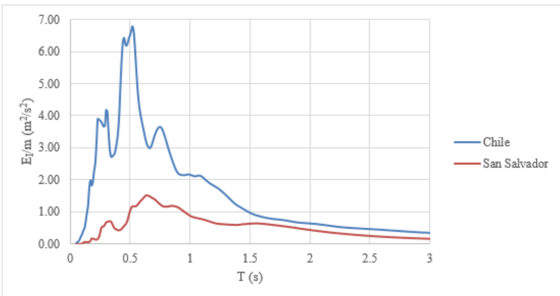

Figure 2.39. Inelastic Input Energy response Spectra of Chile and San Salvador Earthquakes.

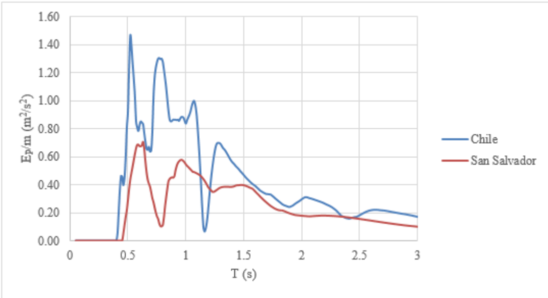

Figure 2.40. Plastic Energy Response Spectra of Chile and San Salvador Earthquakes.

After conducting a thorough search in the literature, such inelastic input energy or plastic energy response spectrum which was derived by performing inelastic dynamic analysis were not found. All the proposed inelastic input and plastic spectra are for seismic design purpose considering specific ductility factors (Clement *et al.* 2002; Decanini and Mollaioli, 2001; Dindar, 2009). Thus, it was not possible to provide a verification by using digital data. However, since the algorithm works properly for computing both dynamic and energy responses in nonlinear analysis, as it is discussed in Sections 2.3.3, it could be inferred that the results are reliable.

2.5. Summary and Conclusion

This Chapter stated with discussion about derivation of absolute and relative energy equations and followed by derivation of relative energy components. Also, whole the formulations of Newmark constant and linear acceleration methods were described. Afterwards, two algorithms were developed using the derived formulations for conducting energy time history and energy response spectra.

Since this study aims to experimentally investigate the validity of the analytic Energy- Based analysis, the results of developed algorithm will be compared with the data, which will be obtained from shake table test for SDOF cantilever steel column specimens in order to investigate the energy components of an individual structural member. It should be mention that it is not possible to predict the energy response values which are going to be obtained from experiments now because, the seismic accelerations which will be read from the sensors in the tests as earthquake-type load will not be the same as what will be applied to shake table. Thus, after the end of each test both developed algorithms in this study will be run using the obtained earthquake data from the shake table consequently the comparison between the experimental and analytic results will be performed.

3. EXPERIMENTAL TESTS

This Chapter discusses the experimental part of this study. Twelve shake table tests has been performed using Chile and San Salvador ground motions with two scale factors (total of four seismic loads) on individual cantilever steel columns. All experiments conducted for three different periods. All the dynamic and energy responses of experimental and analytic parts are compared and in order to maintain on the safe side, all the analyses were controlled by modal analyses in SAP2000. Figure 3.1 represents the test setup sketch.

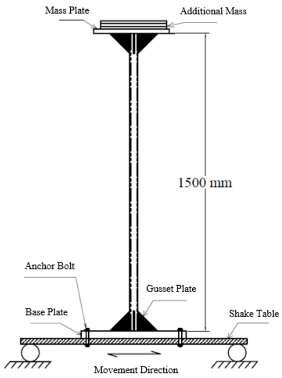

Figure 3.1. Test Setup Sketch.

The Section of the column shown in Figure 3.1 is a structural hollow Section (80x40x2 mm) and the height is 1.5 m. Figure 3.2 shows one of the test setups on shake table.

Figure 3.2. Overview of One the Specimens.

Table 3.1 up to Table 3.3 describes the properties of the specimens used in this study and Figure 3.1 demonstrates the general test setup.

Table 3.1. Properties of Specimens (T=0.40s).

Seismic Loads	m	h	ζ	k	c
	Kg	m	-	kN/m^2	kN.s/m
All the loads	57	1.76	0.0306	14.44	0.056

Table 3.2. Properties of Specimens (T=0.50s).

Seismic Loads	m	h	ζ	k	c
	Kg	m	-	kN/m^2	kN.s/m
All the loads	98.1	1.76	0.0306	14.44	0.071

Table 3.3. Properties of Specimens (T=0.66s).

Seismic Loads	m	h	ζ	k	c
	Kg	m	-	kN/m^2	kN.s/m
0.20 Chile	153.06	1.79	0.0306	13.73	0.089
0.25 Chile	153.06	1.79	0.0272	13.73	0.078
0.20 San Salvador	153.06	1.79	0.016	13.73	0.0585
0.25 San Salvador	153.06	1.79	0.016	13.73	0.0585

Where m is the mass, E is the Elasticity Modulus, I is moment of inertia, h is the height of the column (Cantilever Length), ζ is damping ratio, k is the initial stiffness, T is the period and c is the Damping Coefficient of the SDOF system.

Sensors are included two accelerometers (acceleration gauges), one at the top of the specimen and one on the shake table, two Linear Variable Differential Transducers (LVDT, also known as displacement gauge), one installed to the shake table and one to the top the specimen, and four strain gauges, two installed at front and two at back at the base of the column. Figure 3.3 depicts the instrumental sketch with their general location on the test specimen. Figure 3.4 shows the two accelerometer and the LVDT 1 at the top in red circles and Figure 3.5 shows the strain gauges in one side of the specimen at column base. The distance between two strain gauges on each side is almost 4 cm.

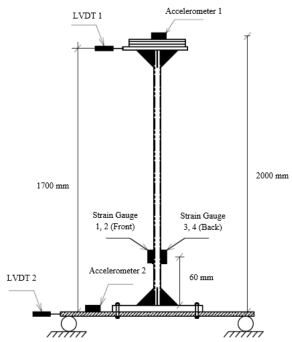

Figure 3.3. Instrumental Sketch.

Figure 3.4. Location of the Sensors.

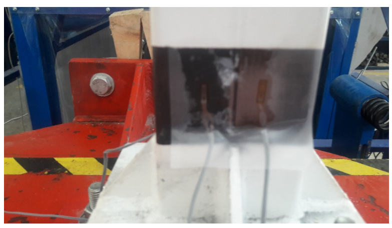

Figure 3.5. Strain Gauges at Column Base.

3.1. Shake Table Compatibility Control

Since any shake table has its own limitations due to three capacities of displacement, velocity and acceleration, the compatibility of the earthquake records which are going to be used, needs to be checked. The experiments of this study is performed on the shake table of Structural and Earthquake laboratory in Civil Engineering Faculty of Istanbul Technical University (ITU) which hold the limitations as below;

- Displacement: $\pm$ 32.5 cm from the resting point.
- Velocity: 100 cm/s
- Acceleration: 2 g

The peak absolute value of the three parameters of Chile earthquake (without scale factor) are as follows;

- Displacement: 11.34 cm from the resting point.
- Velocity: 38.43 cm/s
- Acceleration: 0.71 g

The peak absolute value of the three parameters of San Salvador (without scale factor) earthquake are as follows;

- Displacement: 12.36 cm from the resting point.
- Velocity: 59.31 cm/s
- Acceleration: 0.87 g

As it is observed, both of the seismic records meet the limitations of the shake table located at ITU and they are suitable for the intended experiments even if they used without any scale factor. Besides, since the scale factors (discussed in the next Section) are less than unit, we would be certainly on the safe side during experiments.

3.2. Selected Period and Scaled Factors

The selected periods are T_1=0.4s, T_2=0.5s and T_3=0.66s Since all the experiments were decided to be elastic-ranged, it was necessary to apply some scale factors to the earthquake records. The selected scaled factors are 0.20 and 0.25 applied to both Chile and San Salvador ground motions.

3.3. Experimental Activities before the Main Tests

Before applying the seismic records to the shake table, the capablity of generating data for all the sensors needs to be checked. For this purpose, by giving an initial displacement a free vibration is generated in the system and the capability of producing data for the sensors is obsereved were obsereved. Also, the period of the SDOF system could be calcuted using the data from the generated free vibration in order to make sure that the test will be conducted in the desirable period. That is, by giving an initial displacement to the each specimen and reading data from the accelerometer 1 and LVDT 1, shown in Figure 3.3, the displacement-time gragh (Figure 3.6) was generated. The time needed in which the system needs to complete one cycle in damped vibration is considered as the period of the system. Additionally, damping ratio of the system has to be calculated using the data obtained from the generated free vibration by the Equation 3.1 (Chopra, 1995).

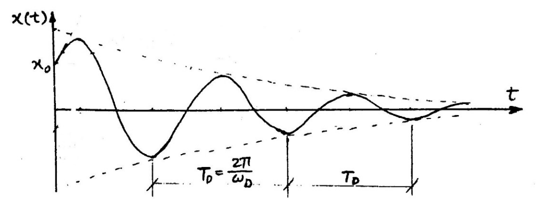

Figure 3.6. Logarithmic Curves in Damped Free Vibration.

$$\varepsilon = \frac{1}{2\pi n} \ln\left(\frac{x\,(t)}{x\,(t + nT_D)}\right) \tag{3.1}$$

where n is the number if cycles between two peaks and T_D is the period of damped vibration of the system that is generally assumed to.be equal as natural period (T_n).

After the mentioned calculations and testing the sensors, the seismic accelerations could be applied to shake table in order to conduct the experiments.

3.4. Trial Tests and Observations During the Tests

Almost twenty trail tests were conducted for many reasons. First, it was necessary to make sure that the signal processing, which is needed to perform after obtaining data from all the sensors, could be conducted adequately. For this purpose, the experimental results were compared with those of the developed algorithm and SAP2000 analyses. The trial tests were first performed without Linear Variable Displacement Transducer (LVDT) 1 as shown in Figure 3.3. In this way, the top displacements were tried to be obtained from the acceleration data read from accelerometer 1 (shown in Figure 3.3). During the filtering (signal processing) it was noticed that the obtained top displacements were not as expected. Therefore it was decided to install the LVDT 1 at the top of all specimens. In this way, it was observed that the damping ratio of the system was increased from 0.0012 (value of damping ratio of the system without LVDT 1) to a higher value (mostly 0.0306 in specimens). It happened since the stiffness of the specimens were low so that the stiffness of the spring inside the LVDT added to the stiffness of the specimens. In specimens with high stiffness the reduction in damping ratio is not expected since the stiffness of the spring in the LVDT is negligible. Thus, the damping ratio of all the specimens were recalculated as explained in the previous Section before the tests. It was also observed that although a high quality glue were used in order to attach the LVDT to the system, it was detached from the specimen while the shake table was subjected to seismic acceleration as shown in Figure 3.7. Therefore, it was decided to use a clamp to make sure the LVDT would not get separated from the specimens during the tests.

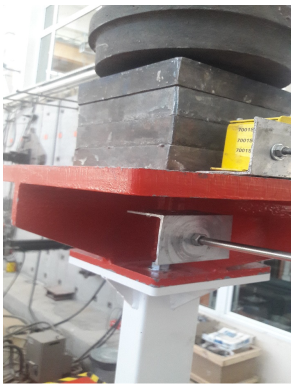

Figure 3.7. Detached LVDT During Trial Test.

In order to satisfy the symmetry of the loading (the mass on the top of the columns), it was necessary to use another similar clamp on the opposite side of mass plate as shown in Figure 3.8.

Figure 3.8. Using Clamps in Both Sides of Mass Plate.

Second, since the moment-curvature and consequently the stain energy was decided to be calculated due to stain gauge data, it was significant to find out the cantilever length in each test. During the trial tests, it was noticed that the distance from the middle of strain gauge location to center of the mass located at the top of the specimen should be considered as the cantilever length. For this purpose, the moment-curvature sub program discussed Chapter 2 was updated. That is to say, instead of gradually increasing the strain values, the data obtained from the strain gauges were utilized in order to perform all the related computations moment-curvature analysis. Then, force-displacement relationship (graph) were derived from the calculated moment values. Ultimately, the values of time history strain energy were calculated from the obtained force-displacement relationship using the Equation 2.15 (as all the experiments of this study are in the elastic region, it is possible to use Equation 2.16).

Third, it was important to check if the developed two algorithms, discussed in Sections 2.3.2 and 2.4.1 are compatible to the conditions of the tests. In this way, it was found that the *P-Delta* effect plays a significant role in the ultimate results as the column is very sensitive due to small dimensions of its cross Section. So, the *P-Delta* effect was added to the time history energy response analysis computer program (the algorithm explained in Section 2.3.2).

Furthermore, it needs to be mentioned that another observation was made during the main test. As it could be noticed from Table 3.1 to Table 3.3, the damping ratio of the most specimens are the same (0.0306). However, in the last three tests a reduction in the value of the damping ratio is observed. The reduction happened because all the twelve main tests were conducted continuously and consequently the bolts at the column base got some loosened.

3.5. Data Obtained from Each Experiment

In this Section all the data obtained from the sensors in each experiment (after filtering) is presented. It needs to be stated that the average of the data received from strain gauges in the front side of specimens (strain gauges 1 and 2) is considered as the front stain values and average of the data obtained from stain gauges in back side of specimens (stain gauges 3 and 4) is considered as the front and back stain values of the specimens. That is, the average values were taken into account in the whole related calculations. Therefore, the mentioned average values are depicted in all of the figures of this part.

3.5.1. First Test (T=0.4s, 0.2 Chile)

Figure 3.9 to Figure 3.14 represent the data obtained from the first test.

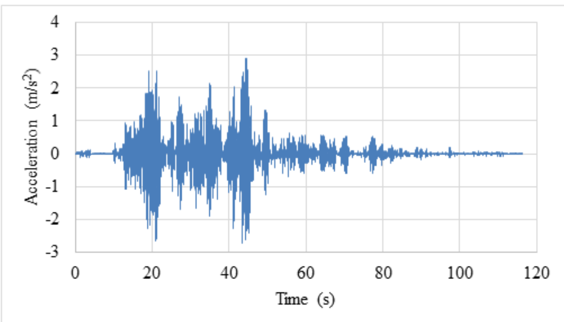

Figure 3.9. Acceleration Data from Accelerometer 1.

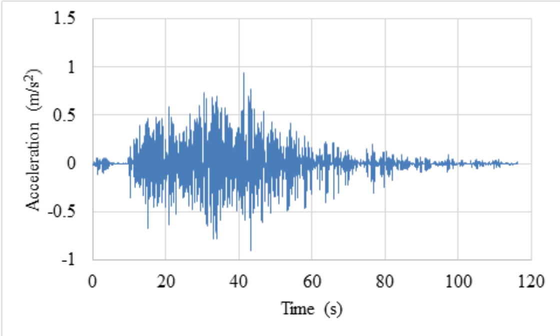

Figure 3.10. Acceleration Data from Accelerometer 2.

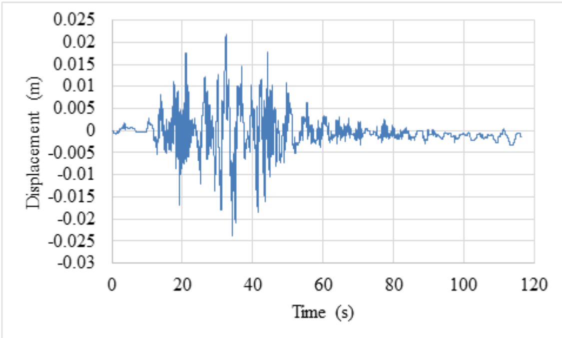

Figure 3.11. Displacement Data from LVDAT 1.

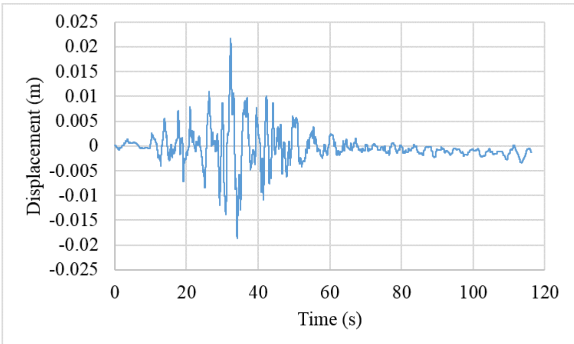

Figure 3.12. Displacement Data from LVDAT 2.

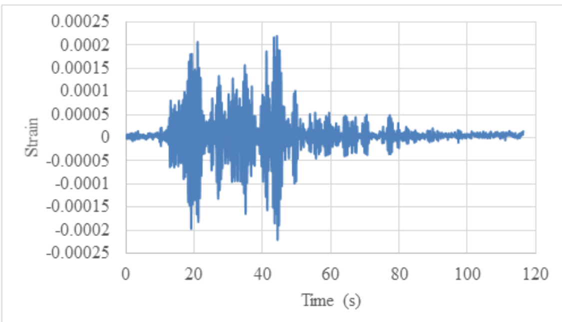

Figure 3.13. Front Strain Data.

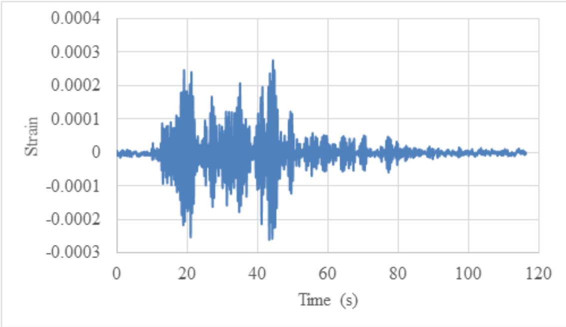

Figure 3.14. Back Strain Data.

3.5.2. Second Test (T=0.4s, 0.2 San Salvador)

Figure 3.15 to Figure 3.20 represent the data obtained from the second test.

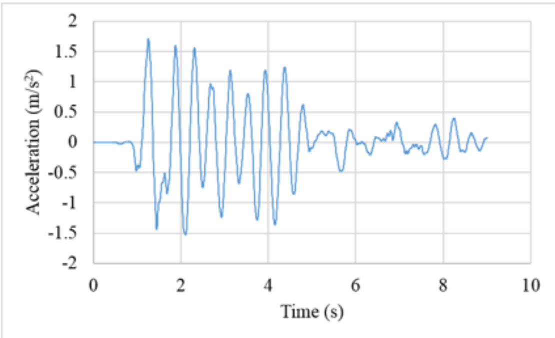

Figure 3.15. Acceleration Data from Accelerometer 1.

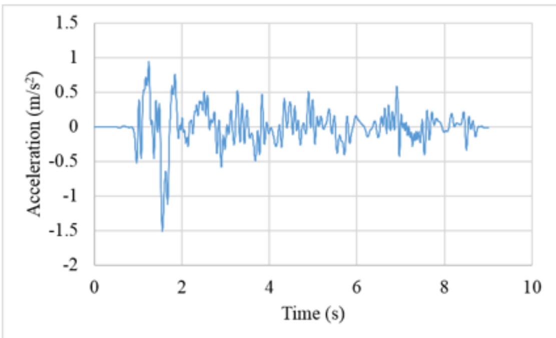

Figure 3.16. Acceleration Data from Accelerometer 2.

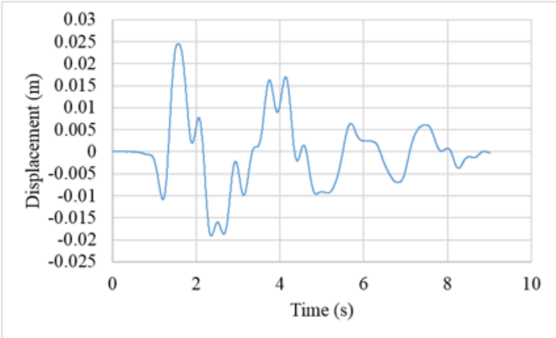

Figure 3.17. Displacement Data from LVDT 1.

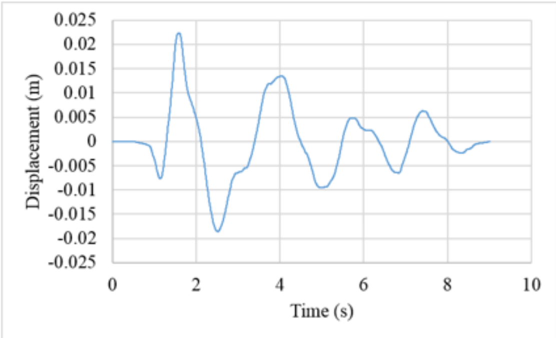

Figure 3.18. Displacement Data from LVDT 2.

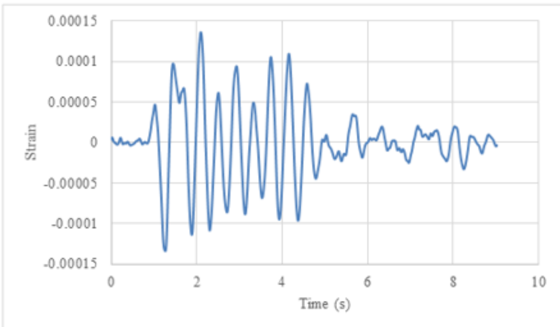

Figure 3.19. Displacement Data from LVDT 2.

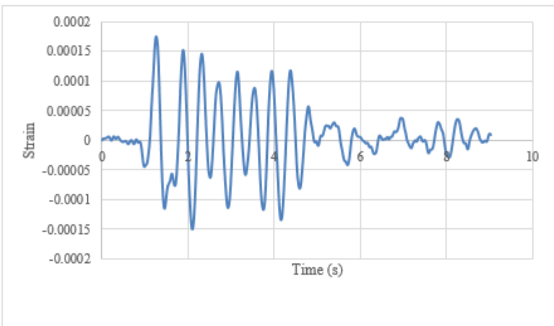

Figure 3.20. Back Strain Data.

3.5.3. Third Test (T=0.4s, 0.25 Chile)

Figure 3.21 to Figure 3.26 represent the data obtained from the third test.

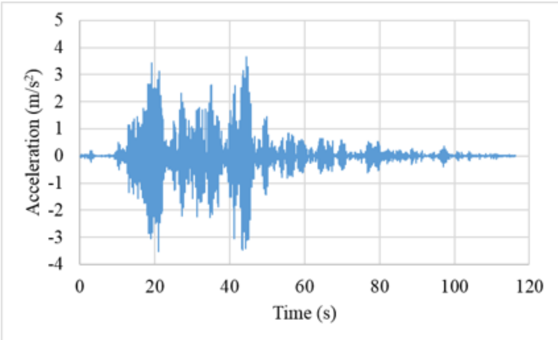

Figure 3.21. Acceleration Data from Accelerometer 1.

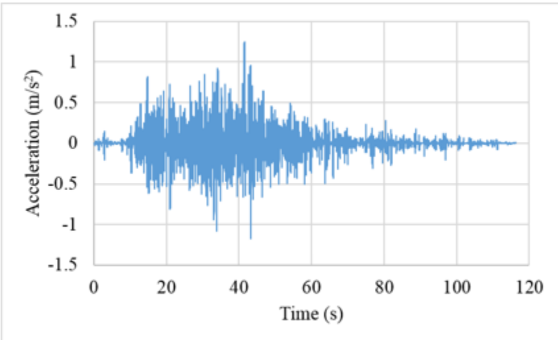

Figure 3.22. Acceleration Data from Accelerometer 2.

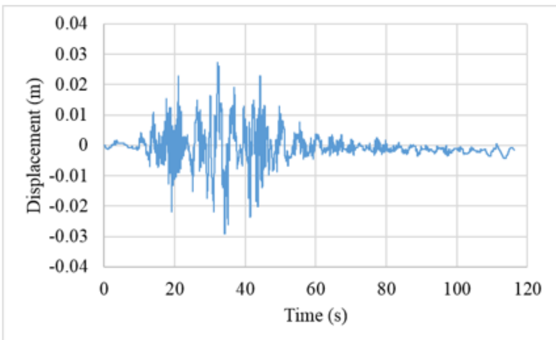

Figure 3.23. Displacement Data from LVDT 1.

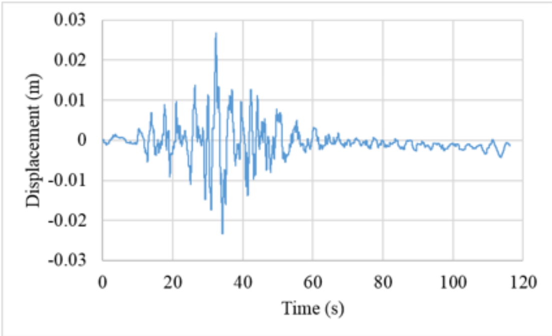

Figure 3.24. Displacement Data from LVDT 2.

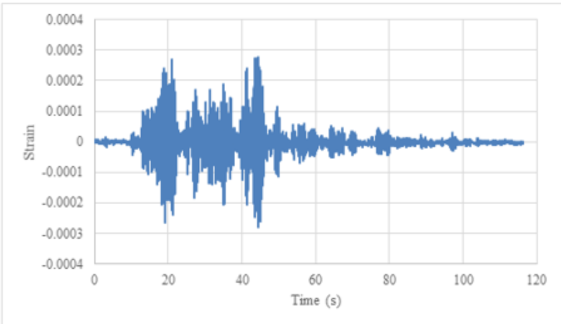

Figure 3.25. Front Strain Data.

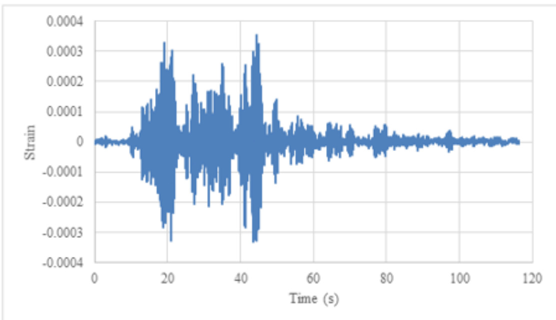

Figure 3.26. Back Strain Data.

3.5.4. Fourth Test (T=0.4s, 0.25 San Salvador)

Figure 3.27 to Figure 3.32 represent the data obtained from the forth test.

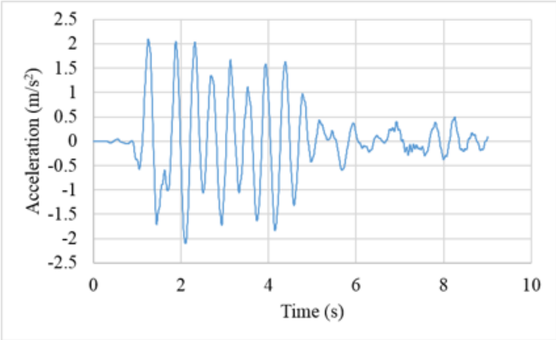

Figure 3.27. Acceleration Data from Accelerometer 1.

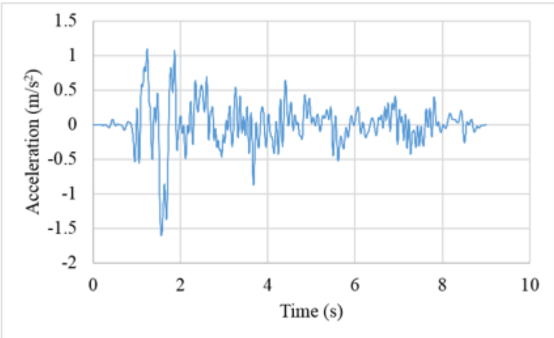

Figure 3.28. Acceleration Data from Accelerometer 2.

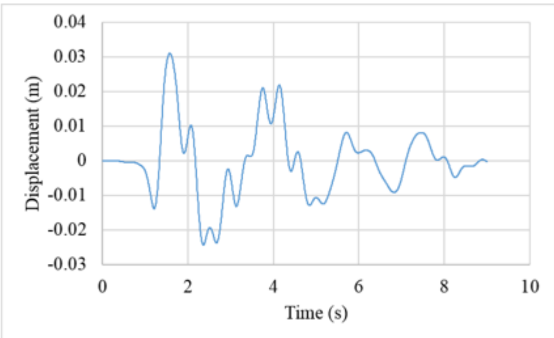

Figure 3.29. Displacement Data from LVDT 1.

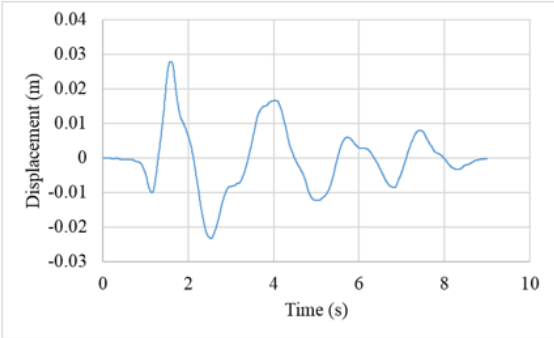

Figure 3.30. Displacement Data from LVDT 2.

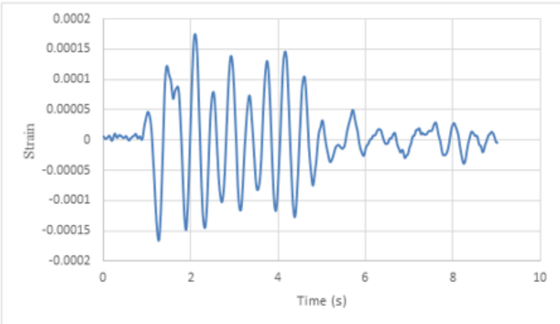

Figure 3.31. Front Strain Data.

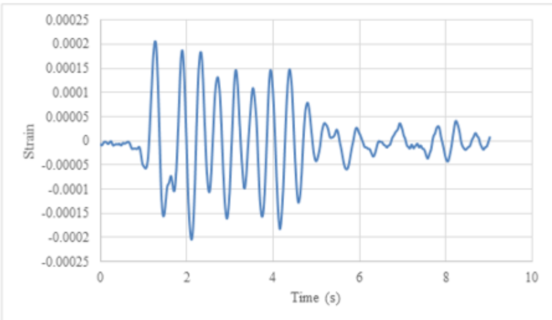

Figure 3.32. Back Strain Data.

3.5.5. Fifth Test (T=0.5s, 0.20 Chile)

Figure 3.33 to Figure 3.38 represent the data obtained from the fifth test.

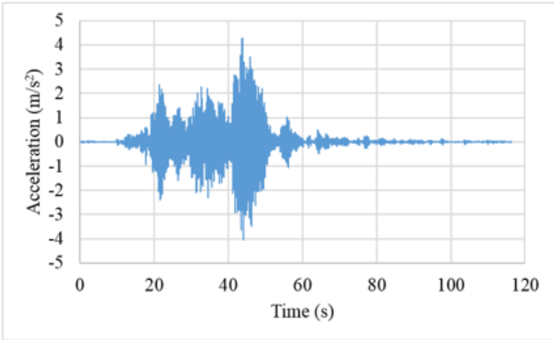

Figure 3.33. Acceleration Data from Accelerometer 1.

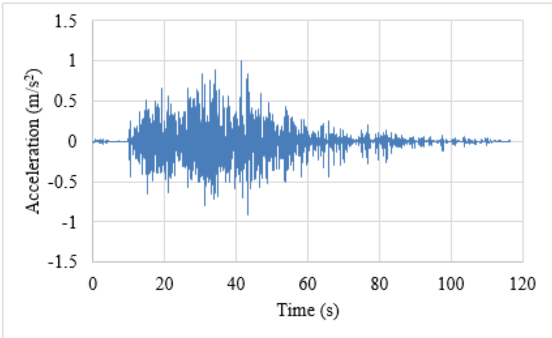

Figure 3.34. Acceleration Data from Accelerometer 2.

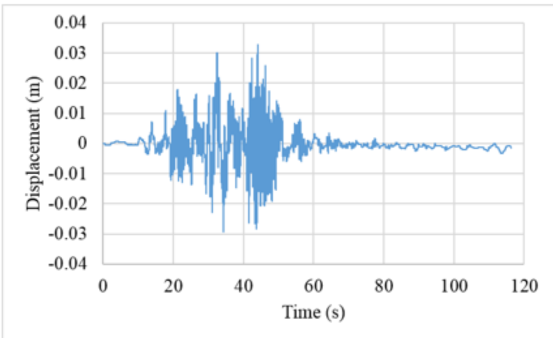

Figure 3.35. Displacement Data from LVDT 1.

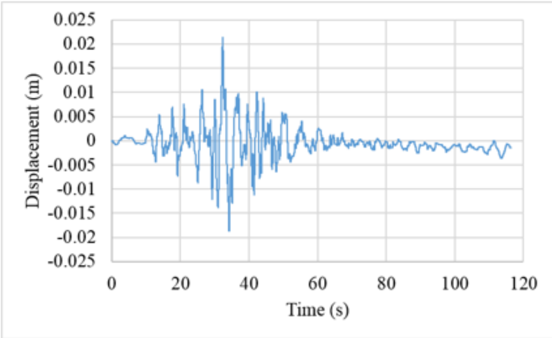

Figure 3.36. Displacement Data from LVDT 2.

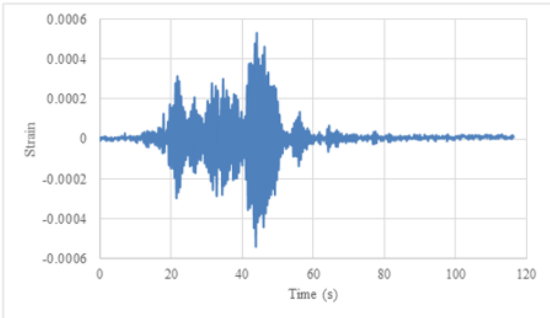

Figure 3.37. Front Strain Data.

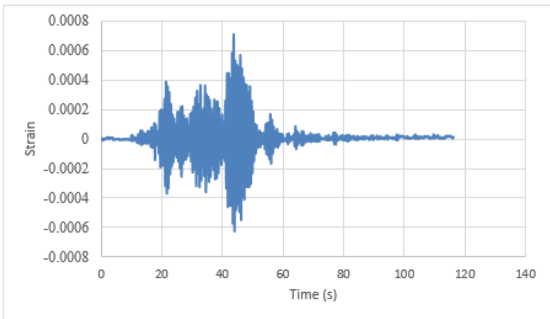

Figure 3.38. Back Strain Data.

3.5.6. Sixth Test (T=0.5s, 0.20 San Salvador)

Figure 3.39 to Figure 3.44 represent the data obtained from the sixth test.

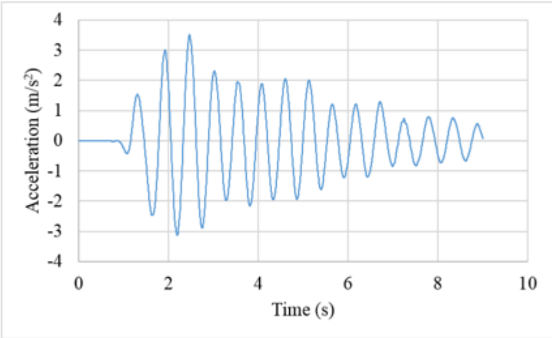

Figure 3.39. Acceleration Data from Accelerometer 1.

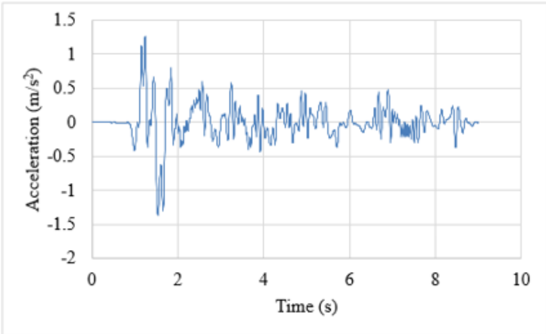

Figure 3.40. Acceleration Data from Accelerometer 2.

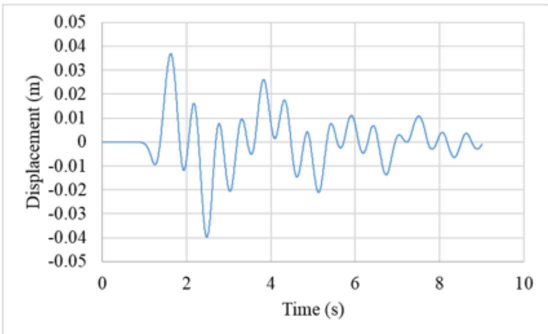

Figure 3.41. Displacement Data from LVDT 1.

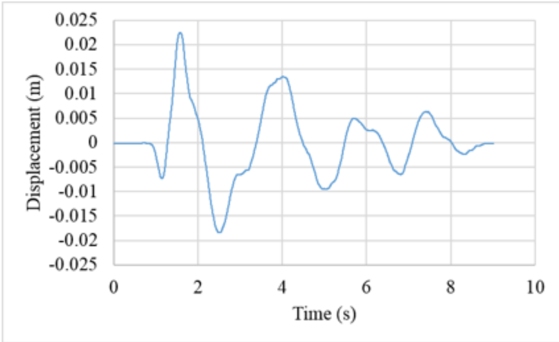

Figure 3.42. Displacement Data from LVDT 2.

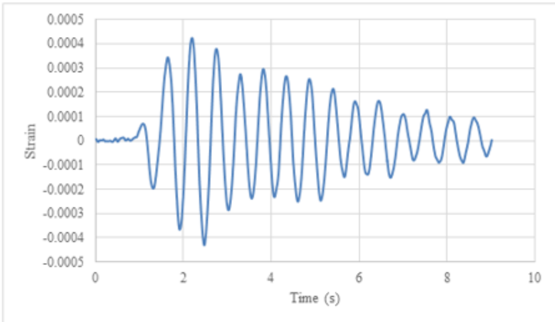

Figure 3.43. Front Strain Data.

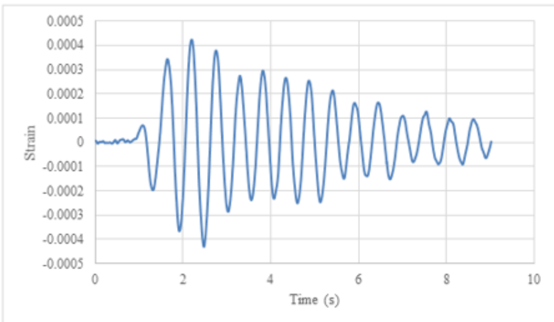

Figure 3.44. Back Strain Data.

3.5.7. Seventh Test (T=0.5s, 0.25 Chile)

Figure 3.45 to Figure 3.50 represent the data obtained from the seventh test.

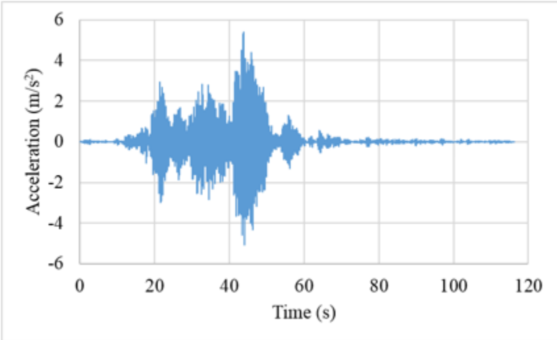

Figure 3.45. Acceleration Data from Accelerometer 1.

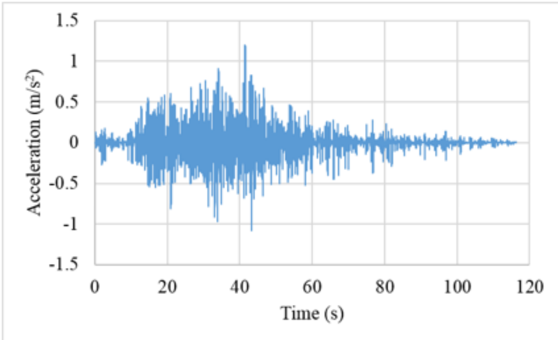

Figure 3.46. Acceleration Data from Accelerometer 2.

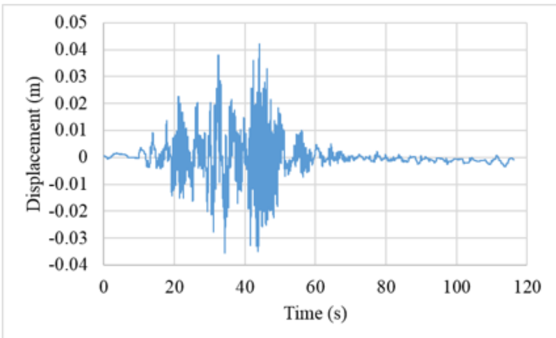

Figure 3.47. Displacement Data from LVDT 1.

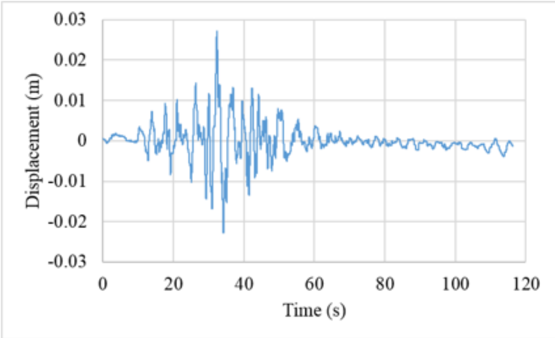

Figure 3.48. Displacement Data from LVDT 2.

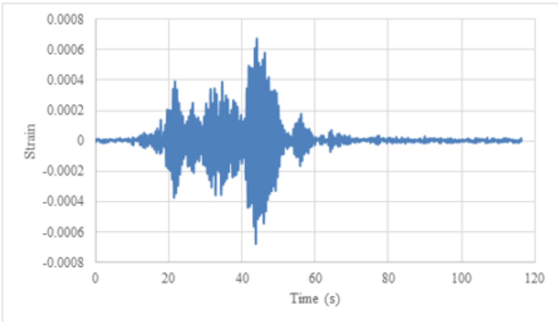

Figure 3.49. Front Strain Data.

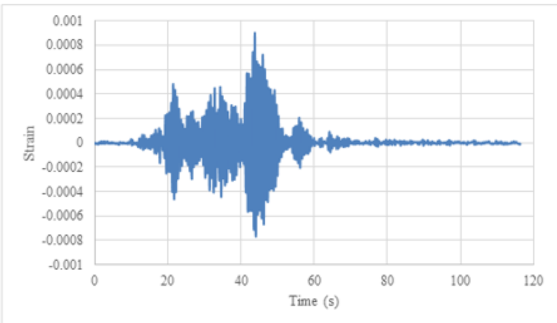

Figure 3.50. Back Strain Data.

3.5.8. Eighth Test (T=0.5s, 0.25 San Salvador)

Figure 3.51 to Figure 3.56 represent the data obtained from the eighth test.

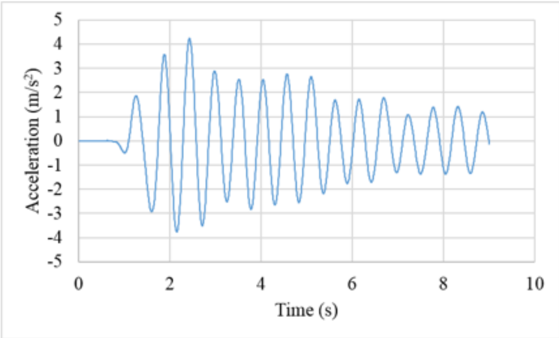

Figure 3.51. Acceleration Data from Accelerometer 1.

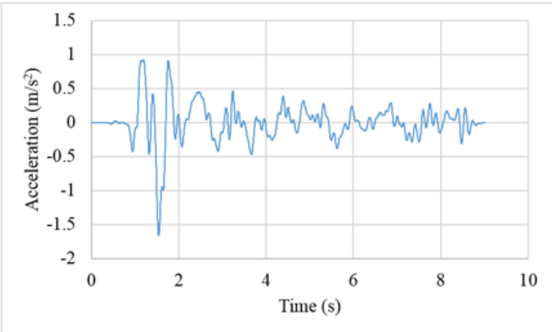

Figure 3.52. Acceleration Data from Accelerometer 2.

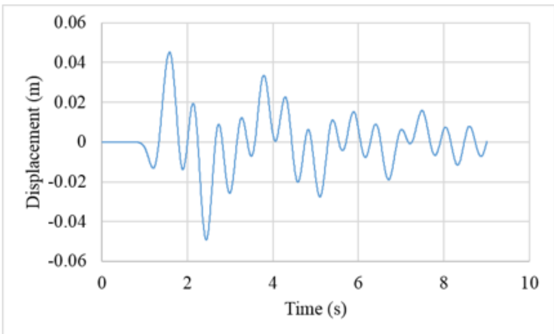

Figure 3.53. Displacement Data from LVDT 1.

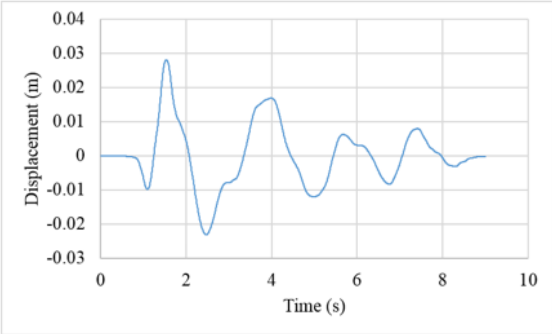

Figure 3.54. Displacement Data from LVDT 2.

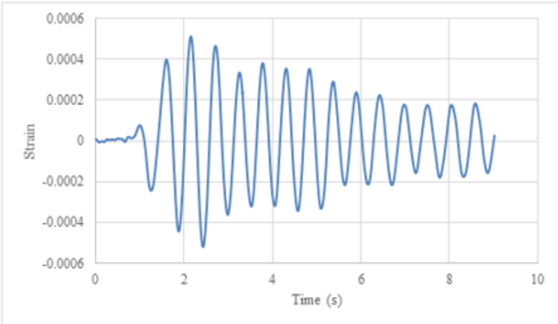

Figure 3.55. Front Strain Data.

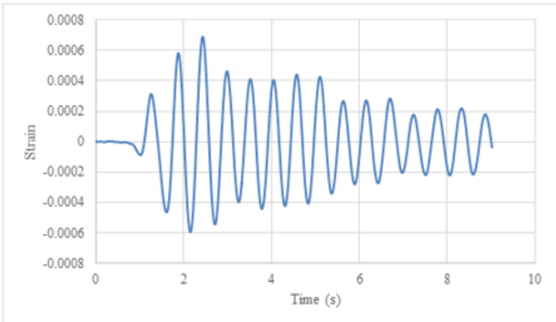

Figure 3.56. Back Strain Data.

3.5.9. Ninth Test (T=0.66s, 0.20 Chile)

Figure 3.57 to Figure 3.62 represent the data obtained from the ninth test.

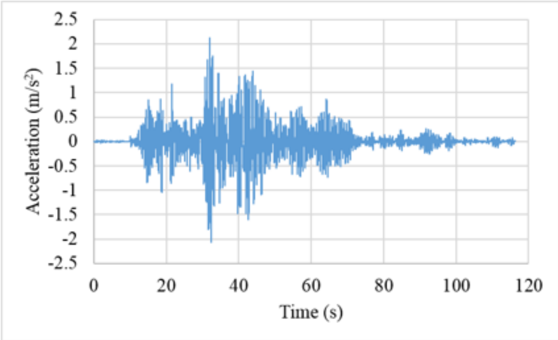

Figure 3.57. Acceleration Data from Accelerometer 1.

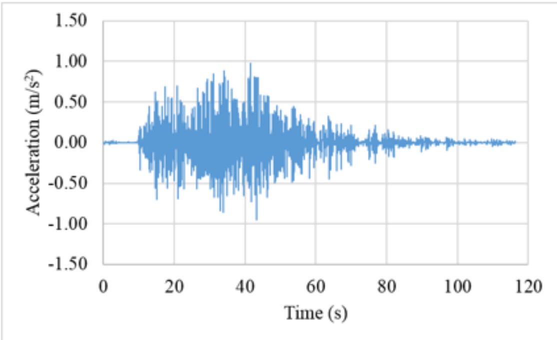

Figure 3.58. Acceleration Data from Accelerometer 2.

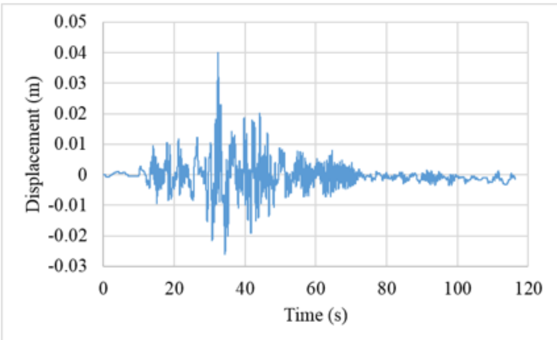

Figure 3.59. Displacement Data from LVDT 1.

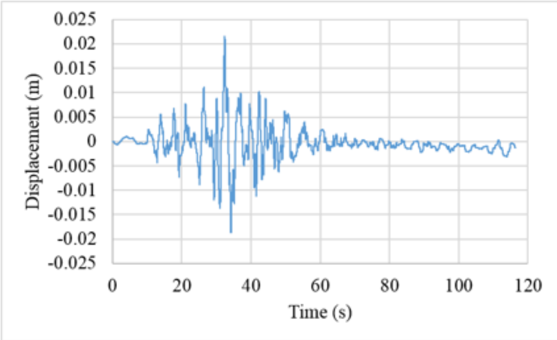

Figure 3.60. Displacement Data from LVDT 2.

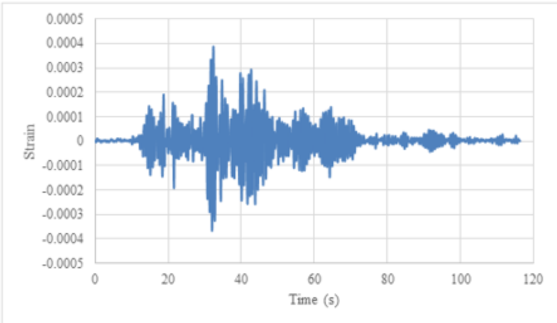

Figure 3.61. Front Strain Data.

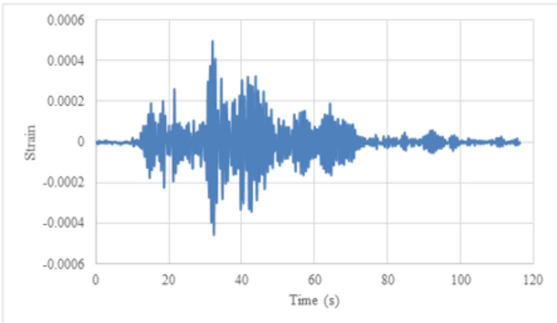

Figure 3.62. Back Strain Data.

3.5.10. Tenth Test (T=0.66s, 0.20 San Salvador)

Figure 3.63 to Figure 3.68 represent the data obtained from the tenth test.

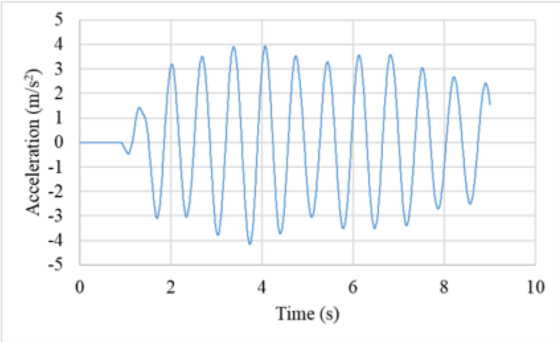

Figure 3.63. Acceleration Data from Accelerometer 1.

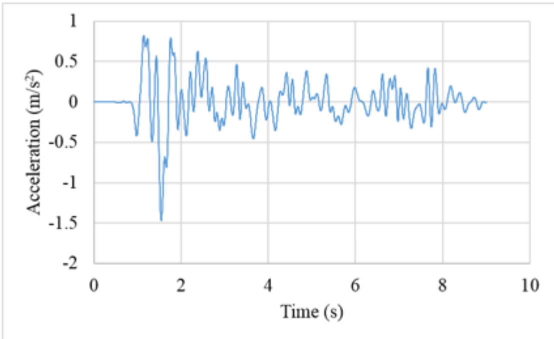

Figure 3.64. Acceleration Data from Accelerometer 2.

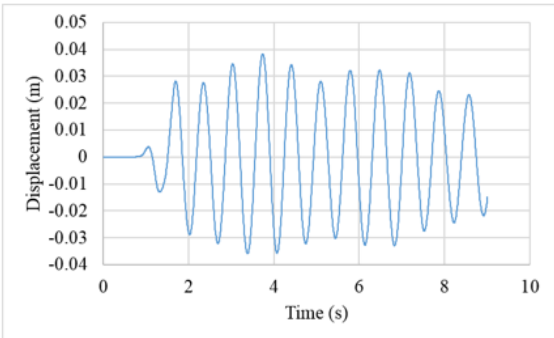

Figure 3.65. Displacement Data from LVDT 1.

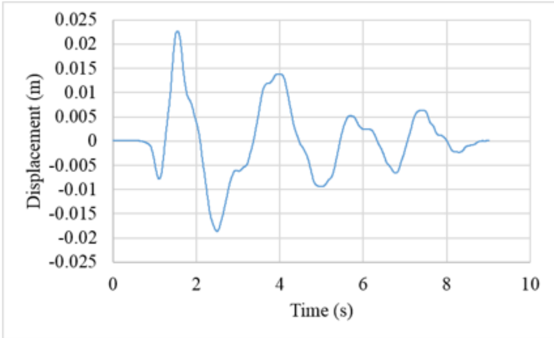

Figure 3.66. Displacement Data from LVDT 2.

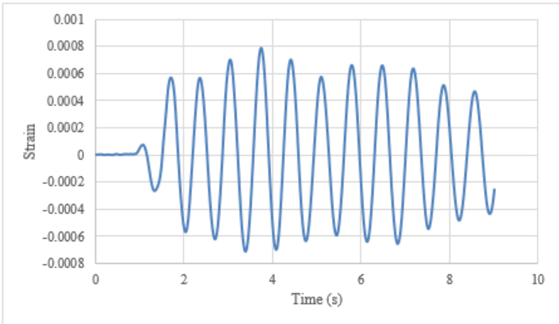

Figure 3.67. Front Strain Data.

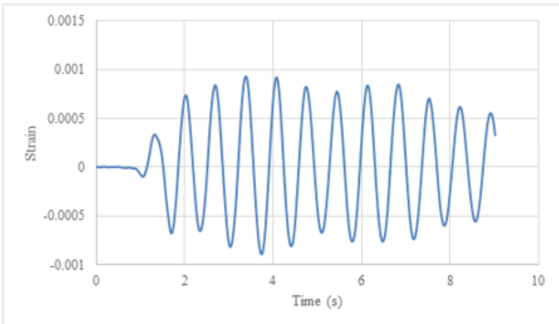

Figure 3.68. Back Strain Data.

3.5.11. Eleventh Test (T=0.66s, 0.25 Chile)

Figure 3.69 to Figure 3.74 represent the data obtained from the eleventh test.

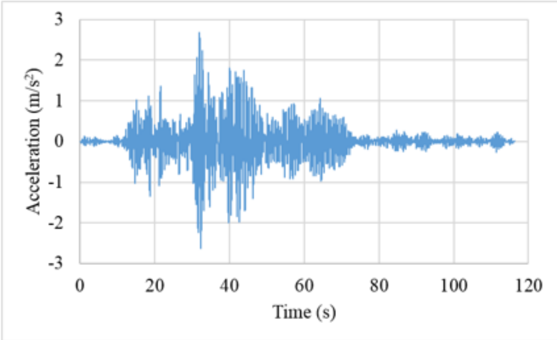

Figure 3.69. Acceleration Data from Accelerometer 1.

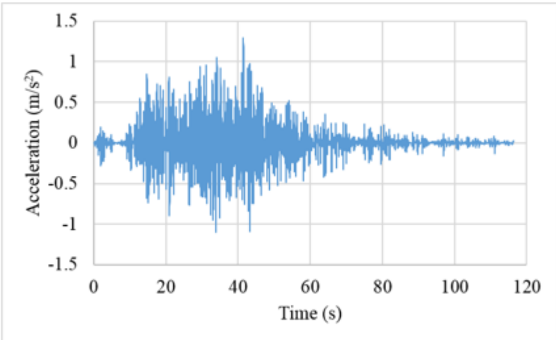

Figure 3.70. Acceleration Data from Accelerometer 2.

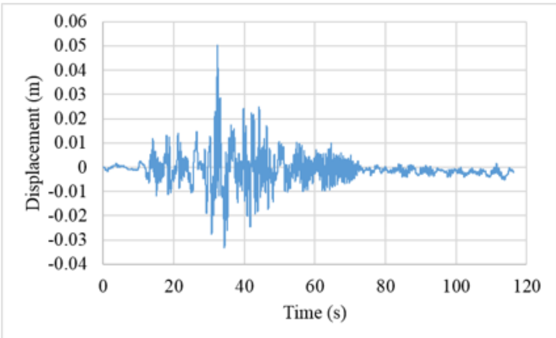

Figure 3.71. Displacement Data from LVDT 1.

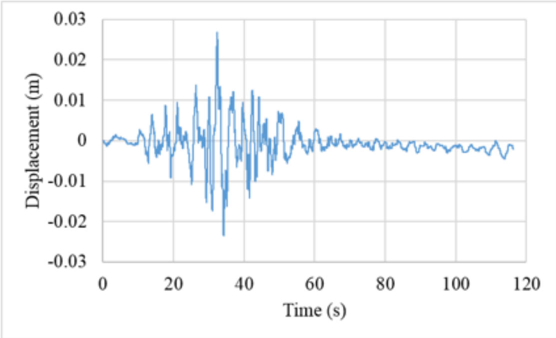

Figure 3.72. Displacement Data from LVDT 2.

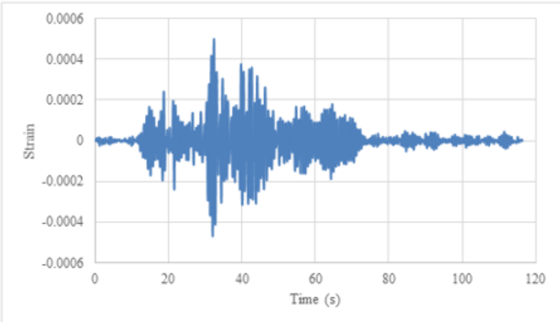

Figure 3.73. Front Strain Data.

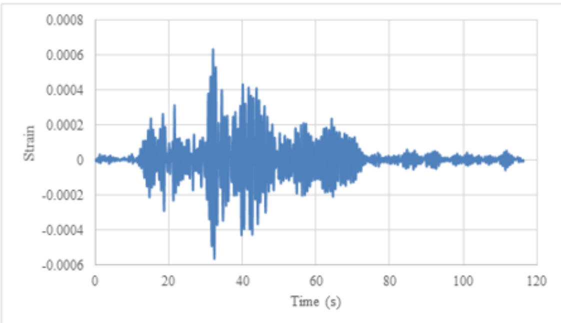

Figure 3.74. Back Strain Data.

3.5.12. Twelfth Test (T=0.66s, 0.25 San Salvador)

Figure 3.75 to Figure 3.80 represent the data obtained from the twelfth test.

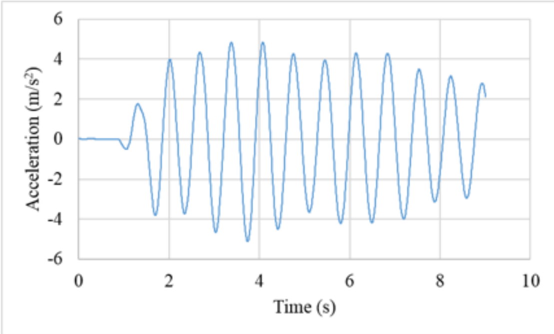

Figure 3.75. Acceleration Data from Accelerometer 1.

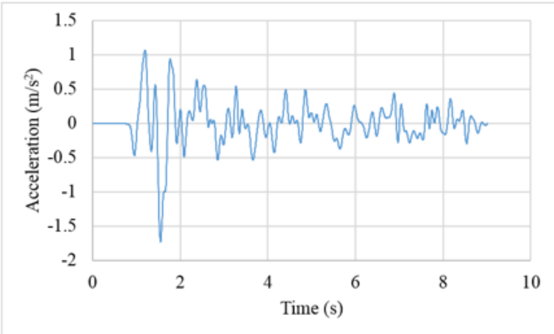

Figure 3.76. Acceleration Data from Accelerometer 2.

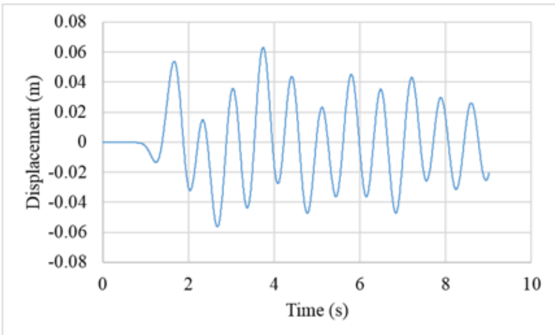

Figure 3.77. Displacement Data from LVDT 1.

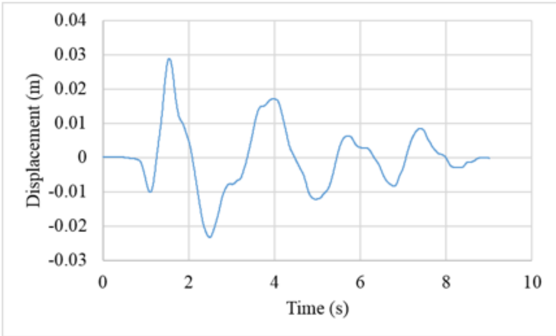

Figure 3.78. Displacement Data from LVDT 2.

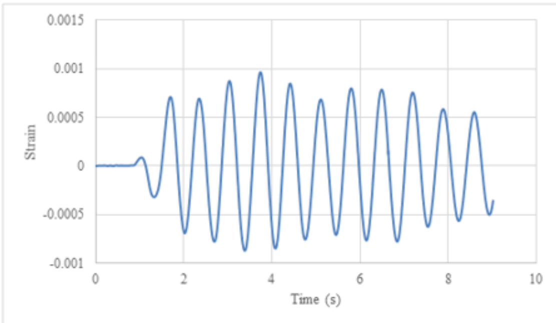

Figure 3.79. Front Strain Data.

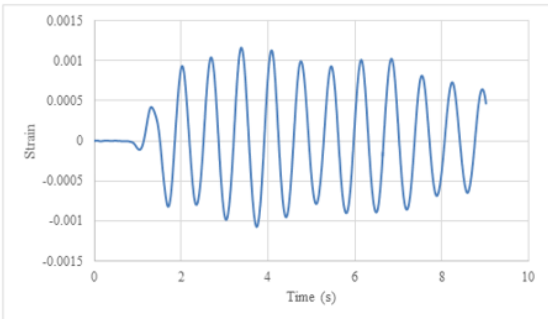

Figure 3.80. Back Strain Data.

4. ANALYSIS AND COMPARISON OF THE RESULTS

In this Chapter, results of all the different energy time history analyses of experimental and analytic results along with those obtained from SAP2000 are compared. In addition, results of moment-curvature, force-displacement and strain energy calculations based on strain data are presented in this Chapter. Also, the obtained experimental time history input energies are compared with the spectral values derived from the developed program in this study. Finally, the envelope of strain data for all the utilized seismic loads in the experiments are presented and compared due to the applied impact factors.

4.1. Displacement and Strain Energy Calculation Using Strain Data

As it is mentioned in the Chapter 3, all the process of Moment-Curvature analysis, which were discussed in Chapter 2, could be performed using the data obtained from strain gauges during the experiments. In order to compute strain energy it is necessary to obtain force-displacement relationship from the results of moment-curvature analysis. Values of force could be easily calculated by dividing the amounts of moment, M, which were obtained from moment-curvature analysis, by the cantilever length. However, the formulation of displacement calculation need to be derived referring to Figure 4.1. As it is discussed in the previous Chapter, *P-Delta* effect needs to be definitely taken into consideration in all the related calculations.

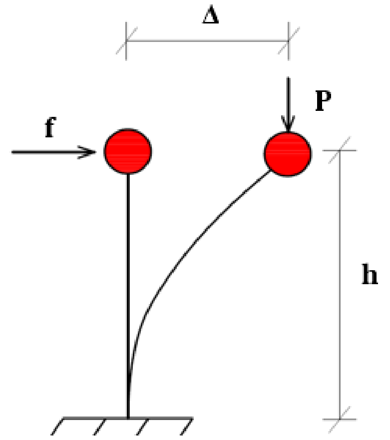

Figure 4.1. SDOF System Subjected by Lateral Force.

The value of displacement could be computed by dividing the force subjected to the system by the stiffness. The stiffness of a cantilever column considering the *P-Delta* effect (Figure 4.1) is as Equation 4.1 (Hibbeler, 1985);

$$k = \frac{3EI}{h^3} - \frac{P}{h} \tag{4.1}$$

where E is the Elasticity Modulus of the material, I is the moment of inertia of the cross section of the column, P is the weight of the mass on the system and h is the cantilever length. The displacement, Δ, of the system is calculated as Equation Equation 4.2.

$$\Delta = \frac{F}{k} = \frac{\frac{M}{h}}{\frac{3EI}{h^3} - \frac{P}{h}} = \frac{Mh^2}{3EI - Ph^2} \tag{4.2}$$

As it is previously mentioned, M is the value of moment derived from moment-curvature analysis. As the values for force and displacement is obtained, the force-displacement and strain energy (based on Equation 2.16) graphs could be drawn.

4.2. Comparison of the Energy Time History Results

In order to calculate experimental values of time history energy components, all the dynamic responses were read from the diverse sensors, which are mentioned at the beginning of Chapter 3, and inserted into the Equations 2.11-Equation 2.13 and Equation 2.16. Since all the experiments are performed in the elastic region of the material, the amount plastic energy is considered as zero (as explained in Chapter 2). In addition, the results of calculation for moment-curvature, force-displacement relationships and strain energy based on strain data is included for all the specimens.

4.2.1. First Test (T=0.4s, 0.2 Chile)

Figure 4.2 to Figure 4.10 depict the time history values of the responses and the energy components derived from the utilized methods along with moment-curvature, force-displacement and moment graphs based on strain data for the first test.

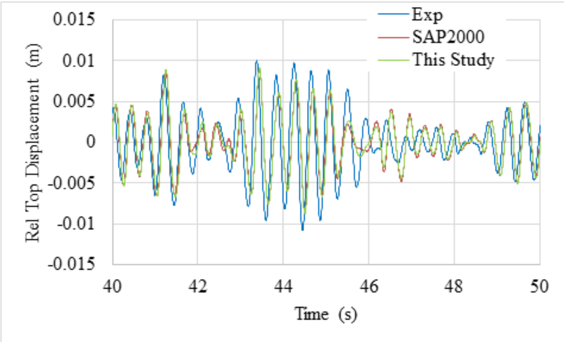

Figure 4.2. Relative Displacement Response.

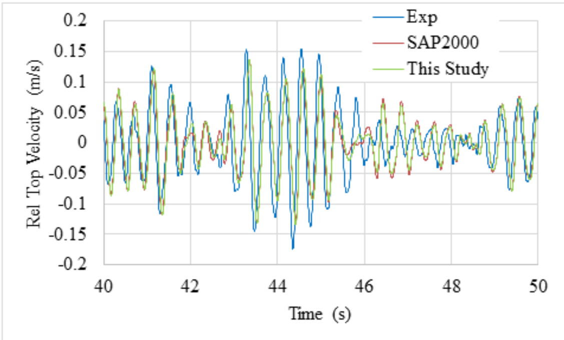

Figure 4.3. Relative Velocity Response.

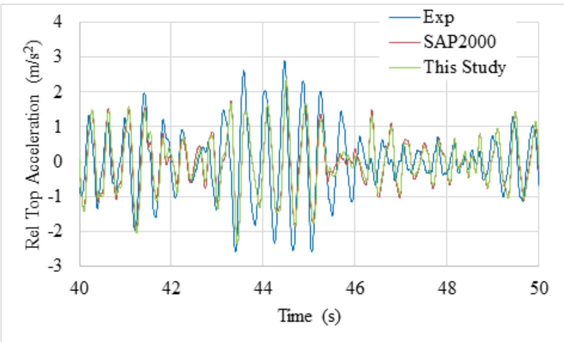

Figure 4.4. Relative Acceleration Response.

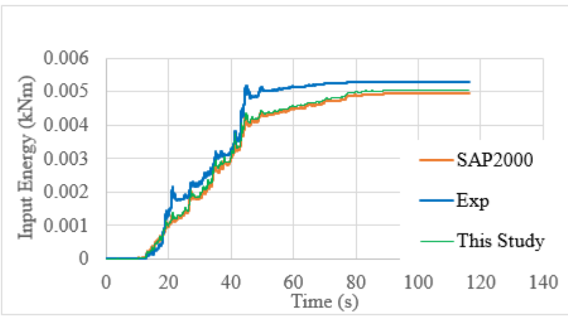

Figure 4.5. Relative Input Energy Response.

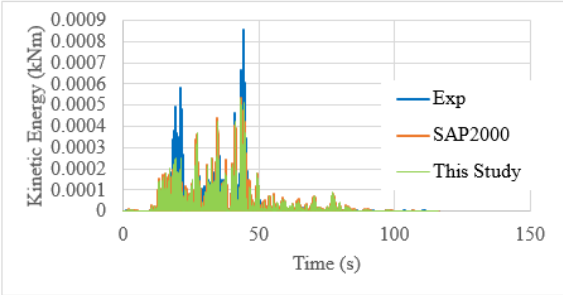

Figure 4.6. Relative Kinetic Energy Response.

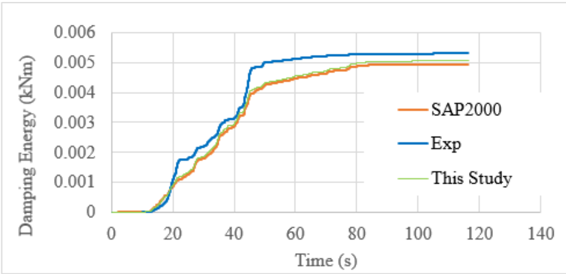

Figure 4.7. Damping Energy Response.

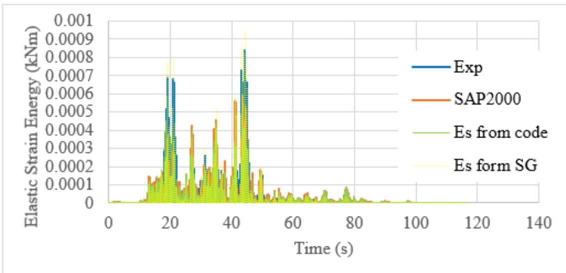

Figure 4.8. Strain Energy Response.

E_s (Strain Energy) from SG (Strain Gauge) in the above Figure refers to the amounts of strain energy calculated using the data obtained from strain gauges.

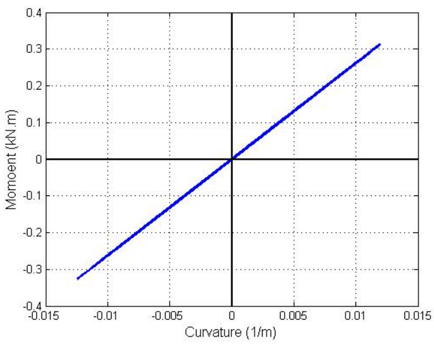

Figure 4.9. Moment-Curvature.

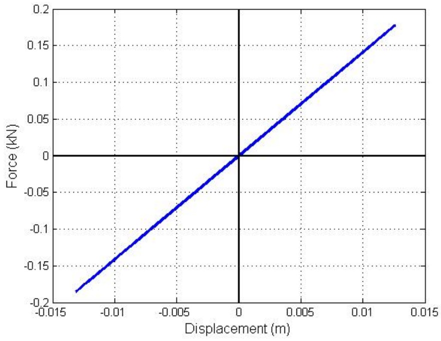

Figure 4.10. Moment-Curvature.

4.2.2. Second Test (T=0.4s, 0.2 San Salvador)

Figure 4.11 to Figure 4.19 depict the time history values of the responses and the energy components derived from the utilized methods along with moment-curvature, force-displacement and moment graphs based on strain data for the second test.

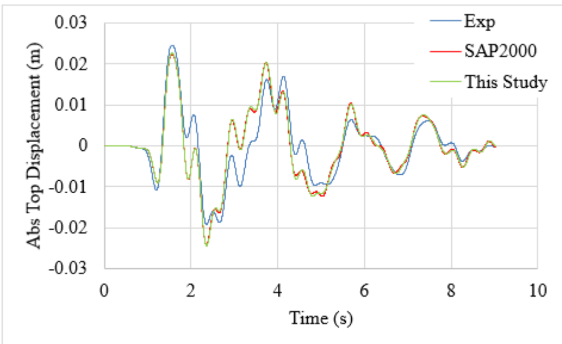

Figure 4.11. Relative Displacement Response.

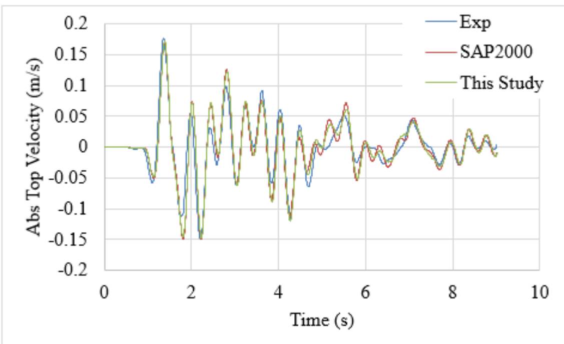

Figure 4.12. Relative Velocity Response.

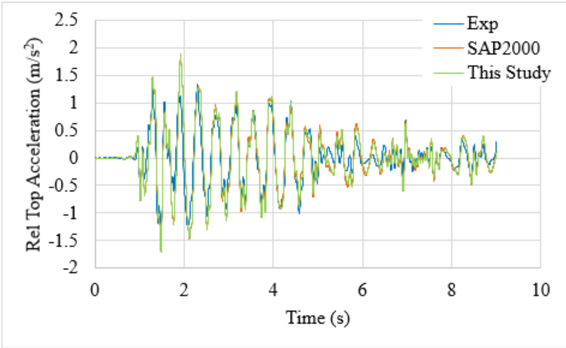

Figure 4.13. Relative Acceleration Response.

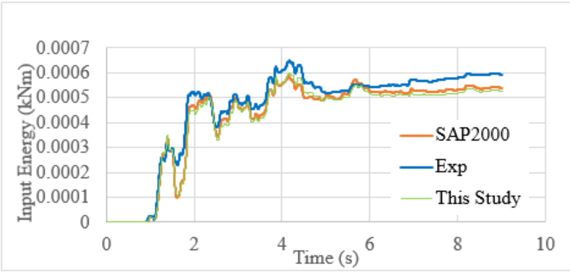

Figure 4.14. Relative Input Energy Response.

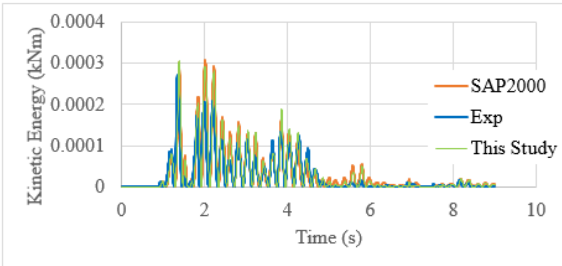

Figure 4.15. Relative Kinetic Input Energy Response.

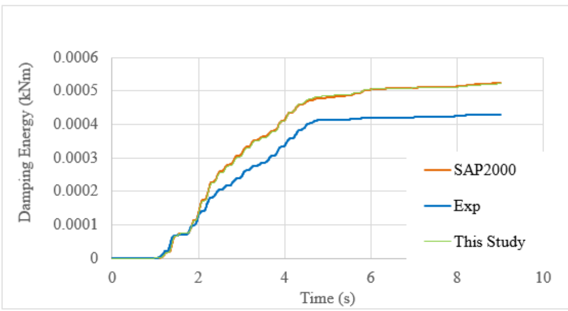

Figure 4.16. Damping Energy Response.

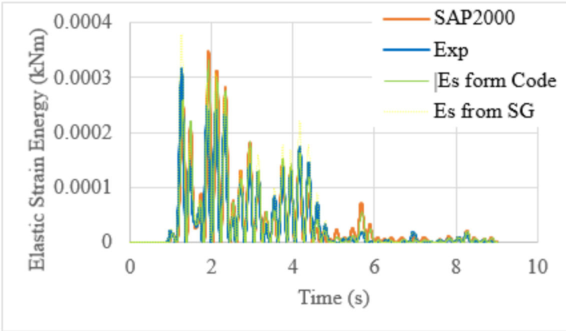

Figure 4.17. Strain Energy Response.

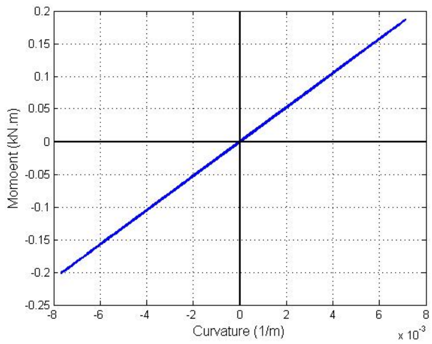

Figure 4.18. Moment-Curvature.

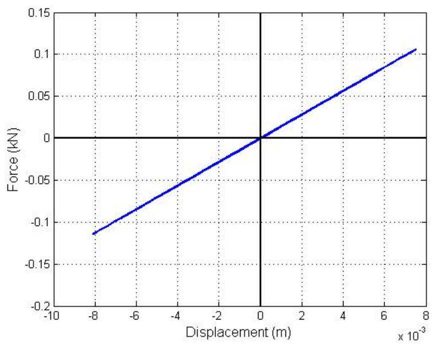

Figure 4.19. Force-Displacement.

4.2.3. Third Test (T=0.4s, 0.25 Chile)

Figure 4.20 to Figure 4.28 depict the time history values of the responses and the energy components derived from the utilized methods along with moment-curvature, force-displacement and moment graphs based on strain data for the third test.

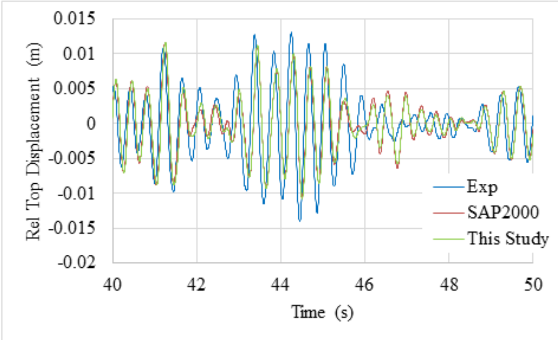

Figure 4.20. Relative Displacement Response.

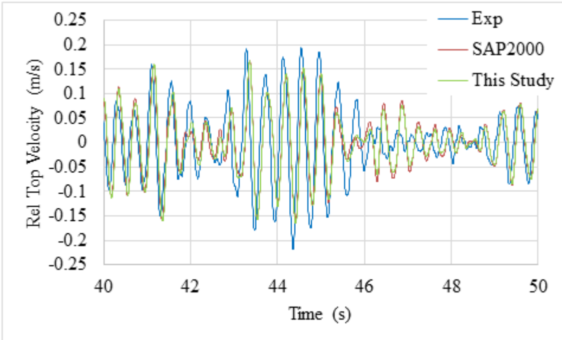

Figure 4.21. Relative Velocity Response.

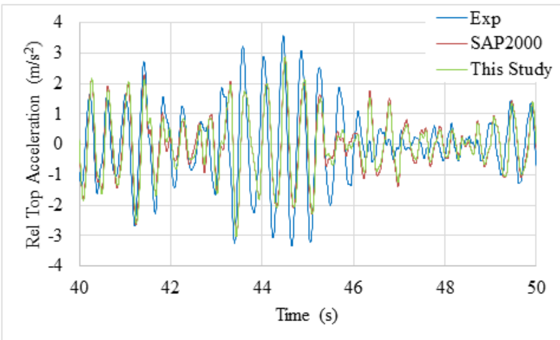

Figure 4.22. Relative Acceleration Response.

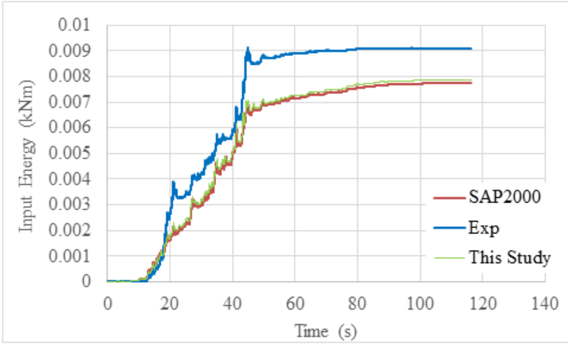

Figure 4.23. Relative Input Energy Response.

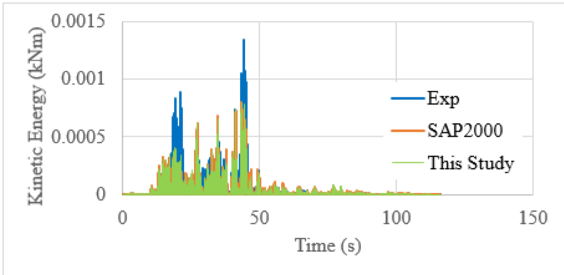

Figure 4.24. Relative Kinetic Energy Response.

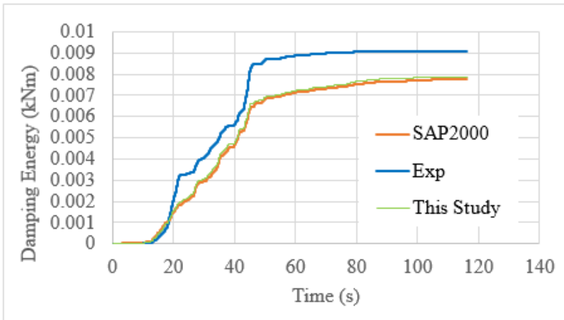

Figure 4.25. Damping Energy Response.

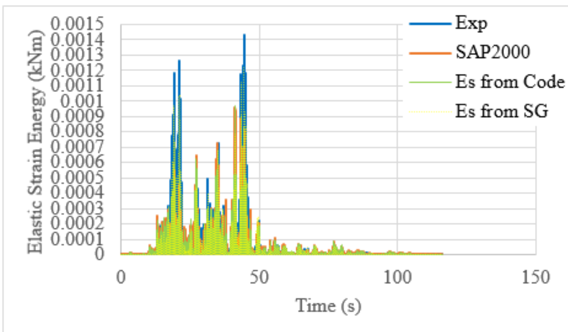

Figure 4.26. Strain Energy Response.

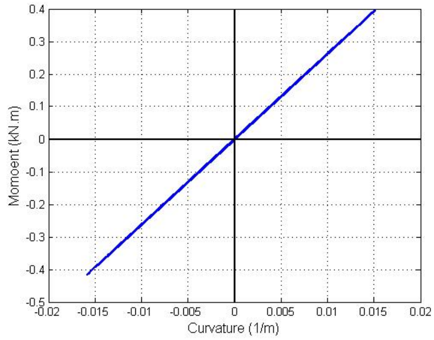

Figure 4.27. Moment-Curvature.

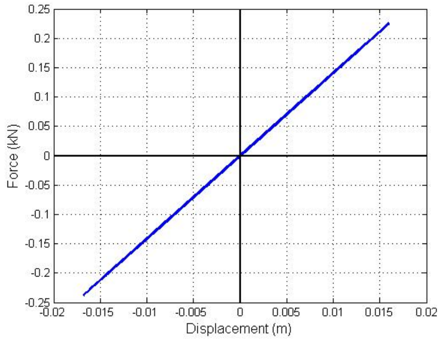

Figure 4.28. Force-Displacement.

4.2.4. Fourth Test (T=0.4s, 0.25 San Salvador)

Figure 4.29 to Figure 4.37 depict the time history values of the responses and the energy components derived from the utilized methods along with moment-curvature, force-displacement and moment graphs based on strain data for the fourth test.

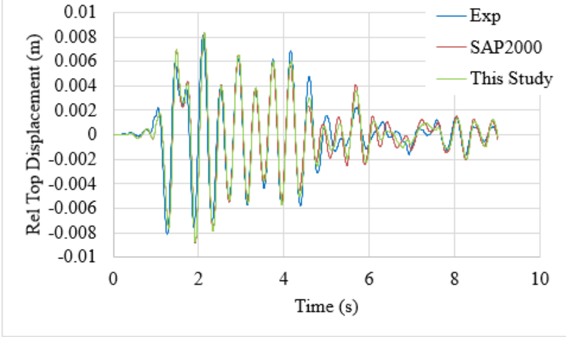

Figure 4.29. Relative Displacement Response.

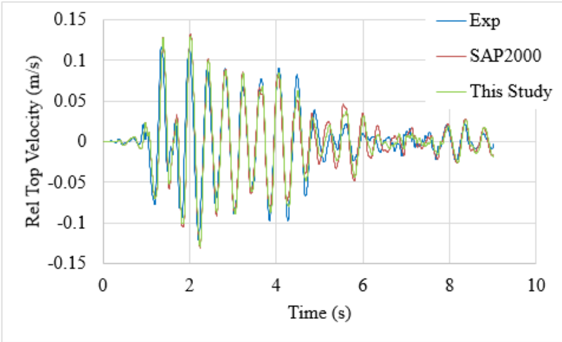

Figure 4.30. Relative Velocity Response.

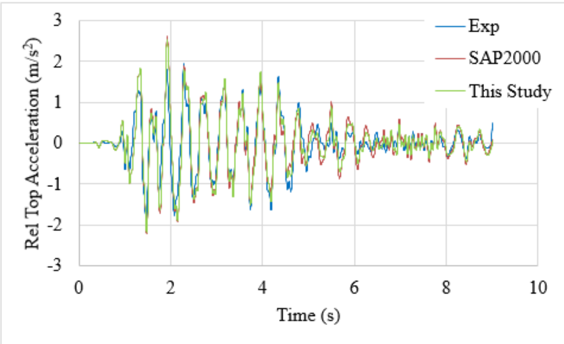

Figure 4.31. Relative Acceleration Response.

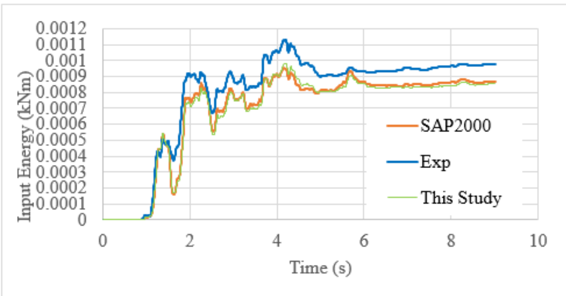

Figure 4.32. Relative Input Energy Response.

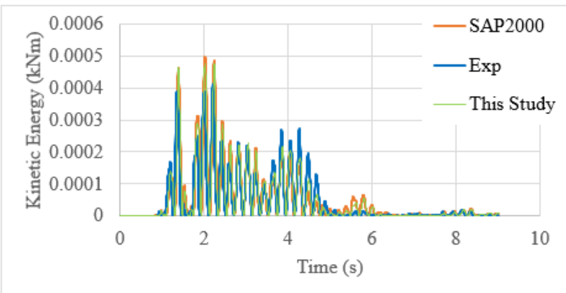

Figure 4.33. Relative Kinetic Energy Response.

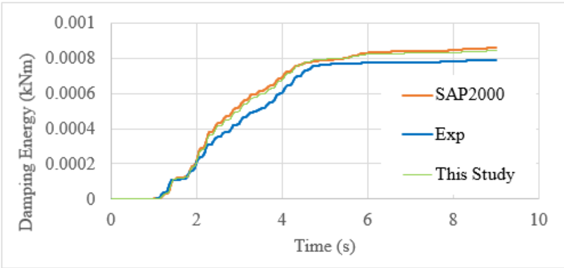

Figure 4.34. Damping Energy Response.

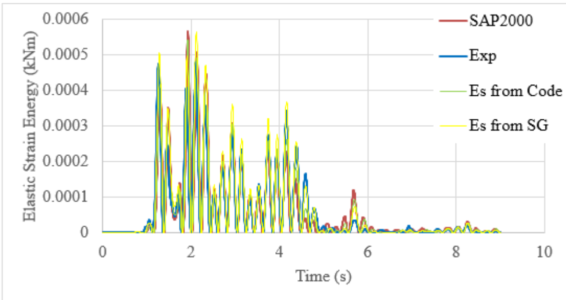

Figure 4.35. Strain Energy Response.

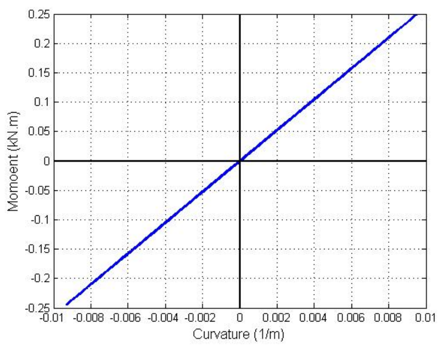

Figure 4.36. Moment-Curvature.

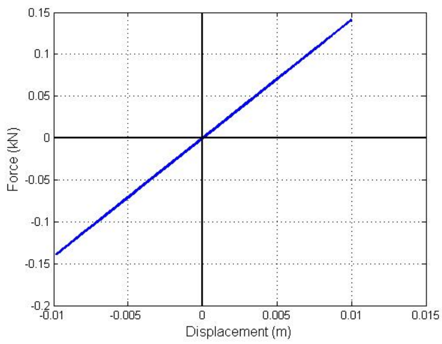

Figure 4.37. Force-Displacement.

4.2.5. Fifth Test (T=0.5s, 0.20 Chile)

Figure 4.38 to Figure 4.46 depict the time history values of the responses and the energy components derived from the utilized methods along with moment-curvature, force-displacement and moment graphs based on strain data for the fifth test.

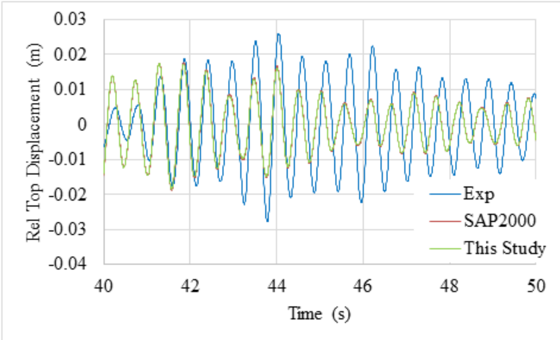

Figure 4.38. Relative Displacement Response.

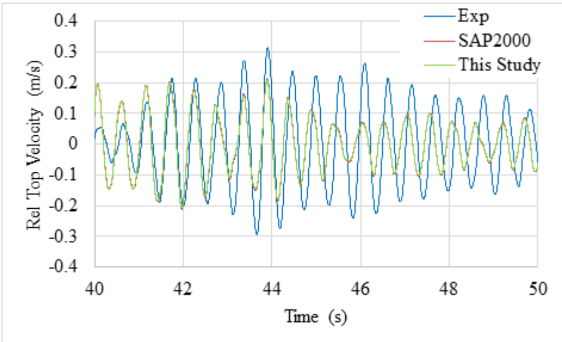

Figure 4.39. Relative Velocity Response.

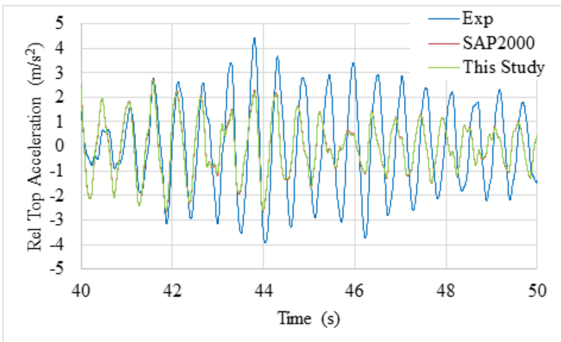

Figure 4.40. Relative Acceleration Response.

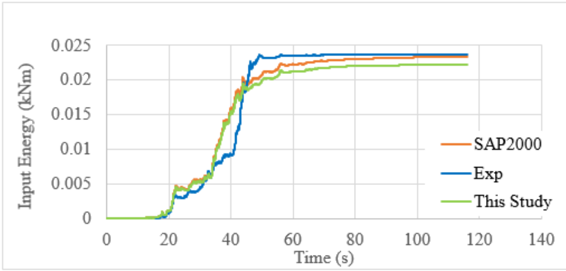

Figure 4.41. Relative Input Energy Response.

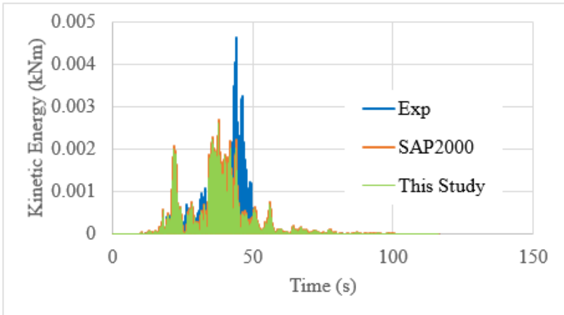

Figure 4.42. Relative Kinetic Energy Response.

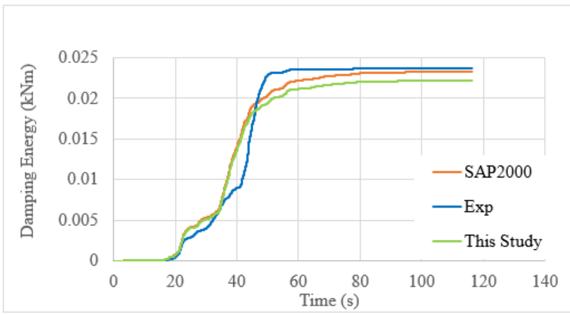

Figure 4.43. Damping Energy Response.

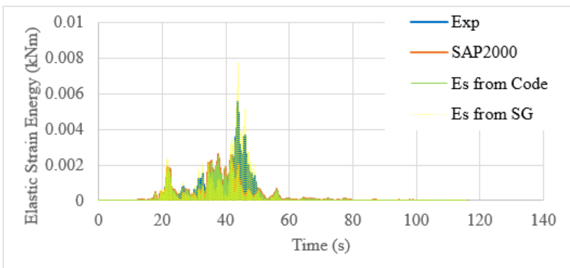

Figure 4.44. Strain Energy Response.

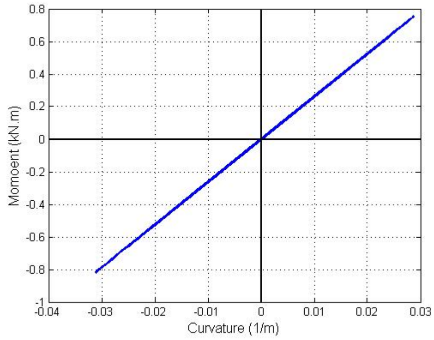

Figure 4.45. Moment-Curvature.

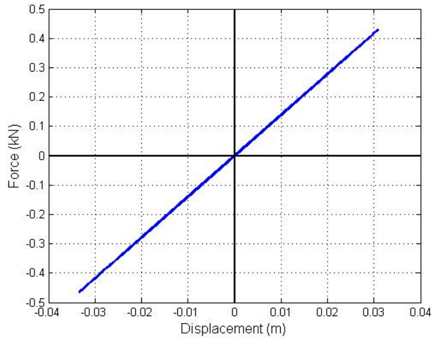

Figure 4.46. Force-Displacement.

4.2.6. Sixth Test (T=0.5s, 0.20 San Salvador)

Figure 4.47 to Figure 4.55 depict the time history values of the responses and the energy components derived from the utilized methods along with moment-curvature, force-displacement and moment graphs based on strain data for the sixth test.

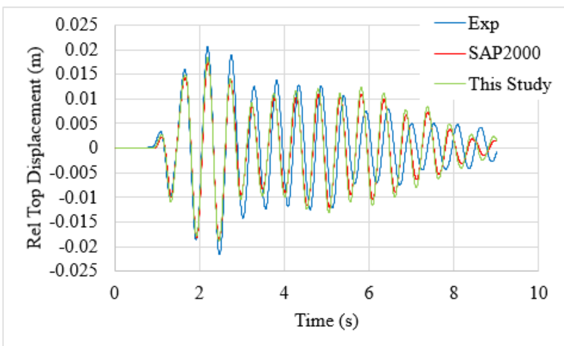

Figure 4.47. Relative Displacement Response.

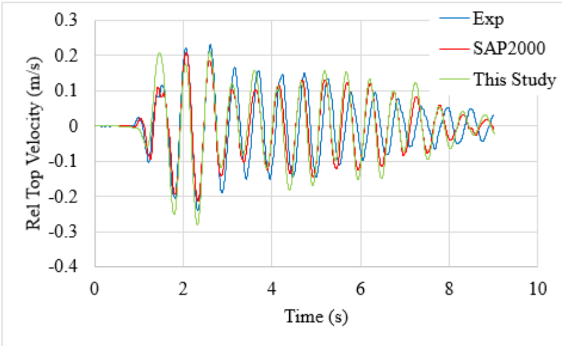

Figure 4.48. Relative Velocity Response.

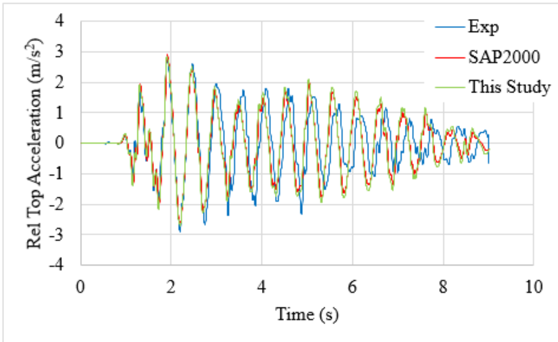

Figure 4.49. Relative Acceleration Response.

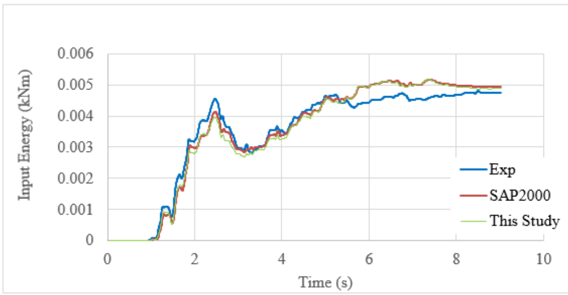

Figure 4.50. Relative Input Energy Response.

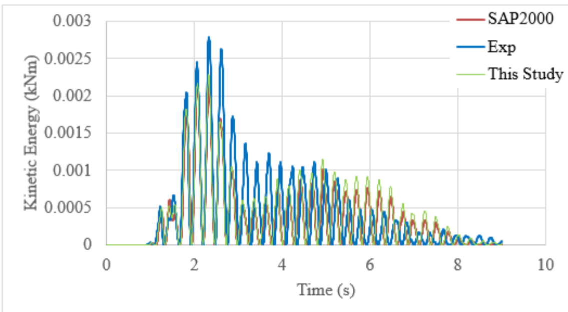

Figure 4.51. Relative Kinetic Energy Response.

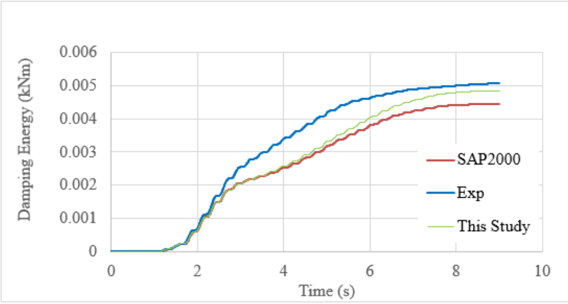

Figure 4.52. Damping Energy Response.

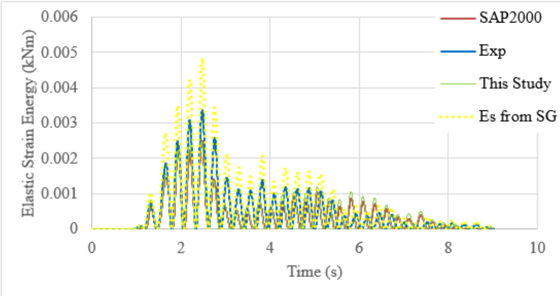

Figure 4.53. Strain Energy Response.

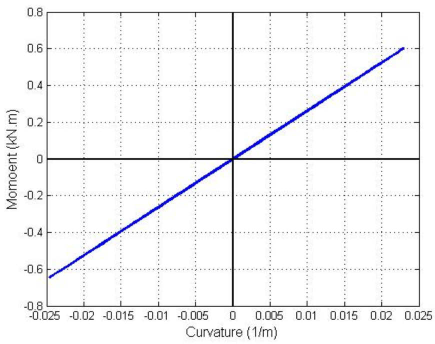

Figure 4.54. Moment-Curvature.

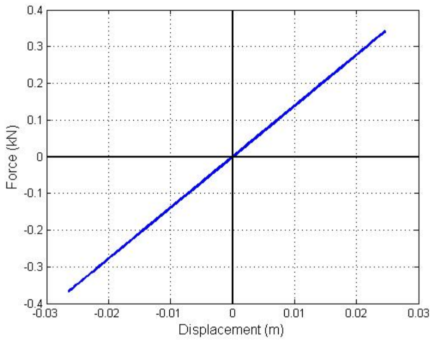

Figure 4.55. Force-Displacement.

4.2.7. Seventh Test (T=0.5s, 0.25 Chile)

Figure 4.56 to Figure 4.64 depict the time history values of the responses and the energy components derived from the utilized methods along with moment-curvature, force-displacement and moment graphs based on strain data for the seventh test.

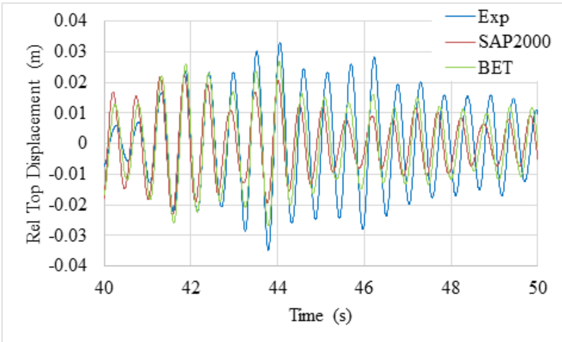

Figure 4.56. Relative Displacement Response.

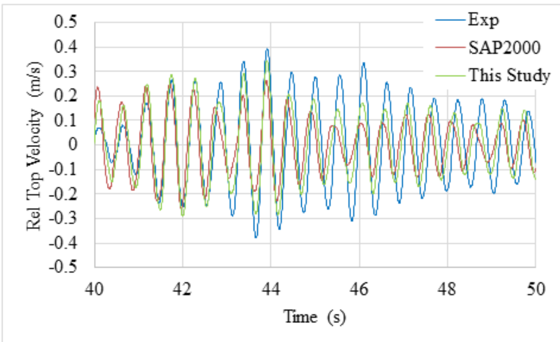

Figure 4.57. Relative Velocity Response.

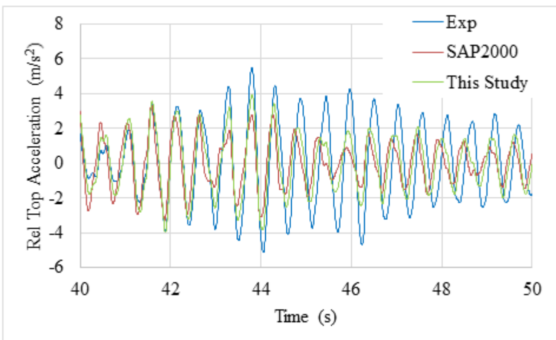

Figure 4.58. Relative Acceleration Response.

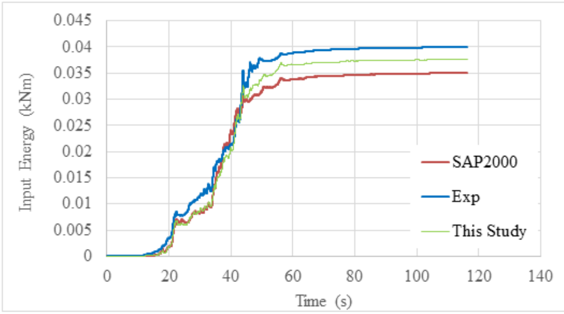

Figure 4.59. Relative Input Energy Response.

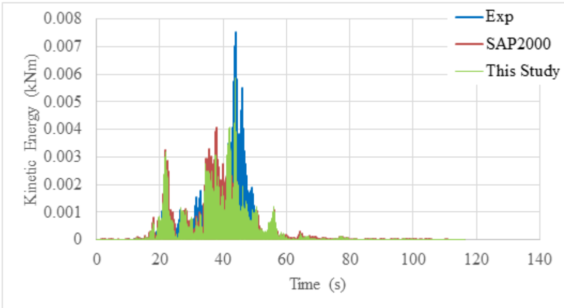

Figure 4.60. Relative Kinetic Energy Response.

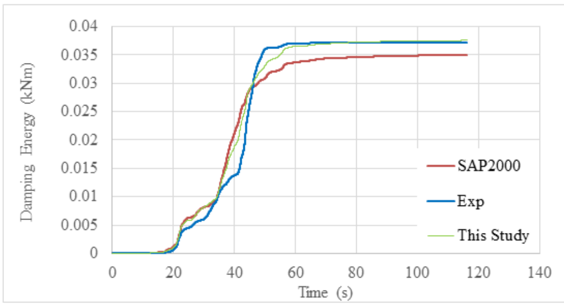

Figure 4.61. Damping Energy Response.

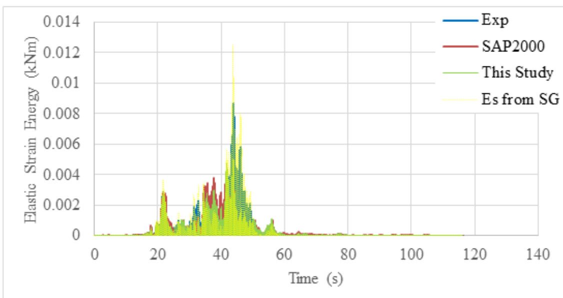

Figure 4.62. Strain Energy Response.

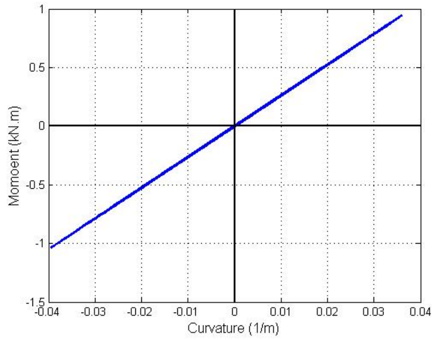

Figure 4.63. Moment-Curvature.

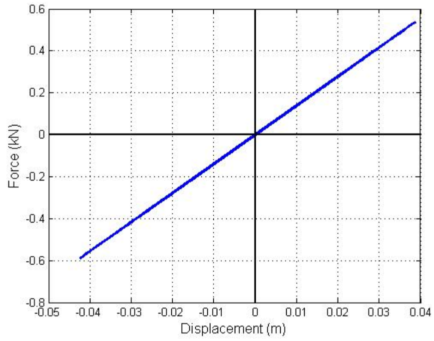

Figure 4.64. Force-Displacement.

4.2.8. Eighth Test (T=0.5s, 0.25 San Salvador)

Figure 4.65 to Figure 4.73 depict the time history values of the responses and the energy components derived from the utilized methods along with moment-curvature, force-displacement and moment graphs based on strain data for the eighth test.

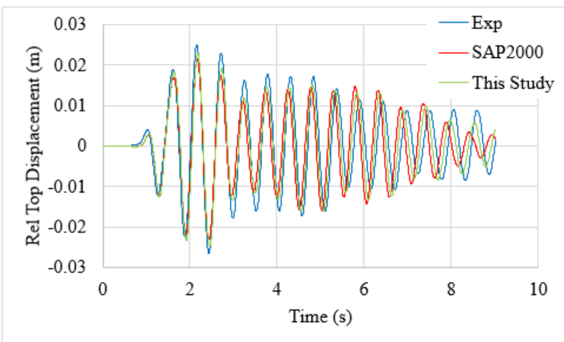

Figure 4.65. Relative Displacement Response.

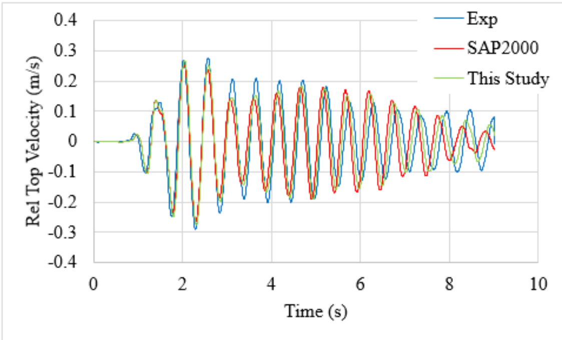

Figure 4.66. Relative Velocity Response.

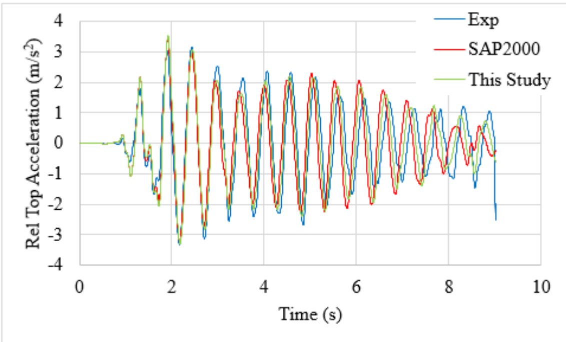

Figure 4.67. Relative Acceleration Response.

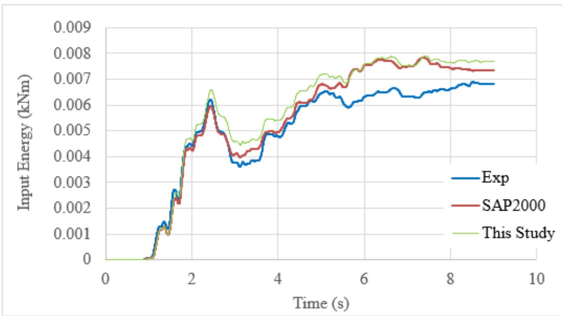

Figure 4.68. Relative Input Energy Response.

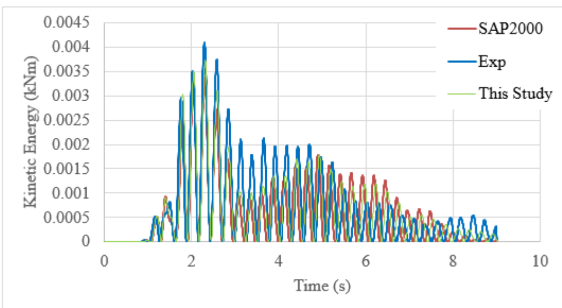

Figure 4.69. Relative Kinetic Energy Response.

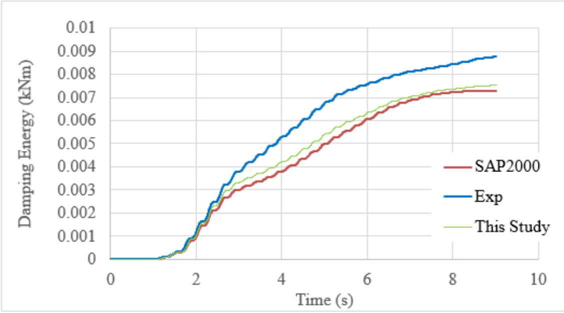

Figure 4.70. Damping Energy Response.

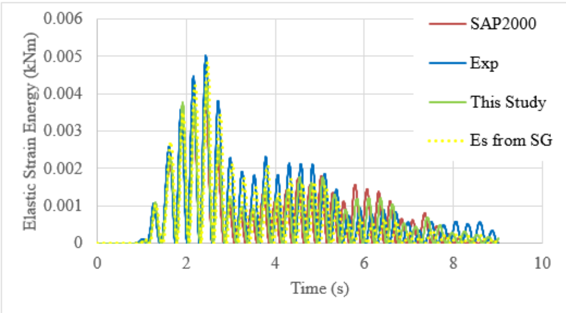

Figure 4.71. Strain Energy Response.

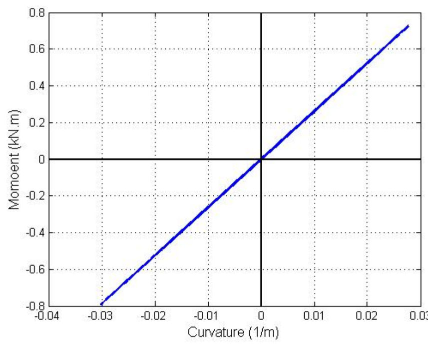

Figure 4.72. Moment-Curvature.

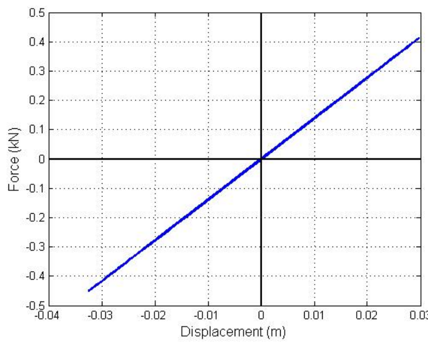

Figure 4.73. Force-Displacement.

4.2.9. Ninth Test (T=0.66s, 0.20 Chile)

Figure 4.74 to Figure 4.82 depict the time history values of the responses and the energy components derived from the utilized methods along with moment-curvature, force-displacement and moment graphs based on strain data for the ninth test.

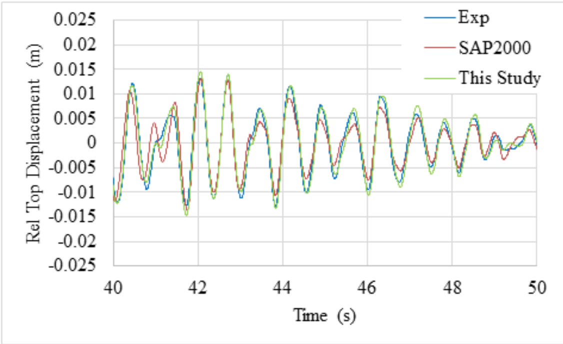

Figure 4.74. Relative Displacement Response.

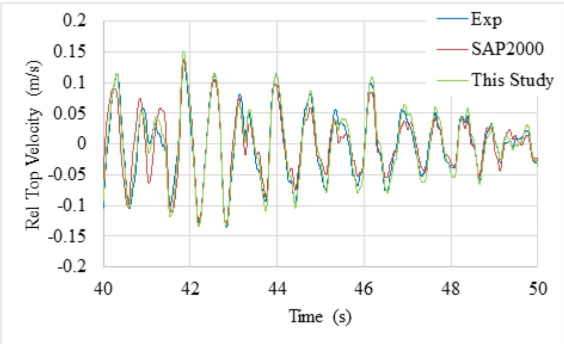

Figure 4.75. Relative Velocity Response.

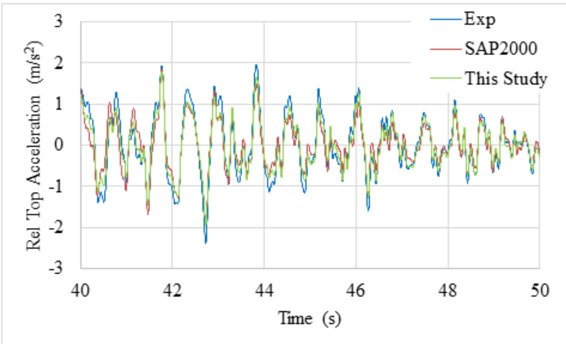

Figure 4.76. Relative Acceleration Response.

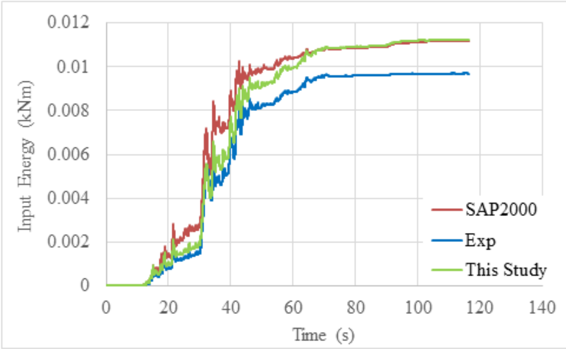

Figure 4.77. Relative Input Energy Response.

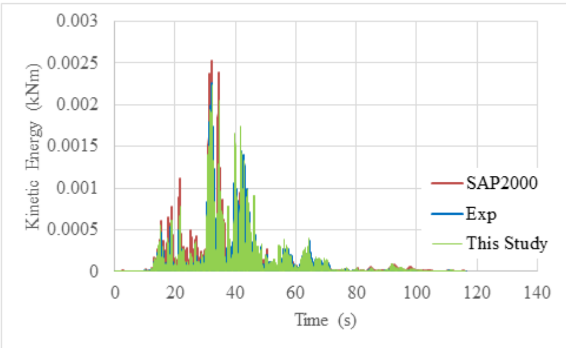

Figure 4.78. Relative Kinetic Energy Response.

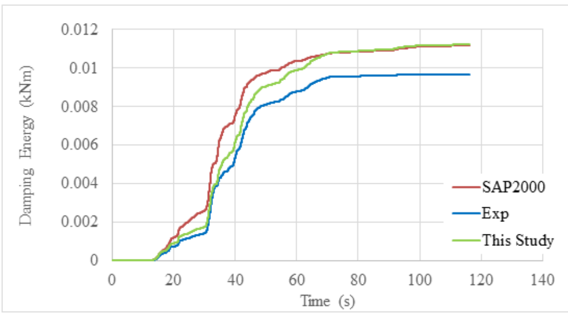

Figure 4.79. Damping Energy Response.

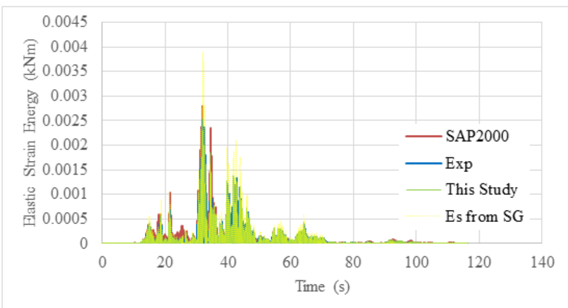

Figure 4.80. Strain Energy Response.

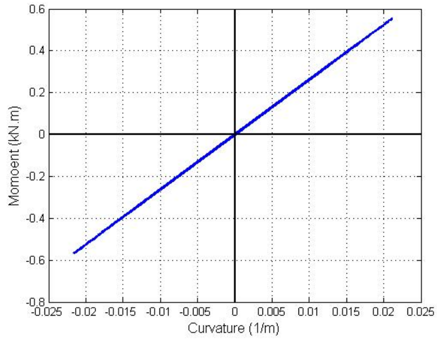

Figure 4.81. Moment-Curvature.

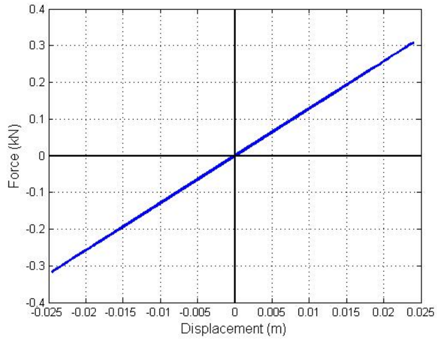

Figure 4.82. Force-Displacement.

4.2.10. Tenth Test (T=0.66s, 0.20 San Salvador)

Figure 4.83 to Figure 4.91 depict the time history values of the responses and the energy components derived from the utilized methods along with moment-curvature, force-displacement and moment graphs based on strain data for the tenth test.

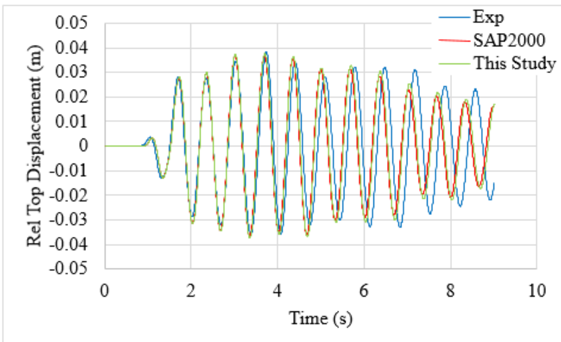

Figure 4.83. Relative Displacement Response.

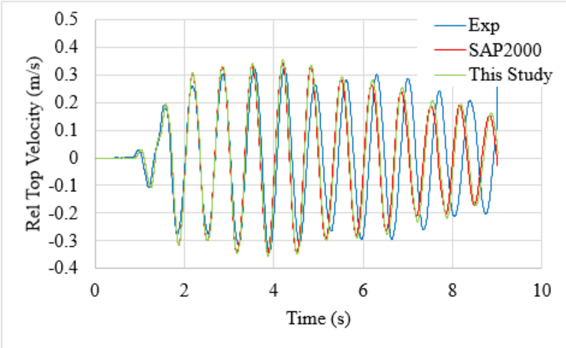

Figure 4.84. Relative Velocity Response.

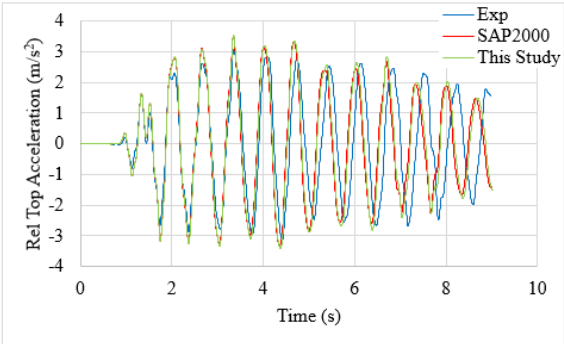

Figure 4.85. Relative Acceleration Response.

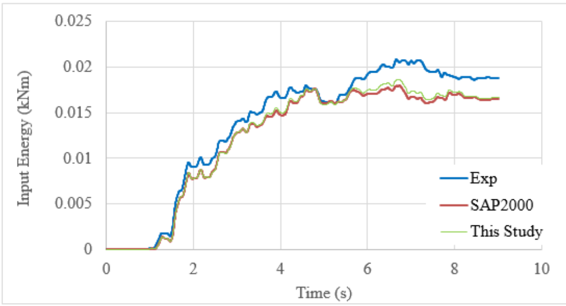

Figure 4.86. Relative Input Energy Response.

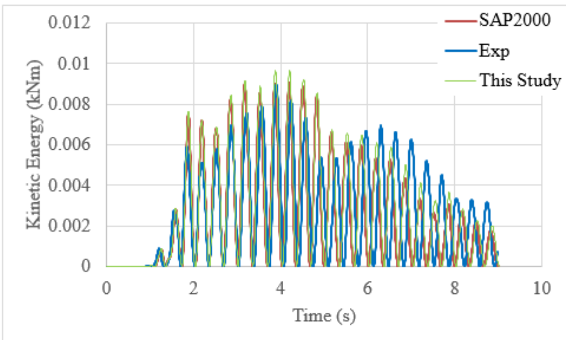

Figure 4.87. Relative Kinetic Energy Response.

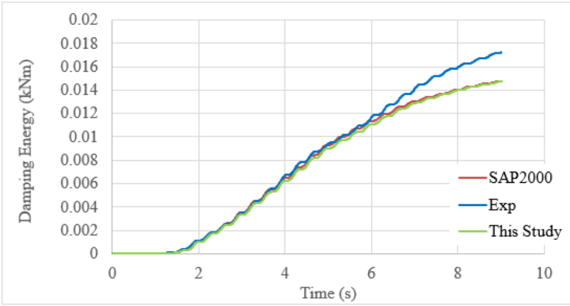

Figure 4.88. Damping Energy Response.

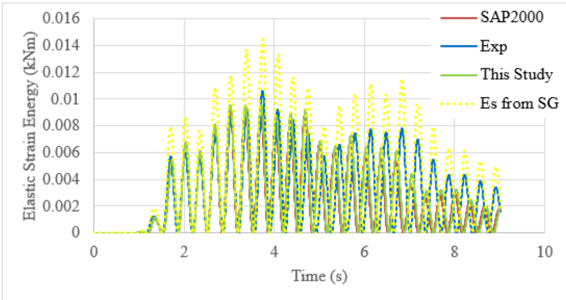

Figure 4.89. Strain Energy Response.

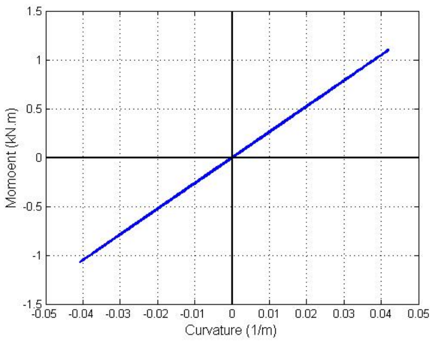

Figure 4.90. Moment-Curvature.

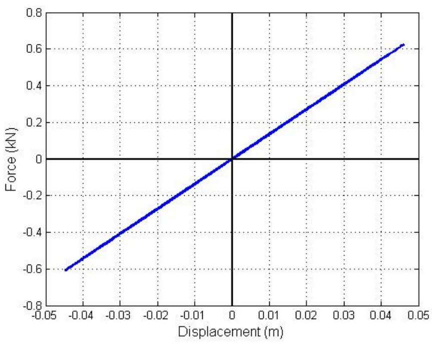

Figure 4.91. Force-Displacement.

4.2.11. Eleventh Test (T=0.66s, 0.25 Chile)

Figure 4.92 to Figure 4.100 depict the time history values of the responses and the energy components derived from the utilized methods along with moment-curvature, force-displacement and moment graphs based on strain data for the eleventh test.

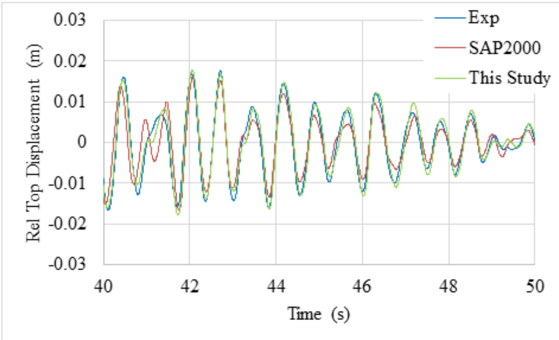

Figure 4.92. Relative Displacement Response.

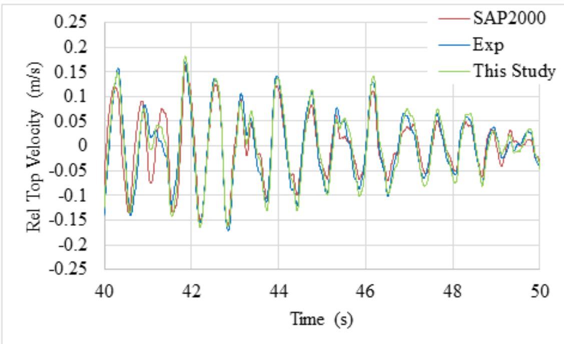

Figure 4.93. Relative Velocity Response.

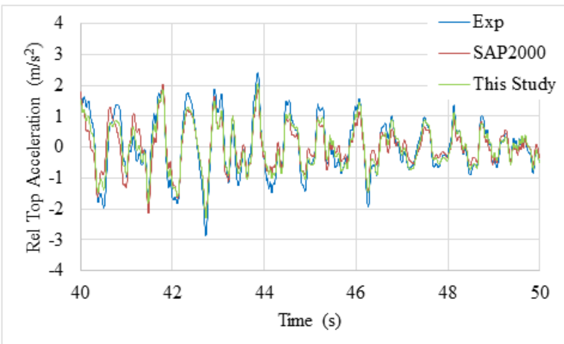

Figure 4.94. Relative Acceleration Response.

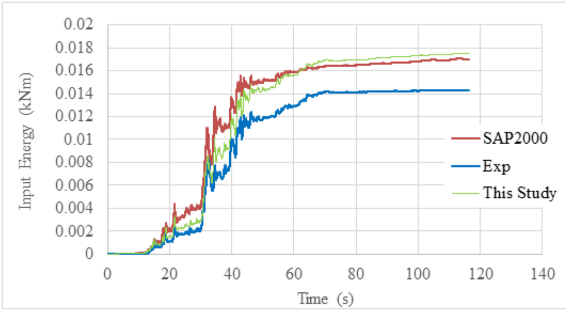

Figure 4.95. Relative Input Energy Response.

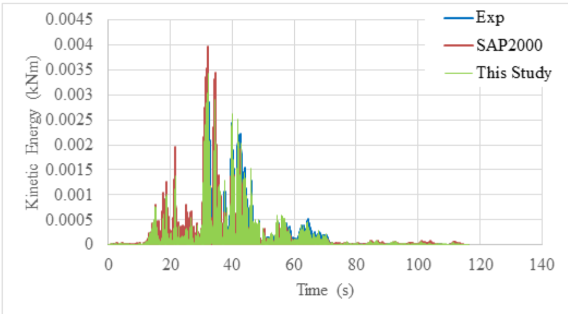

Figure 4.96. Relative Kinetic Energy Response.

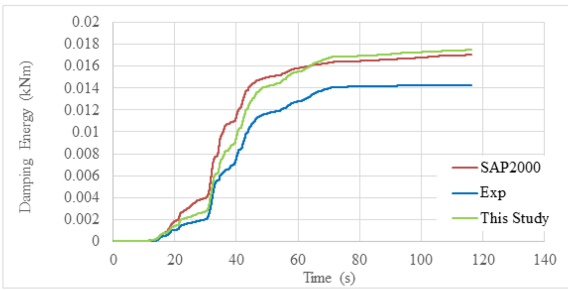

Figure 4.97. Damping Energy Response.

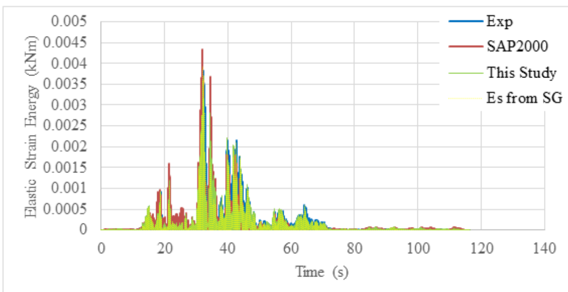

Figure 4.98. Strain Energy Response.

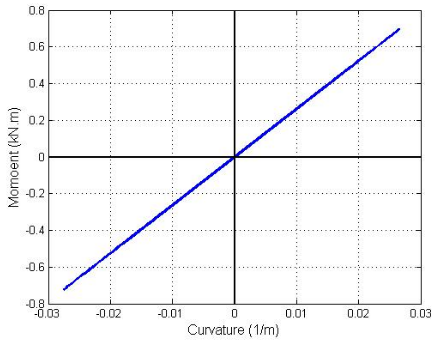

Figure 4.99. Moment-Curvature.

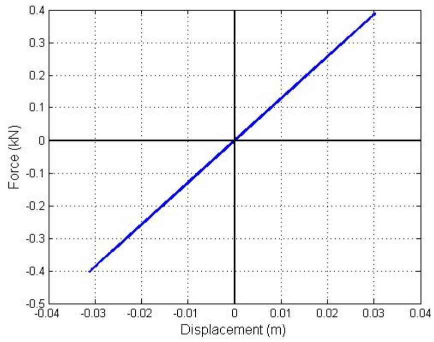

Figure 4.100. Force-Displacement.

4.2.12. Twelfth Test (T=0.66s, 0.25 San Salvador)

Figure 4.101 to Figure 4.109 depict the time history values of the responses and the energy components derived from the utilized methods along with moment-curvature, force - displacement and moment graphs based on strain data for the twelfth test.

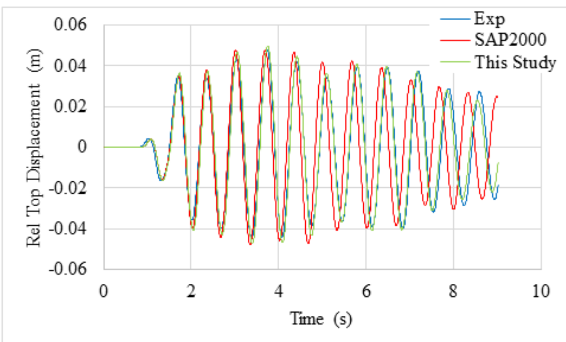

Figure 4.101. Relative Displacement Response.

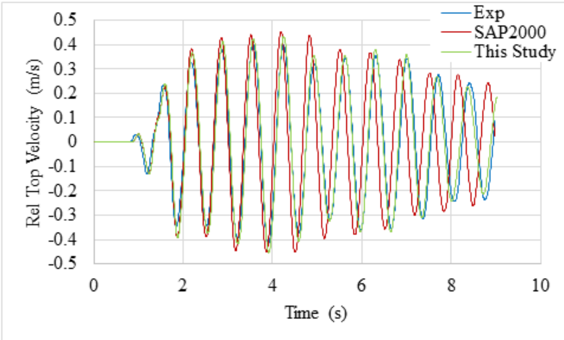

Figure 4.102. Relative Velocity Response.

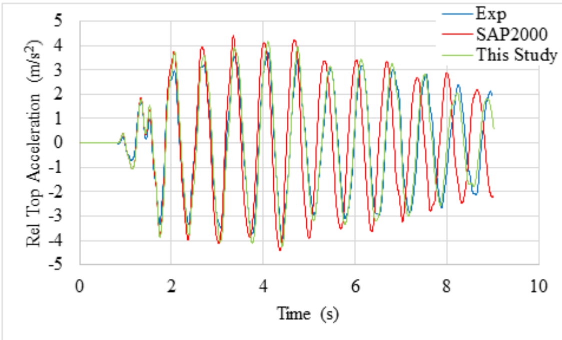

Figure 4.103. Relative Acceleration Response.

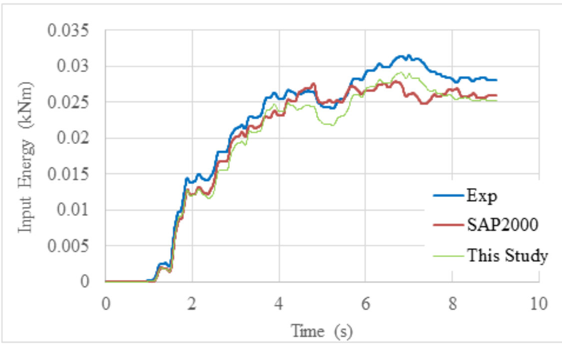

Figure 4.104. Relative Input Energy Response.

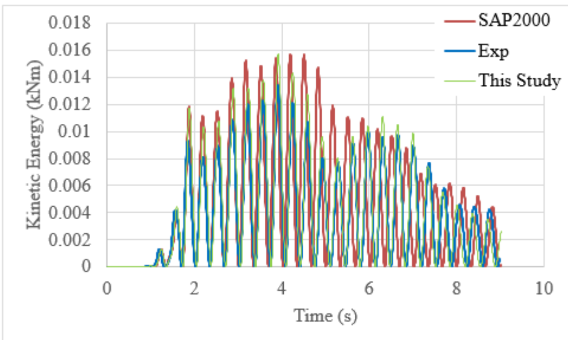

Figure 4.105. Relative Kinetic Energy Response.

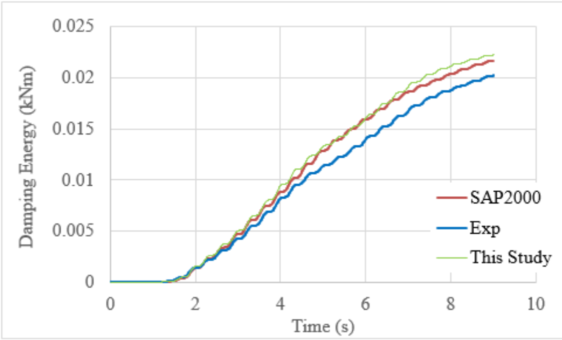

Figure 4.106. Damping Energy Response.

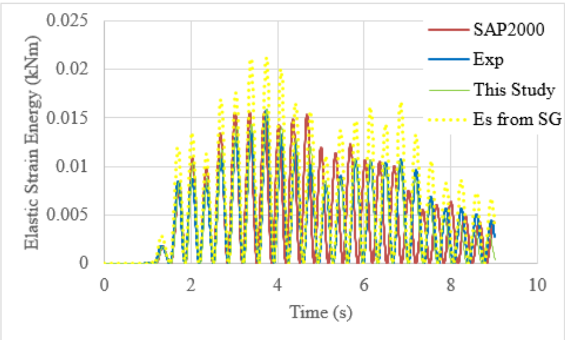

Figure 4.107. Strain Energy Response.

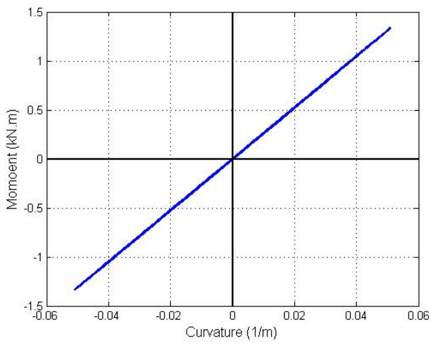

Figure 4.108. Moment-Curvature.

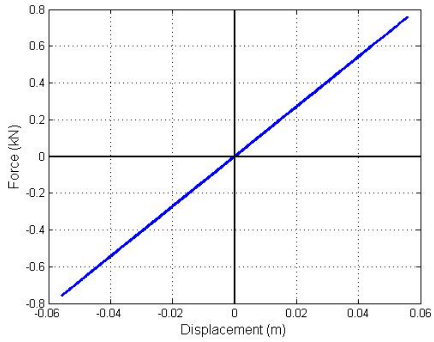

Figure 4.109. Force-Displacement.

Having considered all the figures in Section 4.2, it could be concluded that all the methods used for energy components calculation (experimental, developed algorithm in this study and SAP2000) are in good agreement. In addition, as it could be observed in strain energy graphs, strain energy calculation using the data obtained from strain gauges, installed on both sides of the specimens, is a reliable approach. Also, it is noticed that amount of input energy is approximately equal to that of damping energy in the whole experiments. It implies that all the imparted input energy into the specimens is dissipated by inherent damping of the system.

However, it could be noticed that the results obtained from modal analysis in SAP2000 and the developed program in this study are closer compared to those obtained from experiments. It could be explained due to accuracy of the sensors. That is, by using such sensors which are capable of obtaining data with more exactness, the observed differences could have been negligible.

4.3. Comparing the Test Results with Input Energy Response Spectra

In this Section the values experimental input energy responses are compared with those of analytic analyses. For this purpose, Acceleration Response Spectrum (ARS) and input energy response spectrum of the seismic records are drawn for each test pair (the two test tests which were performed for the same period and scale factor) using the acceleration data obtained from the accelerometer on the shake table. As expected, each loading pair have similar ARS but different input energy response spectra. Next, the comparison between the last input energy time history value and the related spectral value is made for all the twelve experiments.

Figure 4.110 to Figure 4.113 depict the acceleration response spectra and input energy response spectra for the pairs of experiments which their period is 0.40 seconds.

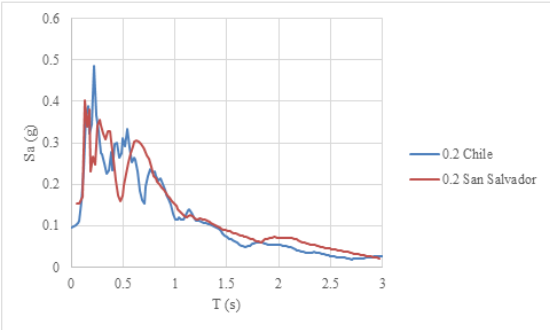

Figure 4.110. Acceleration Response Spectra (T=0.40s).

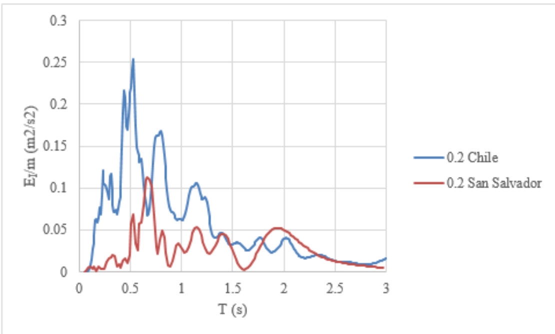

Figure 4.111. Input Energy Response Spectra (T=0.40s).

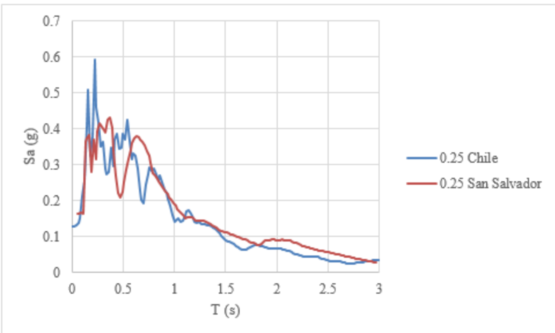

Figure 4.112. Acceleration Response Spectra (T=0.40s).

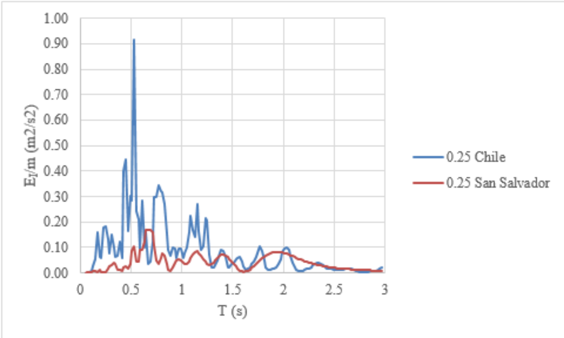

Figure 4.113. Energy Response Spectra (T=0.40).

Figure 4.114 to Figure 4.117 depict the acceleration response spectra and input energy response spectra for the pairs of experiments which their period is 0.50 seconds.

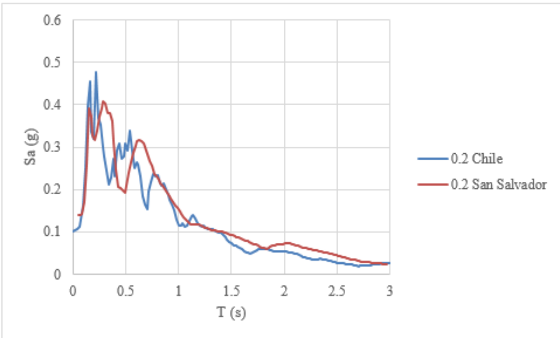

Figure 4.114. Acceleration Response Spectra (T=0.50s).

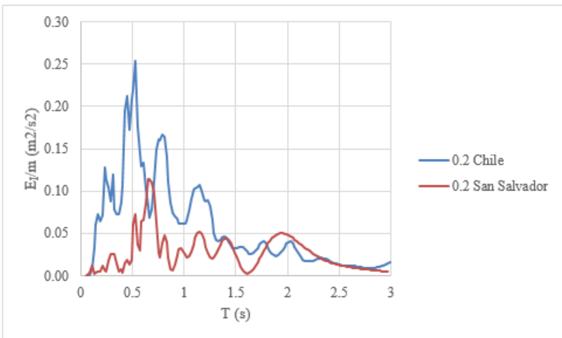

Figure 4.115. Energy Response Spectra (T=0.50).

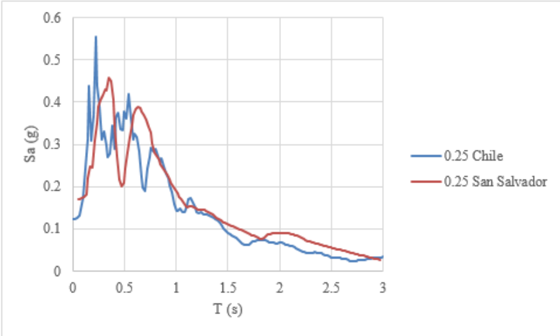

Figure 4.116. Acceleration Response Spectra (T=0.50s).

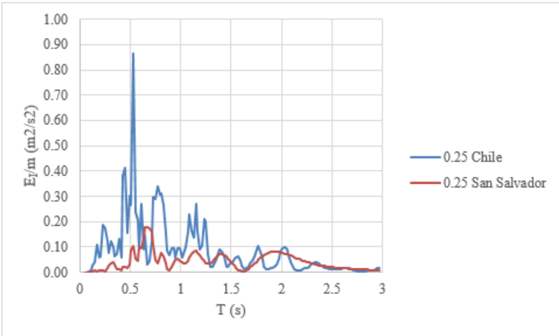

Figure 4.117. Energy Response Spectra (T=0.50s).

Figure 4.118 to Figure 4.121 depict the acceleration response spectra and input energy response spectra for the pairs of experiments which their period is 0.66s.

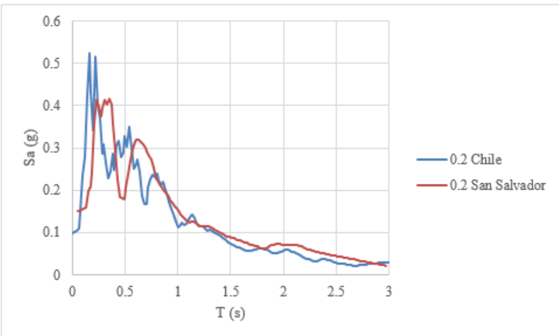

Figure 4.118. Acceleration Response Spectra (T=0.66s).

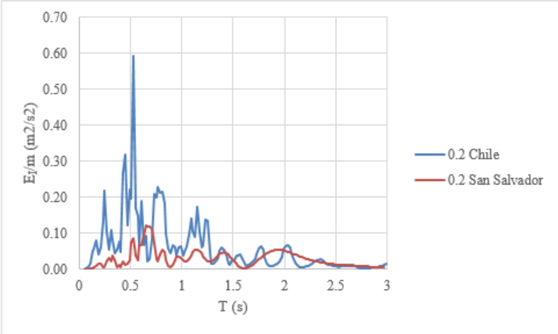

Figure 4.119. Energy Response Spectra (T=0.66s).

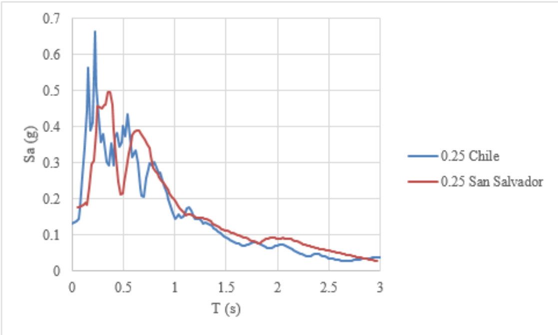

Figure 4.120. Acceleration Response Spectra (T=0.66s).

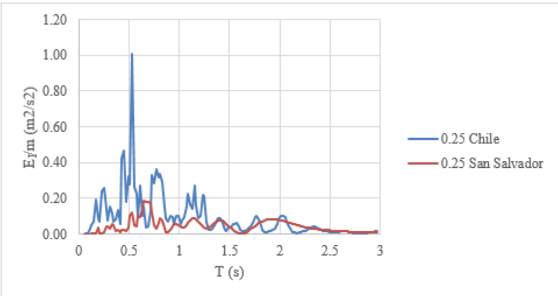

Figure 4.121. Energy Response Spectrum (T=0.66s).

It can be inferred from Figure 4.111, Figure 4.113, Figure 4.115, Figure 4.117, Figure 4.119 and Figure 4.121 that by increasing the duration of earthquake, the amount of imparted input energy is increased.

Table 4.1 provides the comparison of the input energy values obtained from the experiments and the spectra derived from the developed algorithm in terms of Joule. (J), that is equal to Newton multiplied by meter (N.m), for all the tests.

Table 4.1. Experimental and Spectral Values of Input Energy Response (J).

T=0.40s		
Earthquake	Experimental Energy Value	Spectral Energy Value
0.2 Chile	5.3	4.78
0.25 Chile	9.21	7.28
0.2 San Salvador	0.59	0.51
0.25 San Salvador	0.97	0.76
T=0.50s		
Earthquake	Experimental Energy Value	Spectral Energy Value
0.2 Chile	23.62	20.17
0.25 Chile	39.92	29.78
0.2 San Salvador	4.94	3.48
0.25 San Salvador	6.8	5.66
T=0.66s		
Earthquake	Experimental Energy Value	Spectral Energy Value
0.2 Chile	9.7	8.8
0.25 Chile	14.3	14.21
0.2 San Salvador	18.8	18.08
0.25 San Salvador	28.11	28.39

By considering Table 4.1, it can be concluded that the spectra developed algorithm in this study is reliable for estimating the input energy responses of SDOF systems. Therefore, the proposed algorithm may be used in to predict the elastic input energy response for a given earthquake acceleration records.

4.4. Strain Data Envelopes

In order to make a comparison of the damage level for the utilized seismic records, envelope graphs of strain data for the records has been drawn using the absolute peak values of the strain data in each time step. Figures 4.122 and Figure 4.123 depict the strain data envelope graphs for all the experiments conducted using Chile and San Salvador with scale factor of 0.20, respectively.

Although Chile and San Salvador seismic acceleration records with scale factor 0f 0.20 have similar ARSs (Figures 4.111, Figure 4.112 and Figure 4.114), it could be inferred from Figure 4.123 and Figure 4.124 that San Salvador earthquake with scale factor of 0.20 has more potential to make the structural member damaged compared to Chile earthquake with scale factor of 0.20.

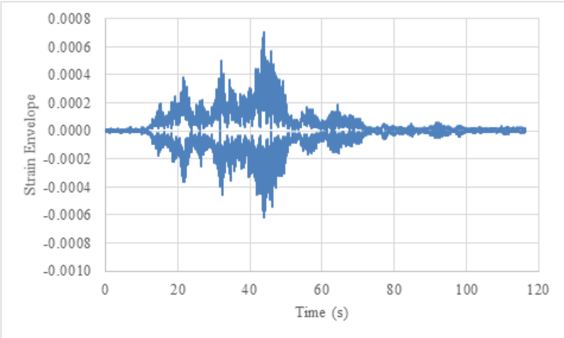

Figure 4.122. Strain Data Envelope for Chile Tests (Scale Factor: 0.20).

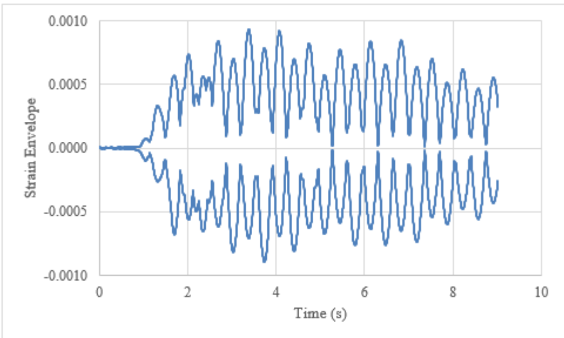

Figure 4.123. Strain Data Envelope for San Salvador Tests (Scale Factor: 0.20).

Figure 4.124 and Figure 4.125 depict the strain data envelope graphs for all the experiments conducted using Chile and San Salvador with scale factor of 0.25, respectively. Similarly, despite having similar ARSs, Chile and San Salvador seismic acceleration records with scale factor of 0.25 (Figure 4.116, Figure 4.118 and Figure 4.120) Figure 4.124 and Figure 4.125 imply that San Salvador earthquake with scale factor of 0.25 has more potential to cause the structural member to get damaged compared to Chile earthquake with scale factor of 0.25.

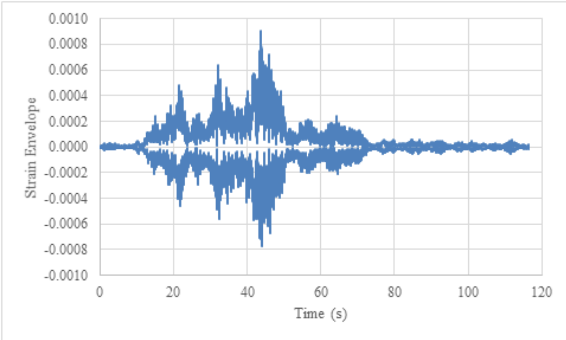

Figure 4.124. Strain Data Envelope for Chile Tests (Scale Factor: 0.25).

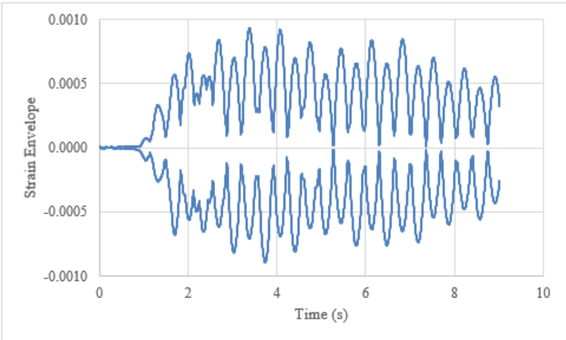

Figure 4.125. Strain Data Envelope for San Salvador Tests (Scale Factor: 0.25).

Although the amounts of input energy in the experiments with Chile earthquake are much than those of experiments with San Salvador earthquake, it could be inferred from Figure 4.122 to Figure 4.125, the amounts of strain in specimens subjected to San Salvador earthquake are higher than those of specimens subjected to Chile earthquake. It could be explained by the higher value of PGA in San Salvador acceleration records. By higher PGA value, more lateral load could be subjected to the specimens and consequently more strain values were resulted.

By drawing envelope cumulative strain graphs the effect of duration of seismic loads gets into consideration. As Figure 4.126 to Figure 4.129 implies the cumulative strain amounts of the specimens while subjected to Chile Earthquake is higher compared to the cumulative strain amounts for the experiments with San Salvador earthquake. As it is widely known, the damage in structural members is directly related to plastic rotation. By considering the duration of the utilized earthquakes it could be concluded that, Chile has more potential to make structural members damaged. In order to make a reliable conclusion regarding the effect of cumulative strain and the plastic rotations and the relationship between cumulative strain values with plastic energy, some inelastic experiments are required.

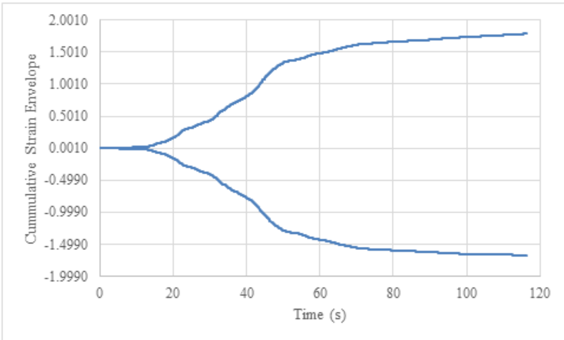

Figure 4.126. Cumulative Strain Data Envelope for Chile Tests (Scale Factor: 0.20).

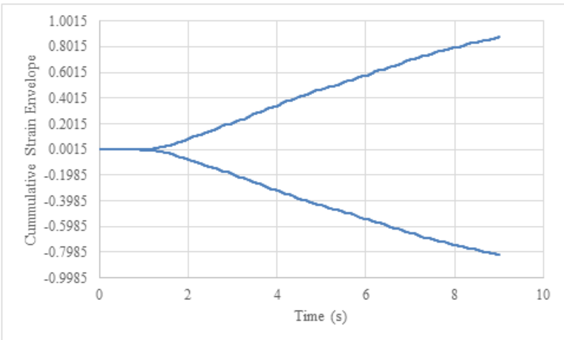

Figure 4.127. Cumulative Strain Data Envelope for San Salvador Tests (Scale Factor: 0.20).

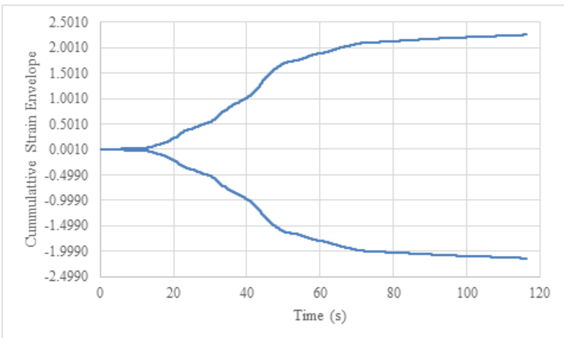

Figure 4.128. Cumulative Strain Data Envelope for San Salvador Tests (Scale Factor: 0.20)Cumulative Strain Data Envelope for Chile Tests (Scale Factor: 0.25).

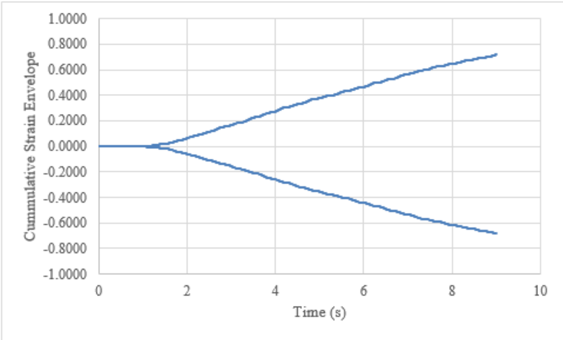

Figure 4.129. Cumulative Strain Data Envelope for San Salvador Tests (Scale Factor: 0.25).

5. SUMMARY AND CONCLUSIONS

In this study, the fundaments of Energy-Based seismic analysis were reviewed and the related equations of absolute and relative energy were derived. Also, an algorithm was developed in order to perform time history response analysis for different energy components and elastic input energy response spectrum. Twelve elastic-range experiments were conducted in order to investigate the validity of the commonly used formulations in Energy-Based seismic analysis. During the trial tests the proposed algorithm was developed in order to include the *P-Delta* effect and to calculate strain energy from the data read from strain gauges. All the time histories of energy components were computed by the proposed algorithm, experimental dynamic responses and modal analysis in SAP2000 and the ultimate of all results were compared. Ultimately, the amounts input energy which resulted from the experiments, are compared with the derived energy spectra of the proposed algorithm.

Having considered the whole results of this study, the following conclusions could be drawn;

- All the experimental results clearly implied that the derived energy formulations are valid in elastic range for the utilized specimens.
- The proposed algorithm may be utilized as a reliable tool in order to estimate the time history of different energy components and generating the elastic input energy response spectrum of a given earthquake-type loading for SDOF systems.
- Increase in the duration of the earthquake makes the imparted input energy into the system increased. Therefore, the effect of the duration of seismic loads needs to be taken into account in order to enhance the seismic analysis and design approaches.
- Almost all the imparted input energy into the tested specimens were dissipated by inherent damping of the systems.
- Comparison of strain envelope graphs illustrated that two earthquake-type loading which have similar ARSs could have different damage levels on members.

Thus, seismic design of structures based upon ARS (or ADS) seems not to be realistic.

This study needs to be extended in a variety of related area such as conducting inelastic tests in order to study the validity of the formulations when system displaces beyond linear behavior. Also, similar tests may be performed for reinforced concrete or other materials in future. The research should be extended to MDOF systems both for linear and nonlinear ranges in order to investigate the related formulations and energy demand and energy dissipating capacity. In addition, since the strength of material was not included in this study, a similar research considering the strength of material is highly recommended.

REFERENCES

Akbas, B., 1997, "Energy-Based Earthquake Resistant Design of Steel Moment Resisting Frames", Ph.D. Thesis, University of Illinois at Urbana-Champaign, Urbana, Illinois, United States of America.

Akiyama, H., 1985, "Earthquake-Resistant Limit-State Design for Buildings", University of Tokyo Press, Japan

Acun, B., and H. Sucuoglu, 2012, "Energy Dissipation Capacity of Reinforced Concrete Columns under Cyclic Displacement", *American Concrete Institute Structural Journal*, Vol. 109, No. 4, pp. 531-540.

Bertero, V.V. and C.M. Uang, 1988, "Implications of Recorded Earthquake Ground Motions on Seismic Design of Building Structures", Research Report, UCB/EERC-88/13, University of California at Berkeley, United States of America.

Bertero, V.V. and C.M. Uang, 1992, "Issues and Future Directions in the Use of An Energy Approach for Seismic - Resistant Design of Structures", *Proceedings of the Nonlinear Seismic Analysis and Design of Reinforced Concrete Buildings*, Vol. 1, pp. 3-22.

Benavent-Climent, A, L.G. Pujades, and F. Lopez-Almansa, 2002, "Design Energy Input Spectra for Moderate Seismicity Regions", *Earthquake Engineering and Structural Dynamics*, Vol. 31, pp. 1151-1172.

Bojorqueza, E., S.E. Ruiza, and A. Teran-Gilmoreb, 2008, "Reliability-Based Evaluation of Steel Structures Using Energy Concepts", *Engineering Structures*, Vol. 30, No. 6, pp. 1745-1759.

Benavent-Climent, A., F. Lopez-Almansa, and D. A. Bravo-Gonzalez, 2010, "Design Energy Input Spectra for Moderate-to-High Seismicity Regions Based on Colombian Earthquakes", *Soil Dynamics and Earthquake Engineering*, Vol. 30, pp. 1129-1148.

Benavent-Climent, A. and R. Zahran, 2010, "An energy-based procedure for the assessment of seismic capacity of existing frames: Application to RC wide beam systems in Spain", *Soil Dynamics and Earthquake Engineering*, Vol. 30, pp. 354-367.

Benavent-Climent A., 2011, "An Energy-Based Method for Seismic Retrofit of Existing Frames Using Hysteretic Dampers", *Soil Dynamics and Earthquake Engineering*, Vol. 31, pp. 1385-1396.

Chopra, A.K., 1995, "Dynamics of Structures: Theory and Applications to Earthquake Engineering", *Prentice Hall*, Englewood Cliffs, New Jersey.

Calvi, G.M. and M.J.N. Priestley, 1997, "Assessment of Existing Buildings, in: Seismic Design of RC Structures for Controlled Inelastic Response", *CEB Bulletin 236 Lausanne*, Vol. 1, pp. 159-204.

Chou, C.C. and C.M. Uang, 2003, "A Procedure for Evaluating Seismic Energy Demand of Framed Structures", *Earthquake Engineering and Structural Dynamics*, Vol. 32, No. 2, pp. 229-244.

Clough, R. W. and J. Penzien, 2003, "Dynamics of Structures, Computers and Structures", Berkeley, California, United States.

Chai, Y.H., 2004, "Incorporating Low-Cycle Fatigue Model into Duration-Dependent Inelastic Design Spectra", *Earthquake Engineering and Structural Dynamics*, Vol. 34, No. 1, pp. 83-96

Decanini, L.D. and F. Mollaioli, 1998, "Formulation of Elastic Earthquake Input Energy Spectra", *Earthquake Engineering and Structural Dynamics*, Vol. 27, pp. 1503-1522.

Decanini, L.D. and F. Mollaioli, 2001, "An Energy-Based methodology for the Assessment of Seismic Demand", *Soil Dynamic and Earthquake Engineering*, Vol. 21, pp. 113-137.

Dimova, S.L. and P. Negro, 2004, "Influence of Construction Deficiencies on the Seismic Response of Structures", *Earthquake Engineering and Structural Dynamics*, Vol. 34, No. 6, pp.613-635.

Dindar, A. A., 2009, "Energy-Based Earthquake Response Analysis and Design of Reinforced Concrete SDOF Columns", PhD Thesis, Department of Civil Engineering, Boğaziçi University, Istanbul, Turkey.

Dindar, A.A., C. Yalçin, E. Yüksel, H. Özkaynak and Oral Büyüköztürk, 2012, "Inelastic Seismic Demand Mapping of the Regions Using Energy Balance Formulation", *The 15th World Conference on Earthquake Engineering*, Lisbon, Portugal.

D'Ambrisi, A. and M. Mezzi, 2015, "An Energy-Based Approach for Nonlinear Static Analysis of Structures", *Bulletin of Earthquake Engineering*, Vol. 13, pp. 1513-1530.

Erberik, M. A., H. Sucuoglu and B. Acun, 2012, "Inelastic Displacement Response of RC Systems with Cyclic Deterioration-An Energy Approach", *Earthquake Engineering*, Vol. 16, pp. 937-962.

Farahmand, B., 2006, "Conceptual Comparison Between Force-Based Design and Displacement-Based Design Methods", M.Sc. Thesis, Sharif University of Technology, Tehran, Iran.

Gupta, A.K., 1990, "Response Spectrum Method", Chemical Rubber Company Press Incorporation.

Gülkan, P. and A.M. Sözen, 1974, "Inelastic Responses of Reinforced Concrete Structures to Earthquake Motions", *American Concrete Institute Journal*, Vol. 71, No.12, pp. 601-609.

Ghosh, S. and K.R. Collins, 2006, "Merging energy-based design criteria and reliability-based methods: Exploring a new concept", *Earthquake Engineering and Structural Dynamics Earthquake*, Vol. 35, pp. 1677-1698.

Haddad Shargh, F. and M. Hosseini, 2010, "A Study on Existence of an optimal Distribution on Stiffness Over the Height of Mid-to High Rise Buildings to Minimize the Seismic Input Energy", *Applied Science*, Vol. 10, No. 1, pp. 45-51.

Hasegawa, T. and H. Kamura, 2008, "Seismic Response Prediction of Steel Frames Utilizing Plastic Strain Energy Obtained from Pushover Analysis", The 14th Word Conference on Earthquake Engineering, Beijing, China.

Hernadez-Montes, E., O.S. Kwon and M.A. Aschheim, 2004, "An Energy-Based Formulation for First- and Multiple-Mode Nonlinear Static (Pushover) Analysis", *Earthquake Engineering*, Vol. 8, No. 1, pp. 69-88.

Hibbeler R.C., 1985, "Structural Analysis", *Prentice Hall New Jersey*, United States of America.

Hosseini, M. and Vaseghinia A., 2008, "A New Insight to the Earthquake Input Energy and Its Variation with Building's Dynamical Characteristics", The 14th World Conference on Earthquake Engineering, Beijing, China.

Kuwamura, H., and T.V. Galambos, 1989, "Earthquake Load for Structural Reliability", *Structural Engineering*, Vol. 115, No. 6. pp. 1446-1462.

Krawinkler, H. and A.A. Nassar, 1992, "Seismic Design Based On Ductility and Cumulative Damage Demands and Capacities", Proceedings of the Nonlinear Seismic Analysis and Design of Reinforced Concrete Buildings, *Bled/Ljubljana*, Vol.1, pp. 23-40.

Kowalsky, M.J., M.J.N. Priestley, G.A. MacRae. 1994, "Displacement-Based Design, a Methodology for Seismic Design Applied to Single Degree of Freedom reinforced

Concrete Structures", Report No. SSRP-94/16. Structural Systems Research, University of California, San Diego, La Jolla, California, United States of America.

Kunnath, S.K., J.B. Mander and F. Lee, 1997, "Parameter Identification for Degrading and Pinched Hysteretic Structural Concrete Systems", *Engineering Structures*, Vol. 19, No. 3, pp. 224-232.

Kalkan, E. and S.K. Kunnath, 2007, "Effective Cyclic Energy as a Measure of Seismic Demand", Earthquake Engineering, Vol. 11. No.5, pp. 725-751.

Ke, K. and Y. Chena, 2014, "Energy-Based Damage-Control Design of Steel Frames with Steel Slit Walls", *Structural Engineering and Mechanics*, Vol. 52, No. 6, pp. 1157-1176.

Khampanit, A., Leelataviwat S., J. Kochanin and P.Warnitchai, 2014, "Energy-Based Seismic Strengthening Design of Non-Ductile Reinforced Concrete Frames Using Buckling-Restrained Braces", *Engineering Structures*, Vol. 81, pp. 110-122.

Leelataviwat, S., S.C. Goel and B. Stojadinovic, 2002, "Energy-Based Seismic Design of Structures Using Yield Mechanism and Target Displacement", *Structural Engineering*, Vol. 128, No.8, pp. 1046-1054.

Lopez-Almansa, F., A.U. Yazgan and A. Benavent-Climent, 2013, "Design Energy Input Spectra for High Seismicity Regions Based on Turkish Registers", *Bulletin of Earthquake Engineering*, Vol. 11, No.4, pp 885-912.

Lin, J.J., A.R. Liu, Q.C. Yu and J.D. Deng, 2014, "Deformation and Energy-Based Seismic Damage Evaluation of Steel Reinforced Concrete and Reinforced Concrete Piers", *Applied Mechanics and Materials*, Vol. 580-583, pp. 1430-1434.

Mahin, S.A. and V.V. Bertero, 1981, "An Evaluation of Inelastic Seismic Design Spectra", *Structural Division*, Vol. 107, No. 9, pp. 1777-1795.

Manfredi, G., 2001, "Evaluation of Seismic Energy Demand", *Earthquake Engineering* *and Structural Dynamics*, Vol. 30, pp. 485-499.

Malhotra, P.K., 2002, "Cyclic-Demand Spectrum", *Earthquake Engineering and Structural Dynamics*, Vol.33, pp. 1441-1457.

Manoukas, G., A. Athanatopoulou, and L. Avramidisc, 2011, "Static Pushover Analysis Based on an Energy-Equivalent SDOF System", *Earthquake Spectra*, Vol. 27, No. 1, pp. 89-105.

Newmark, N.M. and W.J. Hall, 1982, "Earthquake Spectra and Design", Earthquake Engineering Research Institute, Oakland.

Özakgül, K., 2015, "Evaluation of Energy Response of Space Steel Frames Subjected to Seismic Loads", *Structural Engineering and Mechanics*, Vol. 54, No. 4, pp. 809-827.

Park, R. and A.H-S. Ang, 1985, "Mechanistic Seismic Damage Model For Reinforced Concrete", *Journal of Structural Engineering American Society of Civil Engineers*, Vol. 111, No. 4, pp. 740-757.

Priestly, M.J.N., 1997, "Displacement-Based Seismic Assessment of Reinforced Concrete Buildings", *Earthquake Engineering*, Vol. 1, No.1, pp. 157-191.

Prasanth, T., S. Ghosh and K. R. Collins, 2008, "Estimation of Hysteretic Energy Demand Using Concepts of Modal Pushover Analysis", *Earthquake Engineering and Structural Dynamics*, Vol. 37, No.6, pp. 975-990.

Poljansek, K., I. Perus, P. Fajfar, 2009, "Hysteretic Energy Dissipation Capacity And Cyclic To Monotonic Drift Ratio for Rectangular RC Columns in Flexure", *Earthquake Engineering and Structural Dynamics*, Vol. 38, No. 7, pp. 907-928.

Shen, K. L. and T. T. Soong, 1996, "Design of Energy Dissipation Devices Based on Concept of Damage Control", *Structural Engineering*, Vol. 122, No. 1, pp. 76-82.

Sütçü, F., 2006, “Combined of Damper and Displacement Controller for Seismically Excited Structures”, Ph.D. Thesis, Tohoku University, Department of Architecture, Sendai, Japan.

Sucuoğlu, H., and B. Acun 2012, “Energy-Based Hysteresis Model for Flexural Response of Reinforced Concrete Columns”, *American Concrete Institute Structural Journal*, Vol. 109, No. 4, pp. 541-550.

Takewaki, I., 2007, “Earthquake Input Energy to Two Buildings Connected by Viscous Dampers”, *Structural Engineering*, Vol. 133, No. 5, pp. 620-628.

Terapathana, S., 2012, “An Energy Method for Earthquake Resistant Design of RC Structures”, Ph.D. Thesis, Faculty of the USC Graduate School University of Southern California, United States of America.

Uang C.M. and V.V. Bertero, 1986, “Earthquake Simulation Tests and associated studies of a 6-Story Concentrically Braced Steel Structures”, Earthquake Engineering Research Center, Report Number UCB/EERC-86-10, University of California, Berkeley, United States of America.

Uang C.M. and V.V. Bertero, 1990, “Evaluation of Seismic Energy in Structures”, *Earthquake Engineering and Structural Dynamics,* Vol. 19, No. 1, pp. 77-90.

Uçar, T. and O. Merter, 2015, “Determination of Plastic Energy Demands of Reinforced Concrete Frames under Code Specific Earthquake Levels”, *Journal of Gümüşhane University, Faculty of Engineering*, Vol. 5, No. 2, pp. 101-113.

Vidic, T., P. Fajfar and M. Fischinger, 1994, “Consistent Inelastic Design Spectra: Strength and Displacement”, *Earthquake Engineering and Structural Dynamics*, Vol. 23, No. 5, pp. 507-521.

Wong, K.F. and R. Yang, 2002, “Earthquake Response and Energy Evaluation of Inelastic Structures”, *Engineering Mechanics*, Vol. 128, No. 3, pp. 308-317.

Wong, K.F. and Y. Wang, 2003, "Energy-Based Design of Structures Using Modified Force Analogy Method", *The Structural Design of Tall and Special Buildings*, Vol. 12, pp. 393-407.

Xue Q. and Moehle J.P., 1991, "Displacement design approach for Reinforced Concrete Structures Subjected to Earthquakes", *Engineering Structures Research Center*, Report No. UCB/EERC-91/02, University of California, Berkeley, United States of America..

Ye, L., G. Cheng, and Z. Qu, 2009, "Study on Energy-Based Seismic Design Method and the Application for Steel Braced Frame Structures", Sixth International Conference on Urban Earthquake Engineering, Tokyo Institute of Technology, Tokyo, Japan.

Zahrah, T.F. and W.J. Hall, 1984, "Earthquake Energy Absorption in SDOF Structures", *Journal of Structural Engineering*, Vol. 110, No. 8, pp.1757-1773.